

Maclaine, Sarah Elizabeth (2013) *The production of living, tissue engineered, bone graft from progenitor cells using nanotechnology*. MD thesis.

<http://theses.gla.ac.uk/4558/>

Copyright and moral rights for this thesis are retained by the author

A copy can be downloaded for personal non-commercial research or study, without prior permission or charge

This thesis cannot be reproduced or quoted extensively from without first obtaining permission in writing from the Author

The content must not be changed in any way or sold commercially in any format or medium without the formal permission of the Author

When referring to this work, full bibliographic details including the author, title, awarding institution and date of the thesis must be given

The Production of Living, Tissue Engineered, Bone Graft from Progenitor Cells using Nanotechnology

Sarah Elizabeth Maclaine

MBChB MRCS



University
of Glasgow

Submitted in fulfilment of the requirements for the degree of MD.

Centre for Cell Engineering
Institute of Molecular, Cell and Systems Biology
College of Medical, Veterinary and Life Sciences
University of Glasgow, G12 8QQ

February 2013

Abstract

The principal aim of this research was the development of a technique (based upon the effects of nanoscale topography) that facilitates the *in vitro* expansion of bone graft for subsequent implantation.

Nanoscale topography increases the bioactivity of a material and stimulates specific responses at the molecular level (third generation biomaterial properties). Nanoscale topography thus confers these third generation properties upon biomaterials that are otherwise first generation (bioinert) or second generation (bioresorbable or bioactive) in nature.

Two topographies (nanopits and nanoislands) were embossed into the clinically licensed bioresorbable polymer Polycaprolactone (PCL). A protocol was developed which enabled three dimensional cell culture using double-sided embossing of substrates, seeding of both sides, and vertical positioning of the substrates during cell culture.

Human bone marrow was harvested and the mononuclear cell fraction culture expanded. These human bone marrow cells (HBMCs) were used for cellular analysis of substrate bioactivity. In addition, acellular analysis of substrate patterning and degradation was also performed.

The osteogenic behaviour (and cell line specificity) was demonstrated using alizarin red staining, immunohistochemistry, real-time polymerase chain reaction (rtPCR), and quantitative PCR (qPCR). The osteogenicity of PCL was increased by the presence of nanotopography, and by the incorporation of hydroxyapatite (HA) into the PCL forming a hydroxyapatite-PCL composite (HAPCL). The performance of these substrates was compared to exposure to bone morphogenic protein 2 (BMP2), and the use of osteogenic media.

The protocol from shim production to bone marrow harvesting and vertical cell culture on nanoembossed PCL has been shown to be reproducible and potentially applicable to economical larger scale production.

Table of Contents

Abstract	2
List of tables	7
List of figures	8
Publications and presentations relating to this thesis	10
Acknowledgement	11
Author's declaration	12
List of definitions and abbreviations	13
 Chapter 1 General Introduction	 18
1.1 Bone	18
1.1.1 Bone function and structure	18
1.1.2 Bone marrow	18
1.1.3 Bone cells	19
 1.2 The use of bone graft	 20
1.2.1 Bone graft and bone graft substitutes	22
 1.3 Tissue Engineering	 24
1.3.1 Stem Cells	24
1.3.2 Human bone marrow cells (HBMC), MSC & skeletal stem cells (SSC)	26
1.3.3 Clinical applications of chondrocytes and bone marrow stem cells	27
 1.4 Osteoblast differentiation	 30
1.4.1 Control of osteogenic differentiation	30
1.4.2 Osteoblast differentiation and gene expression	30
1.4.3 Phases of <i>in vitro</i> osteoblastic development	32
 1.5 Biomaterials	 34
1.5.1 Development of biomaterials	34
1.5.2 Osseointegration and osteoinduction	35
1.5.3 Topography	37
1.5.4 Chemistry	39
1.5.5 Surface modification of orthopaedic implants: chemistry and or topography	40
 1.6 Tissue responses to the modification of surfaces	 43
1.6.1 Cellular responses to the modification of surfaces	43

1.6.2	Intracellular responses to surface modifications	46
1.7	My hypotheses and the progression to protocol development	48
Chapter 2	Protocol optimisation: Materials and methods	49
2.1	Introduction to materials and methods	49
2.1.1	Nanotopography	50
2.1.2	Materials	51
2.1.3	Cell lines	54
2.1.4	Background to experimental techniques	55
2.1.5	Gene expression and cell phenotype	59
2.2	Methods	63
2.2.1	Shim manufacture	63
2.2.2	Preparation of PCL substrates	63
2.2.3	Acellular analysis of substrates using SEM and AFM	65
2.2.4	HBMC acquisition	66
2.2.5	Cell culture	69
2.2.6	Cell staining and imaging	73
2.2.7	RNA extraction for qPCR	74
2.2.8	RT and PCR	75
2.3	Results	76
2.3.1	Acellular substrate analysis	77
2.3.2	Acellular assessment of substrate degradation	78
2.3.3	HBMC acquisition	81
2.3.4	Single sided cell culture	82
2.3.5	Cell culture on dual sided substrates	84
2.3.6	RNA extraction optimization	91
2.4	Discussion	93
2.4.1	Shim manufacture, substrate preparation and acellular analysis	93
2.4.2	Human bone marrow aspiration and HBMC acquisition	95
2.4.3	Single and dual sided cell seeding and culture	97
2.4.4	Coomassie blue and alizarin red staining	98
2.4.5	Immunostaining and light microscopy	99
2.4.6	RNA harvesting, RT and qPCR	99
2.4	Conclusion	100

Chapter 3	Analysis of nanopit (NSQ50) embossed PCL	101
3.1	Introduction	101
3.2	Materials and methods	101
3.2.1	Shim manufacture	102
3.2.2	Substrate conditions	103
3.2.3	Horizontal single sided culture for Microscopy	104
3.2.4	Horizontal single sided culture for qPCR	104
3.2.5	Vertical dual sided culture for Microscopy	106
3.2.6	Vertical culture for immunofluorescence analysis of phenotype	106
3.2.7	Vertical culture for rtPCR	106
3.2.8	Vertical culture for qPCR	106
3.3	Results	107
3.3.1	Single sided HBMC culture	107
3.3.2	Single sided culture for qPCR analysis of gene expression	108
3.3.3	Dual sided culture and OPN, OCN and Alizarin red staining	109
3.3.4	Preliminary analysis of phenotype	113
3.3.5	QPCR analysis of phenotype	114
3.4	Discussion	115
Chapter 4	Analysis of nanoisland embossed PCL	124
4.1	Introduction	124
4.2	Materials and methods	124
4.2.1	Shim production, substrate manufacture and acellular substrate analysis	125
4.2.2	Cellular substrate analysis using light and immunofluorescence microscopy	126
4.2.3	RUNX2 analysis using qPCR	126
4.3	Results	126
4.3.1	Acellular analysis of planar and nanoisland embossed surfaces	126
4.3.2	Cellular analysis of substrates using microscopy	128
4.3.3	Cellular analysis of substrates using qPCR	130
4.4	Discussion	131
4.5	Conclusion	133

Chapter 5	Discussion and future directions	134
5.1	Background	134
5.2	My Research choices	138
5.3	Conclusion	149
	List of References	150
	Appendix	159
1	Acellular substrate analysis	159
2	Cell culture	160
3	HBMC harvest and HOBs	161
4	Cell microscopy	162
5	RNA extraction	163
6	RT	163
7	QPCR	164
8	RNA yield and integrity	165

List of tables

Chapter 2 Protocol Optimisation: Materials and Methods

Table 2.1	Gene expression and cell phenotype	62
Table 2.2	RNA yield at 33 days, single sided culture combining two Planar substrates	92
Table 2.3	RNA yield at 28 days, double sided culture combining four substrates	92

Chapter 3 Analysis of nanopit (NSQ50) embossed PCL

Table 3.1	Summary of horizontal single sided culture results	116
Table 3.2	Summary of vertical dual-sided culture results	117
Table 3.3	Phenotype analysis at day 11	119
Table 3.4	Phenotype analysis at day 28	120

Chapter 5 Discussion and future directions

Table 5.1	Summary of immunofluorescence results (chapter 3)	143
Table 5.2	Summary of immunofluorescence results (chapter 4)	144
Table 5.3	Summary of qPCR results comparing planar PCL and the NSQ50 nanotopography (chapter 3, figures 3.10 and 3.11)	144

Appendix

Table A.1	RNA yield and integrity vertical culture day 11	165
Table A.2	RNA yield and integrity vertical culture day 28	166
Table A.3	RNA yield and integrity vertical culture day 25	166

List of figures

Chapter 1 General Introduction

Figure 1.1	A proximal and distal femur in cross-section	19
Figure 1.2	MSC differentiation	25
Figure 1.3	The harvest, expansion and orthopaedic uses of SSCs	29
Figure 1.4	MSC differentiation into osteoblasts	30
Figure 1.5	The osteogenic differentiation pathway	31
Figure 1.6	Corundumized and fibre metal surface modification of hip prostheses	38
Figure 1.7	Topographical and chemical surfaces of uncemented hip implants	41
Figure 1.8	The <i>Mayo</i> Conservative hip prosthesis	42
Figure 1.9	A comparison of bone ingrowth and biological fixation of implants	43

Chapter 2 Protocol Optimisation: Materials and Methods

Figure 2.1	The mechanisms of action of BMPs in bone repair	53
Figure 2.2	Direct and indirect immunohistochemical staining	56
Figure 2.3	RT	58
Figure 2.4	PCR	59
Figure 2.5	Real time qPCR	60
Figure 2.6	A model 'real time' qPCR plot	61
Figure 2.7	Cell separation using a Ficoll gradient	67
Figure 2.8	Rotatory bioreactor	70
Figure 2.9	The suspension culture technique	71
Figure 2.10	The vertical culture technique	72
Figure 2.11	SEM images of the NSQ50 nanoembossed substrates	77
Figure 2.12	AFM images of NSQ50 embossed PCL and HAPCL	78
Figure 2.13	AFM images after a 28-day period of exposure to SBF	79
Figure 2.14	AFM images after a 28-day period of exposure to media	79
Figure 2.15	Surface roughness of PCL and HAPCL substrates	80
Figure 2.16	HBMC from bone marrow and fragments	81
Figure 2.17	Coomassie blue staining of HTERT at 30 min and 4 days	82
Figure 2.18	Coomassie blue images of HTERT using varied seeding densities and plasma treatment substrates	83
Figure 2.19	Dual sided culture of HTERT on nanoembossed PCL	84

Figure 2.20	Static (with turning) and rotary bioreactor dual-sided culture of HBMCs	85
Figure 2.21	Macroscopic images obtained after suspension culture	86
Figure 2.22	Coomassie blue staining following suspension culture	87
Figure 2.23	Coomassie blue images after 7 days	88
Figure 2.24	Coomassie blue images after 14 days	89
Figure 2.25	OPN immunofluorescence after 3 weeks	90
Figure 2.26	OCN immunofluorescence after 3 weeks	91
Chapter 3	Analysis of nanopit (NSQ50) embossed PCL	
Figure 3.1	Immunofluorescence analysis of OPN and OCN expression	107
Figure 3.2	Coomassie blue staining and Alizarin red staining of HBMCs	108
Figure 3.3	Relative gene expression at day 7	108
Figure 3.3	Immunofluorescence analysis of OPN expression	110
Figure 3.4	Immunofluorescence analysis of OCN expression	111
Figure 3.5	Analysis of calcium deposition	112
Figure 3.6	Immunofluorescence analysis of phenotype	113
Figure 3.7	Relative gene expression at day 11	114
Figure 3.8	Relative gene expression at day 28	115
Chapter 4	Analysis of nanoisland embossed PCL	
Figure 4.1	AFM micrographs of control and test samples	127
Figure 4.2	Section analysis of substrates A and B	128
Figure 4.3	Temporal immunofluorescence analysis of OPN expression	129
Figure 4.4	Temporal immunofluorescence analysis of OCN expression	130
Figure 4.5	RUNX2 expression at 25 days	131
Chapter 5	Discussion and future directions	

Publications and presentations relating to this thesis

Developments in stem cells- implications for future joint replacements.

Maclaine S. E., McNamara L.E., Bennett A.J., Dalby, M.J., Meek, R.M.D.

Proceedings of the Institution of Mechanical Engineers, Part H: Journal of Engineering in Medicine 0954411912471492, first published online January 10, 2013 as doi:10.1177/0954411912471492

Optimizing the osteogenicity of nanotopography using block co-polymer phase separation fabrication techniques. SE Maclaine, N Gadhari, R Pugin, Dominic RM Meek, M Liley, MJ Dalby J Orthop Res 30(8):1190-7 (2012), PMID 22294345

Enhanced osteogenesis of mesenchymal stem cells by nanostructured surfaces. Maclaine, S., Dalby, M.J., Meek, D.. **Research highlights.** 2010 Nanomedicine: 5 (10) 1497

Presentations

Tissue Engineering Bone Graft, for Orthopaedic Application. Maclaine S. GLORI, Glasgow Oct 2012 Podium presentation

Nanopatterning for the Production of Viable Bone Graft on Biodegradable Constructs. Sarah Maclaine^{*1, 2}, Neha Gadhari¹, Andrew Hart¹, Martha Liley³, R.M. Dominic Meek⁴ and Matthew J. Dalby¹ GLORI, Glasgow May 2010 Poster presentation

Acknowledgement

I would like to thank my supervisors Drs Matthew Dalby, Nikolaj Gadegaard and Mr Dominic Meek for the opportunity to undertake this research and their assistance in its undertaking.

Dominic, thank you for introducing me to Matt and Matt thank you for taking me on as a clinical fellow. Thank you for my two years out and the help and support you have shown throughout.

Thank you to all my friends at CCE, you made a home for me when life was tricky and helped me to change from clinician to student and back again. Thank you all for the coffee friendship and chats.

Andy, Carol-Anne and Josie, you took on a lot when you took on someone who hadn't done biology since school, its appreciated. You all worked hard to help me, and this too is acknowledged and appreciated.

Dr Huabing and Mr Gordon McPhee, thank you for your assistance with the SEM and AFM measurements. Ms Veronique Monnier, thank you for the preparation of nanostructured surfaces fabricated by block copolymer phase separation.

Mr David Large, for your support and that of the training committee throughout, and the study leave at the end.

Bob, Abi and my family, thank you for the hugs and kisses and encouragement in finishing 'my book'.

This work was funded by Chief Scientist Office grant CBZ/4/714.

Author's declaration

I declare that, except where specific reference is made to the contribution of others, that this dissertation is the result of my own work and has not been submitted for any other degree at the University of Glasgow or any other institution.

Sarah Maclaine

August 2013

Definitions and abbreviations

ABI	Appositional bone index
ACI	Autologous chondrocyte implantation
AFM	Atomic force microscopy
ALP	Alkaline phosphate
ALPH	Alkaline phosphatase
α MEM	Alpha modified eagles medium
AML	Anatomical intramedullary locking
ANOVA	Analysis of variance
A=T	Adenine=Thymine
BM	Basement membrane
β ME	β mercaptoethanol
BMPs	Bone morphogenic proteins 1-4
BMPR2	Bone morphogenic protein receptor 2, expressed by multiple tissues, involved in up-regulation of bone mineralisation
BMSC	Bone marrow derived stem cells
BSA	Bovine serum albumin
BSP	Bone sialoprotein
Cbfa1	Core binding factor alpha 1
CD34	A haematopoietic stem cell marker
CD133	A haematopoietic stem cell marker
CD146	Melanoma-associated cell adhesion molecule
cDNA	Complementary deoxyribonucleic acid
c-Fos	A transcription factor
CJD	Creutzfeldt-Jakob disease
Col-1, COL1	Collagen type I

CSTi	Cancellous structured titanium
CT	Cycle threshold
CTGF	Connective tissue growth factor
CVD	Chemical vapour deposited
DAPI	4',6-diamino-2-phenylindole stain for DNA
DLX5/6	transcription factors
DMEM	Dulbeccos modified eagles medium
E-beam	Electron beam
EBL	Electron beam lithography
ECM	Extracellular matrix
EDTA	Ethylene diamine tetra acetic acid
ERK1/2	Extracellular-signal related kinase 1/2
FAK	Focal adhesion kinase
FCS	Fetal calf serum
FDA	Food and drug administration
FGF	Fibroblast growth factor
FITC	Fluorescein isothiocyanate
Fra1	A transcription factor
GAPDH	Responsible for the protein involved in the catalysis of the 6 th step of glycolysis
gDNA	Genomic deoxyribonucleic acid
GF	Growth factor
HA	Hydroxyapatite
HAPCL	Hydroxyapatite polycaprolactone
HAPEX	Hydroxyapatite reinforced polyethylene
HBMC	Human bone marrow cell
HD	Homeodomain protein

HEPES	4-(2-hydroxyethyl)-1-piperazine-ethanesulphonic acid
HS	Hepes saline
Htert	Human telomerase reverse transcriptase immortalised cell line
HOBs	Human osteoblasts
IHH	Indian hedgehog
IL	Interleukin 1, 6
LEF	A transcription factor in the Wnt pathway
M-Csf	Macrophage colony stimulating factor
MACI	Matrix induced autologous chondrocyte implantation
MCAM	Melanoma-associated cell adhesion molecule (also known as CD146)
MG63	A human osteosarcoma cell line
MITF	Microphthalmia-associated transcription factor
MM	Master mix
Mn	Molecular number
MRI	Magnetic resonance imaging
mRNA	Messenger ribonucleic acid
MSCs	Mesenchymal stem cells
MYOD1	Marker of myogenic differentiation
NFATc1	Nuclear factor of activated T-cells
NFkB	Receptor activator of nuclear factor-kappaB
n	Number of repeats
NSQ50	The nanopit topography used
N-V	Nickel-Vanadium
OCN	Osteocalcin (also known as BGLAP)
OPN	Osteopontin
OSX	Osterix
PBS	Phosphate buffered saline

PCL	Polycaprolactone
PCR	Polymerase chain reaction
PDGF	Platelet-derived growth factor
PGE2	Prostaglandin E2, dinoprostone
PMMA	Poly-methylmethacrylate
PPARG	Peroxisome proliferator-activated receptor gamma
PS- <i>b</i> -P2VP	Poly(styrene- <i>block</i> -poly-2-vinylpyridine)
PTHrP	Parathyroid hormone related protein
PU.1	A transcription factor
QPCR	Quantitative polymerase chain reaction
Ra	Roughness average in microns
RANKL	Receptor activator of the nuclear factor kappa-B ligand
RMS	Surface roughness
RQ	Relative quantification
RT	Reverse transcription
rtPCR	Real time (or gel) polymerase chain reaction
RUNX2	Runt related transcription factor 2 or Cbfa1
SBF	Simulated body fluid
s.d.	Standard deviation
SEM	Scanning electron microscopy
SHH	Sonic hedgehog
SLA	A combination of acid etching and sand blasting
SOX9	From the SOX9 gene, marker of chondrocyte differentiation
SSC	Skeletal stem cell
STRO-1	A surface marker expressed by stromal cells
T-cell	A subset of lymphocytes
Taq	Thermostable DNA polymerase

TBE	Tris-boric acid ethylene diamine teta acetic acid buffer
TCP	Tri-calcium phosphate
TCF	A transcription factor in the Wnt pathway
TF	A transcription factor
TGF β	Transforming growth factor beta
THR	Total hip replacement
TNFSF11	Tumour necrosis factor ligand superfamily member 11
TRAP	Tartrate-resistant acid phosphatase
TRITC	Rhodamine phalloidin
TUBB3	Beta tubulin 3, marker for neural cells
TV	Trypsin-versene
Twist 1,2	Transcription factors
V	Versene
Wnts	From the wnt gene
18S	Responsible for ribosomal RNA, important random target in PCR

Chapter 1 General Introduction

1.1 Bone

1.1.1 Bone function and structure

Bone functions to provide skeletal support for body tissues and acts as a lever against which muscles can exert the forces that facilitate movement (Ramachandran, 2007). In the form of the ribs and skull, bone facilitates respiration and protects internal organs. It has a haematological role in the manufacture of blood components, which adds to its involvement in calcium homeostasis and metabolism (Ramachandran, 2007). Bone consists of osteoid (uncalcified matrix of type 1 collagen (COL1) and glycosaminoglycans), calcium apatite or hydroxyapatite (HA), and a heterogeneous population of cells (Khurana, 2009; Ramachandran, 2007). The organic portion of bone forms approximately 40 % of its dry weight and includes COL1, osteopontin (OPN), osteocalcin (OCN), osteonectin, bone sialoprotein (BSP), and alkaline phosphatase (ALPH) (Khurana, 2009; Ramachandran, 2007).

Three types of bone have been described, trabecular (cancellous or spongy) bone, compact (cortical) bone, and woven (immature) bone (Ramachandran, 2007). Trabecular bone (figure 1.1) is located between layers of compact bone. Bone marrow occupies the spaces between trabeculae giving this type of bone its metabolic primary function (Khurana, 2009). Cortical bone is dense in nature and undertakes a primarily mechanical role. Concentric rings forming tubular osteons or Haversian systems are aligned along lines of force and are approximately 50 μm in diameter (Ramachandran, 2007).

1.1.2 Bone marrow

Bone marrow consists of haemopoietic tissue (responsible for the formation of blood components) and stroma (Khurana, 2009). There are two types of human bone marrow, medulla ossium rubra (red marrow) and medulla ossium flava (yellow marrow) (Bain and Clark, 2001). Adult bone marrow is approximately 50 % red marrow and 50 % yellow marrow. Red marrow is primarily haematopoietic in nature and is located in the flat bones and cancellous regions of long bones. Stroma is found in small concentrations in red marrow and makes up the

majority of yellow marrow. The cellular constituent of yellow marrow is primarily adipocytic although fibroblasts, macrophages, osteoblasts, osteocytes, endothelial cells, endothelial stem cells, and mesenchymal (marrow stromal) stem cells are also present. Mesenchymal stem cells (MSCs) form the osteocytic (bone), adipocytic (fat), chondrocytic (cartilage) and fibroblastic (fibrous) lineages (Bonfield and Caplan, 2010; Oreffo et al., 2005).

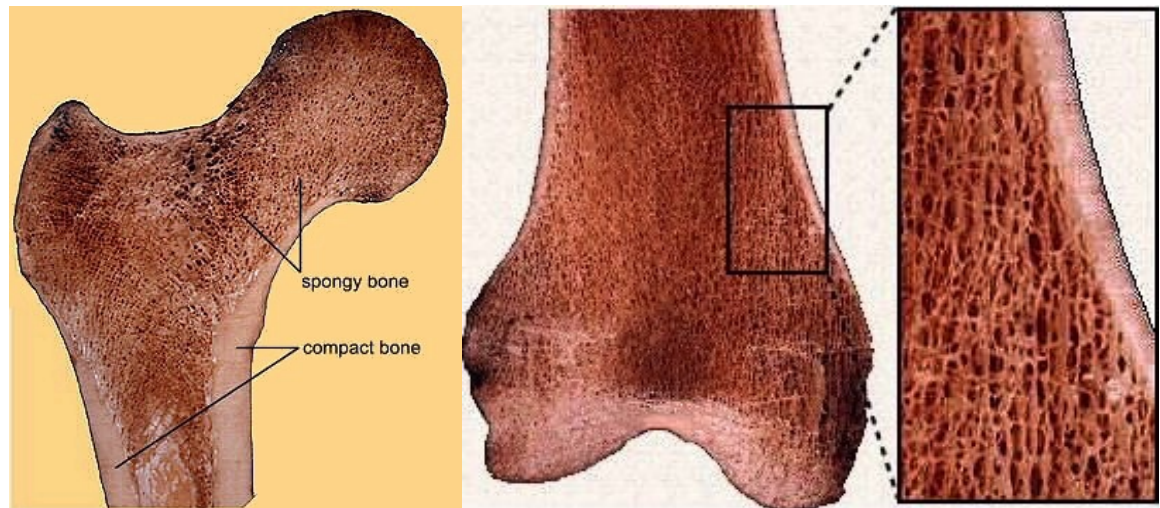


Figure 1.1 A proximal and distal femur in cross-section (Adapted from functional anatomy and biomechanics (Shaw-Dunn J)). The cancellous (spongy) nature of the proximal and distal femur can be seen. Thinning of the cortical (compact) bone from the shaft to the metaphysis of both regions is evident.

1.1.3 Bone cells

Osteoblasts are responsible for the production and mineralization of matrix (osteoid) (Khurana, 2009). Cuboidal during rapid osteogenesis, these cells become thin, flat and elongated on the surface of slowly forming mature bone. Cytoplasmic processes extend toward adjacent osteoblasts and into bone canaliculi where they join the processes of osteocytes. Histological studies in the orthopaedic literature describe osteoblasts as 20-30 μm in diameter and arranged closely in a dense single layer covering the surface of forming bone, except in areas of active bone formation in which there may be several layers of cells (Wheless, 2013). This layer may be seen to thicken during periods of active bone formation. Osteoprogenitor cells develop from MSCs and form the precursors of osteoblasts.

Osteoclasts are the large multinucleated cells responsible for bone resorption (Khurana, 2009). They form through the combination of a number of precursors from the monocytic (macrophage) cell line and are significantly larger than osteoblasts and just a little smaller than the 100+µm long lacunae for which they are thought to be responsible (Wheeless, 2013). Osteocytes form secondary to the encasing of osteoblasts in bone. Previously described as dormant it appears that osteocytes can synthesise collagen, control mineralization within their lacunae and may assist bone resorption (Wheeless, 2013).

1.2 The use of bone graft

The expansion of orthopaedics as a specialty has brought with it an increasing number of challenges. Bone loss is associated with trauma, fracture non-union, tumours, infection, implant loosening and arthroplasty loosening. Bone grafting and the use of bone graft substitutes is now commonplace, and in many cases preferable to the alternatives of endoprosthetic replacement, bone transport, distraction osteogenesis, and in more extreme cases limb amputation.

Over one million fractures occur annually within the United Kingdom (UK), of which between 5 % and 10 % are considered to have problems with bone healing (Johansen et al., 1997). Large areas of bone loss due to trauma exceed the body's regenerative capabilities. Delayed healing or non-union occurs in 5 % of all fractures, and 20 % of high impact fractures (Dickson et al., 2007).

Secondary bone healing is the method by which the majority, but not all, fractures unite. In order to achieve union fracture stability is a requirement, but in addition to this a potent osteogenic population of undifferentiated multipotent MSCs and committed osteoprogenitor cells, an osteoinductive stimulus and an osteoconductive matrix scaffold are also vital (Giannoudis et al., 2007). Six months is not an unusual time frame for union to occur, and up to two years a possibility, however achieving union of a previously un-united fracture is a time consuming and costly process.

Since the first bone graft in Glasgow in 1880, the number performed annually has continued to grow, each year an estimated 300,000-600,000 patients require one, in the United States alone (Rea et al., 2004). A dearth of bone graft material remains an ongoing problem.

Atrophic non-unions are primarily caused by defective biology and cancellous bone grafting should be undertaken. Hypertrophic non-union results from fracture instability or premature weight-bearing is primarily managed through alteration of the biomechanics, treatment by cancellous bone grafting is optional (Wheless, 2013).

Prosthetic implants, such as total hip replacements (THR), have an adverse effect on the quality of the surrounding bone; stress shielding and aseptic loosening are associated with a loss of bone stock. 25-year revision rates of primary cemented Charnley femoral components were shown, by the Mayo Clinic, to be 18 % for patients <40 years old, and 100 % for those over 80 years of age (Charnley, 1970). A Norwegian study revealed that 26 % of 4762 revision THR failed within 10 years (Berry et al., 2002). It is common practice for bone grafting, with either cancellous bone chips or femoral and tibial strut grafts, to accompany a change in implants during hip revision surgery. Impaction grafting using fresh-frozen morsellised allograft, for the management of acetabular bone stock loss in revision THR is effective as shown by long-term studies. It carries with it problems of cost, supply and potential infection (Gaston and Simpson, 2007; Giannoudis et al., 2007; Jager et al., 2007; Nishida and Shimamura, 2008; Stevens and George, 2005).

Limb reconstruction and salvage procedures are increasingly undertaken within the field of bone tumour surgery. Over the past 30 years improvements in imaging, chemotherapy, surgical technique and biomechanical engineering have made this change possible. Amputation is no longer the mainstay of surgical treatment with limb salvage being the patients' preferred option. Combinations of bone graft and bone transportation operations may fill the often large

skeletal defects, forming a living alternative to endoprostheses or amputation (Myers et al., 2007). Massive bone allografts, used for the reconstruction of limbs following bone resection for tumour, are plagued by a 19 % incidence of fracture, 14 % rate of non-union and 10 % chance of infection (Mankin et al., 1992).

1.2.1 Bone graft and bone graft substitutes

Across the world, 4 million operations involving bone graft or bone graft substitutes are performed each year (Reid, 1968). The demand for bone graft in the surgical market is clear; currently the demand is met through the use of autograft, allograft and bone graft substitutes, all of which are associated with their own specific list of limitations. The optimal bone graft would be safe and possess osteoinductive factors to recruit the recipient's MSCs and subsequently induce or modulate bone formation. Osteogenic cells, with the potential to differentiate into osteoblasts, would be present in an osteoconductive matrix, with sufficient structural integrity to provide the mechanical support necessary for fusion to occur.

Osteoconduction occurs when a bone graft material acts as a scaffold onto and into which native osteoblasts can spread and generate new bone. Osteoinduction involves the stimulation of osteoprogenitors to differentiate into osteoblasts and begin new bone formation, an example of osteoinductive cell mediators are bone morphogenic proteins (BMPs). Osteogenesis is new bone growth and an osteogenic indicates the presence of osteoblasts.

Autograft (cancellous and/or cortical bone) harvested from within the recipient remains the 'gold standard' bone graft for the replacement of diseased, absent or excised bone (Khan et al., 2012). It forms the only clinically available material that is osteogenic, osteoinductive, and osteoconductive whilst avoiding the risks inherent in transplanting viable cells or tissues from other individuals (Pountos et al., 2006). The major disadvantage of autograft remains the paucity of its available volume (Khan et al., 2012). Collected from cadavers or living

donors, bone graft is available from tissue banks in the form of massive allografts, demineralised bone matrix, processed bone chips and cortical struts. Allograft is obtained from bone graft donors and is similar to autograft in its human origin, but differs in terms of its processing. In Scotland the source of most allogenic bone is the femoral heads obtained from living donors at the time of hip replacement for osteoarthritis (Holt et al., 2004).

Retaining its mechanical properties, fresh-frozen donor bone that has not undergone the formal sterilization process is the most frequently used form of allograft despite the transmission of viral infections to some recipients (Emms et al., 2009). The transfer of highly resistant infective agents, including certain viruses and prions, remains a concern. Although the rate is low, unprocessed allogenic bone is associated with a risk of both disease transmission (e.g. Creutzfeldt-jakob disease) and immune reactions (Boyce et al., 1999; Dick and Strauch, 1994). The cellular component of bone graft may be sacrificed in order to minimize these risks. The remaining osteoconductive mineral scaffold assists bone healing but lacks the osteogenic properties of autograft. Demineralised bone matrix contains collagen, BMPs, proteoglycans and glycoproteins, and is the only form of allograft that is osteoinductive (Delloye et al., 2007).

Synthetic bone substitutes are predominantly void fillers providing reconstructive surgeons with off-the-shelf osteoconductive alternatives to autograft and allograft. An increased potential for success in the management of bone defects is seen when bone substitutes are used in combination with osteoinductive agents, or when bone substitutes are rendered osteogenic through the addition of autograft or bone marrow aspirate. Calcium sulphate (CaSO_4) pellets have combined successfully with autograft in the performance of instrumented short segment posterolateral spinal fusions for degenerate spines (Chen et al., 2005).

Distraction osteogenesis techniques produce significant quantities of new bone *in vivo* but are currently limited to the lengthening of ‘long bones’. Circular frames and intramedullary devices facilitate the distraction and stabilization necessary for new bone formation to occur following an osteotomy (or bone division). In addition to limits in its application (limited to diaphyseal lengthening) one disadvantage of this method of bone growth is the duration of treatment, a 6 cm length of new bone takes a minimum of 180 days (Miller, 2008).

1.3 Tissue Engineering

Tissue engineering aims to augment, replace, or restore the complexity of human tissue function through the combination of synthetic and living components under optimised environmental conditions (Langer and Vacanti, 1993). It is envisaged that, with time and an appropriate amount of scientific interest, tissue engineering will facilitate the development of *in vitro* expanded autologous bone graft in order to overcome the pressing clinical need. Autologous chondrocyte implantation (ACI) is already undergoing multicentre clinical trials using a very similar process for generating cartilage to that which we propose for bone (Hench and Polak, 2002).

In recent years tissue engineering has focused on the importance of stem cells as a potential autologous cell source. The *in vitro* production of osteogenic bone graft requires a population of osteoblast cells that can be derived from osteogenic progenitor cells, mesenchymal, skeletal (or even embryonic) stem cells.

1.3.1 Stem Cells

The invention of the microscope in the 1800s facilitated both an increase in the understanding of human cells and the discovery in the early 1900s that red blood cells, white blood cells and platelets originated from a single ‘stem’. Transplantation of human stem cells began in the 1950s as a management for

depleted functional bone marrow caused by haematological and oncological conditions, and in 1963 Ernest McCulloch and James Till quantitatively described the self-renewing properties of murine bone marrow cells (Till and McCulloch, 1963).

Stem cells can differentiate into multiple lineages; for example, MSCs form the mesenchymal lineages (predominantly osteogenic, adipogenic, chondrogenic and fibroblastic) (Bonfield and Tanner, 2002) (figure 1.2), whilst embryonic stem cells form all of the tissues found in a developing embryo (endoderm, mesoderm and ectoderm). Composite grafts, formed from the combination of two or more materials, are being used to harness stem cell multipotency (Brady et al., 2010).

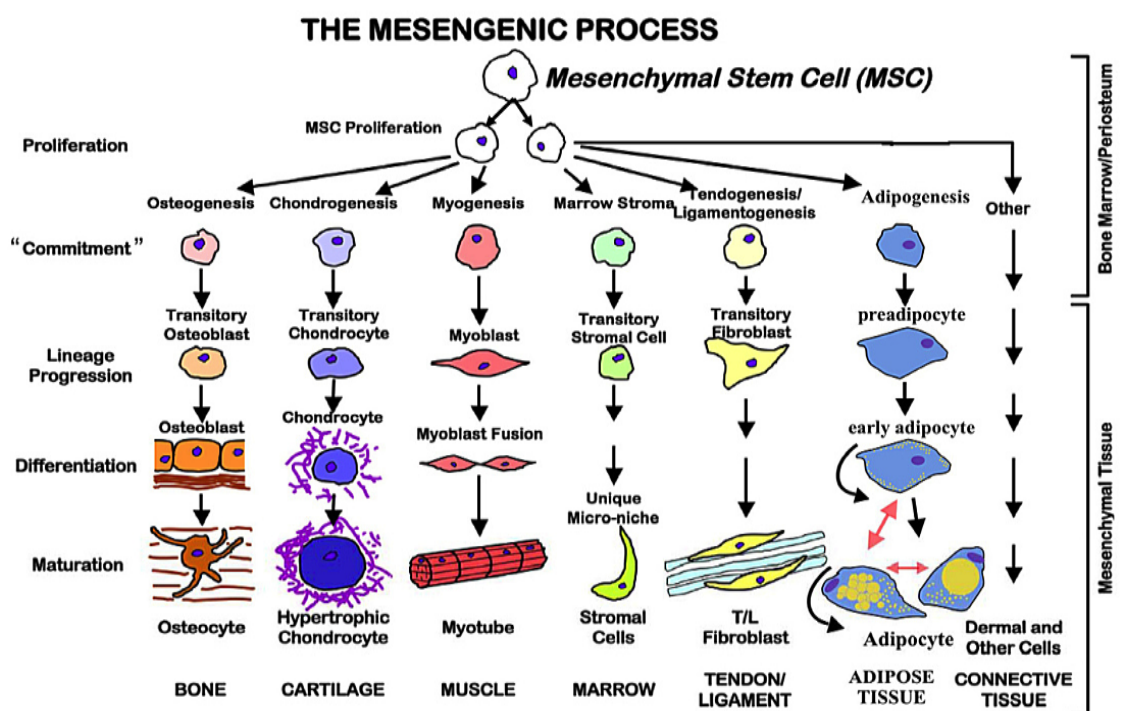


Figure 1.2 MSC differentiation (taken from Bonfield and Caplan (Bonfield and Caplan, 2010)). Post-proliferative commitment of MSCs to the lineages of bone, cartilage, muscle, marrow, tendons, adipose and other tissues precedes cell differentiation and maturation in the development of mesenchymal tissues.

Stem cells ‘self renew’ maintaining their own number through time. Debate continues with respect to the pattern of stem cell turnover (Lopez-Garcia et al., 2010). In asymmetric division one of the two daughter cells of a dividing stem cell remains a stem cell, while the other forms a committed progenitor (Robey and Bianco, 2006), during symmetrical stem cell division two daughter stem cells are produced. In tissues in which cell division of mature cells is slow or in which the division of differentiated cells does not occur, the promotion of symmetrical stem cell division is necessary for population expansion.

Potentially the most interesting property of stem cells is their potential to completely reform a tissue when transplanted. In 2008 groundbreaking research into the use of stem cells was published in the *Lancet* by Macchiarini *et al.* A decellularised trachea (a cell depleted donor airway) colonized with epithelial and MSC-derived chondrocytes was successfully transplanted into a 30 y old suffering from the after effects of tuberculosis. The result was an improvement in her lung function and a resumed ability to climb stairs. The combination of cell depletion and coating with autologous, stem cells gave the benefits of a functional airway with the avoidance both rejection and the use of immunosuppressant drugs (Macchiarini et al., 2008).

1.3.2 Human bone marrow cells (HBMCs), MSC and skeletal stem cells (SSC)

The harvest of stem cells and human bone marrow has become more widespread. Human bone marrow provides a source of MSC (as more MSC niches have become known many now refer to the cells by origin e.g. SSCs referring to MSCs from bone marrow) that can be extracted using a combination of diffusion gradients and sub-grouped through antibody selection. Despite nearly four decades of research specific cell-surface markers that can uniquely identify and select for the MSC/SSC phenotypes remain elusive (Tare RS, 2009). Alternatives include the selective harvesting of heterogeneous populations of stem cell enriched skeletal progenitor cells using the stromal cell monoclonal antibody (STRO-1) (Gronthos et al., 1994; Simmons and Torok-Storb, 1991), and the identification and acquisition of bone and stroma regenerating progenitors using

the melanoma-associated cell adhesion molecule (MCAM/CD146) (Sacchetti et al., 2007). MCAM selected progenitors can establish a haematopoietic microenvironment *in vivo* in addition to the formation of bone.

MSCs are being harvested from arthroplasty patients at the time of joint replacement surgery. These cells display much of the phenotypic character of the cell population encountered by orthopaedic devices and substrates on implantation. Research into these cells is therefore fundamental to understanding the properties of bone and its interactions with biomaterials at micrometric and nanometric levels. The proliferative capacity and cellular spectrum of stem cells harvested from bone marrow affect their usefulness as a source of autogenic cells. Importantly these factors are independent of age and osteoarthritis (Scharstuhl et al., 2007). Isolated and culture expanded MSCs, from donors cleared of any identifiable infective load, may be useful in the future as a source of osteogenicity for implantation with cell deplete osteoconductive scaffolds. Prior to differentiation MSCs have been regarded as non-immunogenic (Chamberlain et al., 2007) and potentially transplantable into allogenic recipients without the use of immunosuppressants. Allogenic MSCs would have the benefit of availability to a recipient at the time of diagnosis, without the lag that would result from culture expansion of their own MSCs.

Cell culture media is supplemented with serum, commonly obtained as fetal calf serum (FCS) although an alternative source is autologous platelet lysate. Some have concerns regarding the use of animal-derived media supplements for culture purposes. A potentially damaging mixed lymphocyte reaction modulated through an induction of T-cell proliferation (MacDermott and Bragdon, 1983) has been associated with long-term expansion of MSCs in FCS. This phenomenon can be prevented through the use of autologous human platelet lysate as an alternative media supplement (Centeno et al., 2010).

1.3.3 Clinical applications of chondrocytes and bone marrow stem cells

ACI was first introduced in Sweden in 1987, and initially described as the harvesting of cartilage slices from minor load-bearing areas of a joint, chondrocyte extraction, and culture within media supplemented with autologous serum. *Ex vivo* expansion for a period of 3-4 weeks or more was undertaken prior to open implantation under an autologous periosteal flap taken from the proximal tibia (Brittberg et al., 1994): (Hench and Polak, 2002). ACI has undergone a number of modifications: in some cases porcine membranes are used, and in others chondrocytes are cultured within a collagen matrix. The technique known as matrix-induced ACI (MACI) requires a reduced surgical access for implantation.

SSCs have been isolated, culture expanded and used in the form of injectable scaffolds or loaded into solid scaffolds. Some of their orthopaedic applications are illustrated in figure 1.3. Fresh and culture expanded SSC have also been used for the regeneration of cartilage within knee joints. SSCs obtained using a cell separator have been mixed with both a protein matrix and a collagen/HA scaffold. The cell containing matrix was transplanted into prepared osteochondral defects using minimally invasive arthroscopic techniques involving the use of a small camera (arthroscope) (Assor, 2010). Wakitani et al culture-expanded the autologous bone marrow derived stem cells (BMSCs) prior to placement on collagen sheets, gelation and transplantation into full thickness defects (Wakitani et al., 2007). Figure 1.3 illustrates the uses of SSCs in primary fracture fixation, the management of fracture non-unions and the treatment of osteochondral defects of the knee (Pountos et al., 2006).

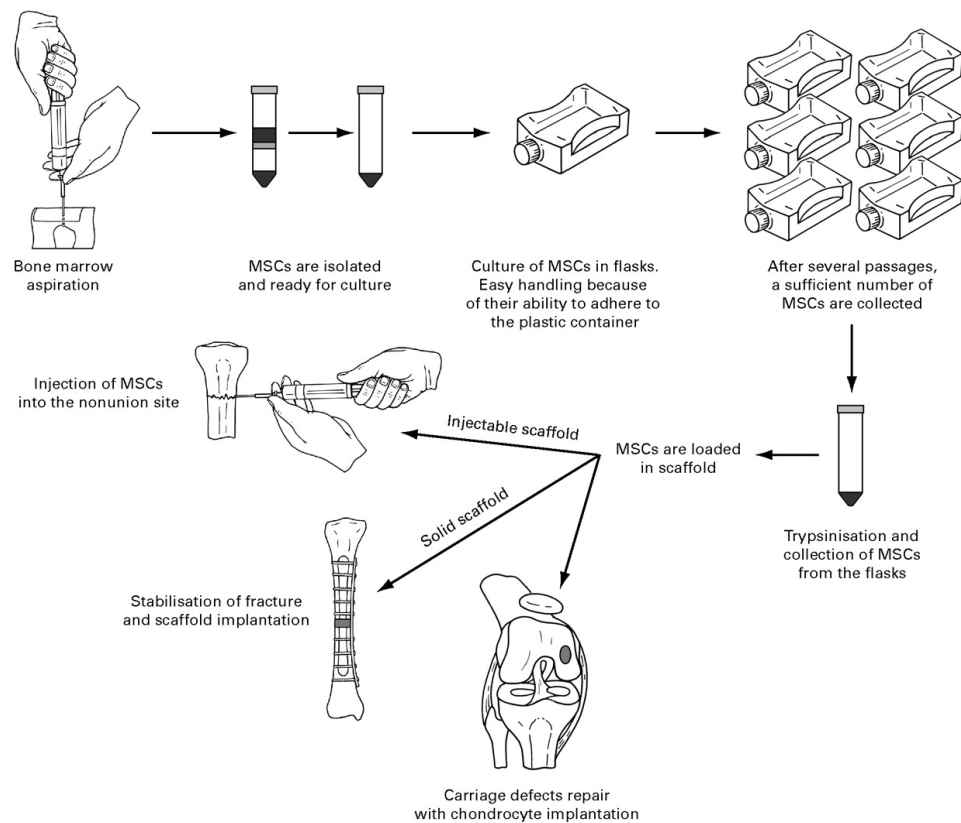


Figure 1.3 The harvest, expansion and orthopaedic uses of MSCs (taken from (Pountos et al., 2006). Bone marrow derived MSCs are culture expanded producing sufficient numbers to aid union of fresh and previously un-united fractures as well as aid repair of cartilage defects.

Patients (with a degenerative condition of the knee of moderate severity (gonarthrosis II-III)) are being recruited for a feasibility and safety study in which BMSCs are isolated and culture expanded for the treatment of arthritis. Twenty-one days later, a single intra-articular injection of approximately 40 million autologously derived SSCs is undertaken. The theory is that the injected SSCs will have a sufficiently regenerative effect on articular cartilage, that it will be evident on magnetic resonance imaging (MRI) (Coll R, 2010). Animal and human trials are also investigating the efficacy of preloading implants with SSCs for use in spinal fusion and fixation of non-unions.

1.4 Osteoblast differentiation

During early development bone is formed by osteoblast differentiation (figure 1.4) from MSCs, directly in the form of membranous bone formation and indirectly through MSC condensation into a cartilage template, endochondral bone formation (Lian et al., 2006).

Mesenchymal stem cells

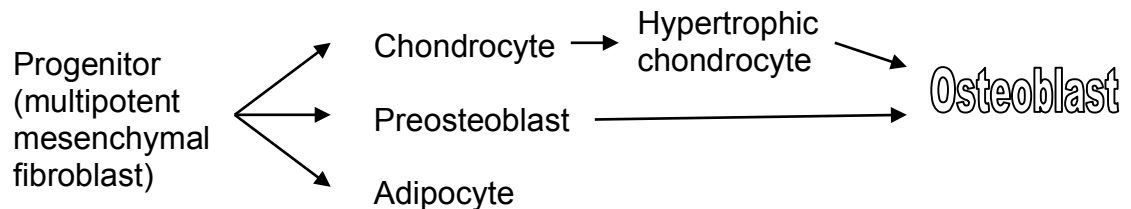


Figure 1.4 MSC differentiation into osteoblasts

MSC differentiation into osteoblasts involves the commitment of MSCs into the osteogenic lineage with the production of progenitors, pre-osteoblasts, chondrocytes and subsequently osteoblasts.

1.4.1 Control of osteogenic differentiation

As they proliferate and differentiate from MSCs, marrow precursors, chondrocytes, osteoblasts and osteoclasts express various proteins including growth factors (GFs), transcription factors (TFs) and extracellular matrix (ECM) proteins (figure 1.5). Based upon its location along the differentiation pathway each GF, TF or ECM protein has a distinct pattern of expression.

1.4.2 Osteoblast differentiation and gene expression

Involved in osteogenesis, cell growth and differentiation BMPs, are multifunctional members of the transforming growth factor beta (TGF β) superfamily of ligands. Acting through runt related transcription factor 2 (RUNX2 - also known as core binding factor alpha 1 (cbfa1)) they are involved in the regulation of the sequential stages of osteoblastic phenotype development, promoting cell phenotype commitment and osteogenesis (Lian et al., 2006). The path from multipotent stem cell to osteoblast is controlled by two key TFs, RUNX2 and osterix (OSX) (Ducy and Karsenty, 2000).

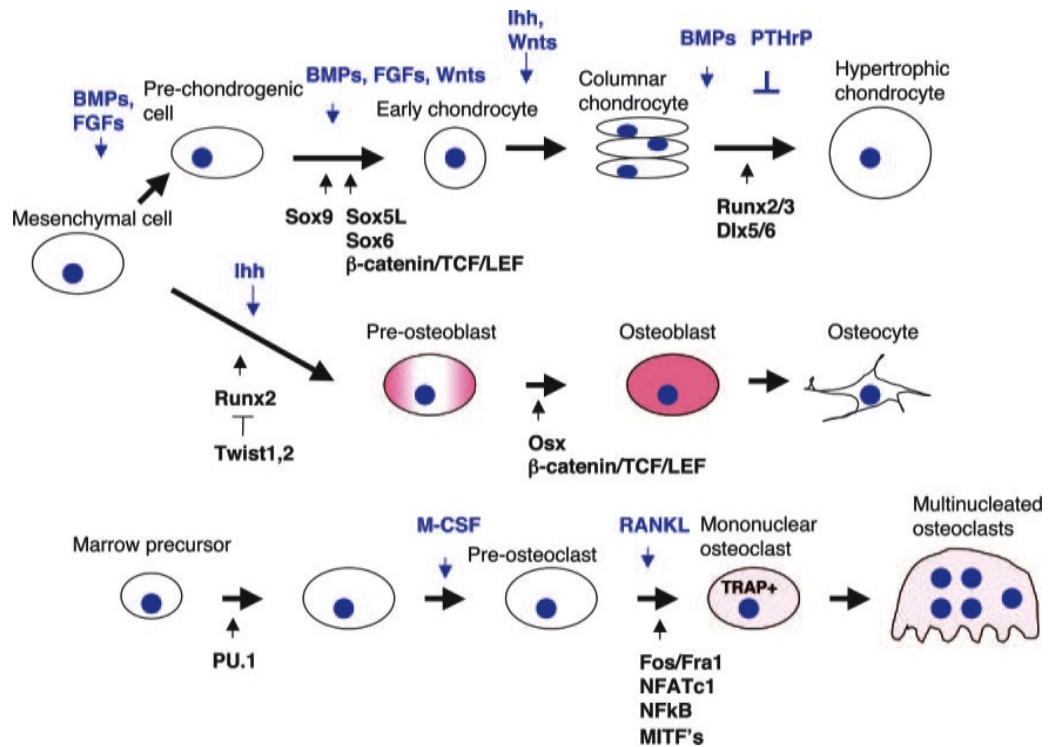


Figure 1.5 The osteogenic differentiation pathway (from (Kobayashi and Kronenberg, 2005)) The major differentiation steps from MSC to hypertrophic chondrocyte, osteocyte and multinucleated osteoclast are associated with growth and transcription factors. In contrast to osteoblasts and osteocytes, osteoclasts (responsible for bone resorption) are derived from the monocyte/macrophage haematopoietic lineage. Abbreviations are shown on pages 13-17.

BMPs act early in embryogenesis to up-regulate many homeodomain (HD) proteins. HD proteins directly regulate many of the key matrix proteins including collagen, OPN, alkaline phosphate (ALP), OCN, and the TFs RUNX2 and OSX (Lian et al., 2006). Binding of BMP to the type II receptor causes recruitment of the BMP 1 receptor, initiating the BMP pathway and its role in transcriptional regulation. BMPs are used clinically as osteoinductive agents. Atrophic non-unions in which defective biology is thought to have been responsible and spinal fusion surgery are two of the surgical indications. Associations between their usage and adverse effects have now been documented (Woo, 2012a, b).

RUNX2 is expressed at early stages of the MSC line, prior to bone formation, and has been described as the ‘principal osteogenic master gene for bone formation’ (Lian et al., 2006). RUNX2 is essential for osteoblastic differentiation and skeletal morphogenesis, and is involved in the differentiation from pluripotent MSCs to osteochondroprogenitors, and from osteochondroprogenitors to osteoblasts. RUNX2 may be involved in cells exiting the cell cycle, and in the change from proliferation to differentiation (Lian et al., 2006). RUNX2 is also the major TF for chondrocyte development (Kobayashi and Kronenberg, 2005). RUNX2 whilst appearing to be down regulated in the progression of cells down the chondrogenic lineage is increasingly expressed at the change from columnar to hypertrophic chondrocytes, and in the progression towards endochondral ossification (Lian et al., 2006).

OPN, a protein with a high affinity for calcium (Sodek et al., 2000), is synthesized by a number of cell types (primarily within the mesenchymal cell line) including pre-osteoblasts, osteoblasts, osteoclasts, fibroblasts, dendritic cells, chondrocytes, myoblasts, and endothelial cells. RUNX2 and OSX are among a number of TFs required for the expression of OPN. Binding of RUNX2 and OSX to promoters of osteoblastic specific genes COL1 alpha 1 and OPN results in their up-regulation.

OCN is a bone specific marker for mature osteoblasts and contributes to the regulation of bone mineralization. Osteonectin (a glycoprotein secreted by osteoblasts) is involved in cell-matrix interactions, collagen binding and bone mineralization. It is involved in the mineralization stage promoting the formation of mineral nodules.

1.4.3 Phases of *in vitro* osteoblastic development (adapted from (Lian and Stein, 1995; Stein and Lian, 1993))

Three phases of osteoblastic development have been identified: the growth phase; ECM development, maturation and organization; and ECM mineralization.

When placed in culture bone-related genes are down regulated and the cells enter a proliferation phase. The initial period of cell proliferation and ECM deposition takes the first 10-12 days. This phase proceeds into a phase of ECM development, maturation, and organisation (days 12-18). ECM mineralization forms the final phase, from day 18 onwards.

This first 10-12 days shows the enhanced mitotic activity associated with cell proliferation. The genes expressed primarily are those associated with ECM formation such as COL1, fibronectin and TGF β . Towards the end of this phase these genes are down-regulated, although COL1 remains at a basal level throughout. OPN expression is active in this proliferative phase. The genes responsible for ECM production and deposition must be expressed for differentiation to progress.

Days 12-18 are associated with a reduction in the expression of the proliferative proteins, and a greater than ten fold increase in the expression of ALPH, although this is not picked up histochemically until the third phase. A decrease in cell proliferation is associated with the increasing osteoblast differentiation that inhibits BMP2, 3, and 4 expression. OCN expression is post-proliferative.

Initially ALPH levels continue to rise, although they reduce again when the ECM becomes heavily mineralized. The expression of other bone related genes (BSP, OPN, and OCN) increases in parallel with increasing mineralization. OCN expression correlates with mineralization, restarting at the onset of mineralization and peaking at days 16-20. OCN expressing cells are only found within mineralizing nodules.

The time taken for these three phases to occur can be manipulated to an extent. Culture on a COL1 film accelerates progression towards the osteoblastic phenotype, has an inductive effect on osteoblast differentiation and enhances

ALPH and OCN expression. High levels of collagen synthesis and ECM accumulation are associated with a cessation of cell proliferation at a lower than normal cell density.

Dexamethasone in media accelerates differentiation and increases expression of post-proliferative genes and relatively early mineralised nodule formation. Dexamethasone may deplete the pool of proliferating undifferentiated cells by pushing cells to a terminal degree of differentiation beyond the natural rate.

Culture of MG-63 (human osteosarcoma cell line) on cell matrix and purified COL1, results in morphological changes inducing the formation of long extracellular processes. In addition osteonectin levels increase up to 2.5 fold immediately after cell seeding, and ALPH increases up to 2.5 fold. These transient changes were maximal on days 6-8 after cell seeding, and reduced as cell confluence was achieved (Andrianarivo et al., 1992). The transient nature of the increases would be reflected in transient increases in mRNA levels. When considering qPCR results multiple time points or comparison with the levels of proteins expressed is therefore important.

1.5 Biomaterials

1.5.1 Development of biomaterials

Tissue engineering requires the development of materials that will precisely control cellular morphology and the functions of adhesion, proliferation, differentiation and gene expression (Curtis and Wilkinson, 2001; Du et al., 1999).

The first generation of biomaterials was inert in nature, developed to perform a supportive role with minimal toxic effects. As such they produced neither beneficial nor detrimental effects in the surrounding tissues. The second-generation of biomaterials was designed to be either resorbable or bioactive. The third-generation of biomaterials was designed to stimulate specific, reproducible, cellular responses at the molecular level (Hench and Polak, 2002).

My aim in this thesis is to develop a third generation biomaterial combining bioactivity with bioabsorbability in order to aid bone regeneration.

First generation biomaterials can be rendered second generation through a change in the material topography (configuration or shape), chemistry (by alteration of the material used or adhesion of substances to the surface), or by chemically augmenting topographically modified surfaces. In a smooth form metals (such as titanium), ceramics and plastics used in the manufacture of orthopaedic implants can be described as first generation biomaterials, tending to be bioinert in nature. Clinical experience has shown that a fibrous capsule forms around an implant in the presence of a smooth surface, whereas bone forms more readily on rough surfaces. The uncemented implantation of smooth surfaced first generation biomaterials was associated with implant loosening in the absence of active stimulation of osteogenesis.

In 1911 contact guidance was noted by R.G. Harrison (Harrison, 1911) and in 1964 the reaction of cells to the topography of their environment was popularized (Curtis and Varde, 1964). Clinical findings support laboratory findings in which *in vitro* osteoblast-like cells attach more readily and differentiate faster, with enhanced HA formation, on rough surfaces (Blumenthal N, 1989). A region of roughness, porosity or chemical (for example HA) coating adds bioactivity to inert implants and hence renders them second generation. This thesis will focus on defined topography as a move to third generation biomaterials (as defined surfaces will provide reproducible response), but it is acknowledged that much prior work has focused on simple roughening.

1.5.2 Osseointegration and osteoinduction

The processes of osseointegration and osteoinduction represent the positive tissue responses to material chemistry and topography sought in the fields of orthopaedics and tissue engineering.

A large proportion of the work relating to the interaction between mesenchymal and osteogenic cells and substrates has been undertaken in the field of implant (joint replacement) manufacture. Differing opinions dominate this subspecialty. Debates regarding cemented versus uncemented fixation, and optimal bearing surface continue among hip and knee arthroplasty surgeons, as well as debate about the surface modifications chosen by users of the uncemented implant group. The primary aim of uncemented prostheses is the elimination of the osteolysis associated with the wear and loosening of cemented arthroplasty components.

Osseointegration refers to a direct structural and functional connection between an implant and living bone, and is associated with an absence of intervening soft tissue. Representing a combination of bone apposition to the implant with functional fixation (Petrie T, 2008) osseointegration is a prerequisite for the success of uncemented orthopaedic implants. This requires a surface to which osteoblasts and supporting connective tissue can attach, or pores into which these cells and tissues can migrate. Osseointegration can be verified microscopically or radiologically by the presence of spot welds of new endosteal bone contacting a porous surface or by the absence of reactive lines around an implant (Engh and Bobyn, 1988).

Osseointegration can be achieved through the modification of surface topography, chemistry or both. Topography is traditionally altered for implants by sintering (coalescing heated solid particles onto the surface of implants), sandblasting, etching (using acid (Amrich and Burghouwt, 2010; Cho and Park, 2003; Engh and Bobyn, 1988), laser, or plasma), or machining. Chemistry is commonly altered through the addition of HA, tricalcium phosphate (TCP) or a composite HA/TCP to a material or its surface.

Bioactive materials, such as HA coated implants, are generally considered to be osteoconductive, producing a physico-chemical bond between the bone and the coating that ankyloses it to bone. Osteoblastic cells need to be able to adhere

and proliferate, osteoblastic precursors, such as SSCs, need to differentiate osteogenically, and terminally differentiated mature osteoblasts need to adhere, secrete and initiate mineralization of bone matrix. Sceptics of the use of chemistry in order to add bioactivity express concerns primarily relating to the stability of the chemical-implant interface, and the potential ease of its disruption.

1.5.3 Topography

Every surface has an inherent topography that is dependent on its mode of manufacture and the material used. The topography of even the flattest of materials is referred to according to its average roughness (Ra). It is worth pointing out that Ra is a term to consider carefully as two surfaces can have similar Ras but look very different and this is a big problem in comparing response of random topographies. Topography may be randomly produced or more carefully controlled. Topographies may be applied to a surface for example sintered, embossed onto it, or cut into it (sandblasting, etching, or machining).

Corundumization or blasting with Corundum (Aluminium oxide, the second hardest mineral) produces a roughened surface, in the case of the VerSys hip system 24-grit (1035 μm) (Zimmer, 2010). A corundumized surface finish can be created throughout an implant surface or in combination with a porous option developed using a fibre mesh circumferentially wrapped around the proximal femoral stem (Anatomic Fibre Metal Plus Stem and VerSys Fibre Metal Taper Hip Prosthesis, Zimmer (figure 1.6)). An alternative porous option uses sintered beads (VerSys Beaded Fullcoat Plus, Zimmer).

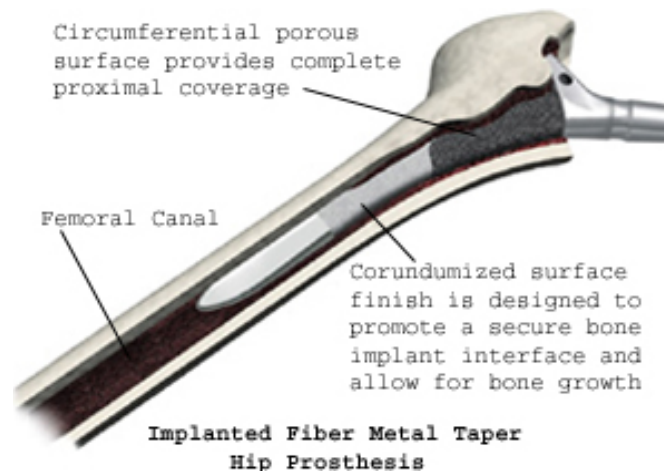


Figure 1.6 Corundumized and fibre metal surface modification of hip prostheses (obtained from Zimmer (Zimmer, 2010)). The femoral stem is shown within a sectioned proximal femur. The smooth distal stem has been corundumized in the mid portion of the implant and is accompanied by a circumferential fibre metal porous surface at the intertrochanteric region.

Well-designed topographical features can be retained over time although concave topographies are more resistant to abrasive wear than convex alternatives. Despite long-term clinical studies that show good to excellent implant longevity, beads from sintered bead surfaced implants cause third body wear should they debond. The design basis of certain implants has been developed to mimic the trabecular structure of bone and includes a porous trabecular surface incorporated on the surface of a solid titanium (Ti) implant (Delta TT, Lima Corporate (Corporate, 2013)). High trabecular strength within the porous component aims to reduce the likelihood of topography loss, and particulate debris formation.

The cemented vs uncemented debate with respect to total hip arthroplasty continues. The perceived advantages of uncemented topographically or chemically enhanced implants in part relate to the effects of polyethylene wear. Wear debris (e.g. from polymeric components) inhibits the osteoblast functions associated with bone formation, and induces secretion of factors capable of influencing nearby osteoclasts and macrophages. Osteoblasts may themselves

play a role in the events leading to granuloma formation, osteolysis, and implant failure (Dean et al., 1999). It is proposed that the osseointegration of the implant to bone prevents the osteolytic effects of polyethylene by sealing the proximal implant bone interface.

1.5.4 Chemistry

The surface chemistry of a biomaterial can be altered through a change in the material composition or through the addition of a soluble or insoluble surface chemistry to the material surface. These two options have both been used in orthopaedics. A disadvantage of soluble mediators is that following detachment they may be transported away from the site of implantation, which carries an inherent risk of undesirable effects systemically.

Different chemical factors have been added to implant surfaces. Osteogenic biomolecules, such as BMP2 (Kashiwagi et al., 2009) and fibroblast growth factor (FGF) (Park et al., 2006) covalently bonded to Ti may be gradually degraded or lost as a consequence of the tissue environment. HA coating of smooth acetabular implants has failed with retrieval analysis showing cell-mediated HA resorption. Conversely, HA is commonly applied to the surfaces of femoral stems with enhanced osseointegration.

It should be remembered that the environment into which an implant has been implanted can change from the normal tissue environment and for which it was designed into a tissue environment developing in response to the presence of the implant. For example in the case of an uncemented acetabular cup, polyethylene wear at screw hole insertion points in the outer shell of the cup (the notch effect) leads to an associated reduction in oxygen content of the body fluid creating a localized acidosis resulting in corrosion of the biomaterial (Antoniac et al., 2003).

An interesting example of use of HA chemistry is HAPEX, a composite of HA with polyethylene that mimics the HA collagen composite bone. Osteoblasts have been shown to grow over the surface of HAPEX attaching to the surface HA particles. *In vivo* testing revealed that a strong and stable interface had developed between the implant and surrounding bone. HAPEX has been used to treat orbit deficiencies; it had the advantage over blocks of HA in that it could be shaped during the procedure with standard tools. HAPEX middle ear implants have been shaped in the operating theatre and restored sound conduction in the recipients (Bonfield and Tanner, 2002). Work is ongoing into the use of HAPEX as the outer surface of a multicomponent inter-vertebral disc replacement, the mechanically sound HAPEX surface would provide the osseointegration to the vertebra above and below whilst the fiber reinforced hydrogel would provide functional benefit (Gloria et al., 2011).

1.5.5 Surface modification of orthopaedic implants: chemistry and or topography

Topography can have a more significant effect than chemical composition of a matrix (Dalby et al., 2000). Controlled topography can be used in isolation or in combination with a chemical composition designed to increase osseointegration.

In 1977 De-Puy introduced the anatomical medullary locking (AML) hip replacement (Engh, 2013). A porous coating of cobalt chrome alloy (CoCr) beads sintered to the proximal 1/3 of the implant facilitated dense cortical-cancellous bone ingrowth (Whiteside et al., 1993). In the 1980s they introduced a chemically modified alternative, the Corail, a fully HA coated non-porous stem manufactured in forged titanium alloy. The literature suggests that this stem design should be implanted with cancellous autograft impacted proximally (DePuy, 2013a).

De Puy combined the chemical and topographical approaches in the design of the Pinnacle acetabular cup system. An aluminium shell is combined with a porocoat of sintered Ti, a duofix porous coating with 30 µm depth of HA or a high friction porous option. The Gription high friction option combines macro

and micro topography in order to increase cell adhesion and cell proliferation. The pore size and porosity of the Ti increases incrementally from the implant to the bone interfaces (DePuy, 2013b).

At least five different surfaces including plasma spray coating, sintered beads, trabecular metal, fibre metal, HA/TCP coated fibre metal surfaces are used alone or in combination in the design of Zimmer hip prostheses (figure 1.7) (Zimmer, 2003b). Zimmer has developed a ceramic coating that can be applied to fibre mesh. The HA/TCP composite applied using plasma spray technology coats the mesh to a thickness of approximately 70 μm and has a biphasic resorption profile.

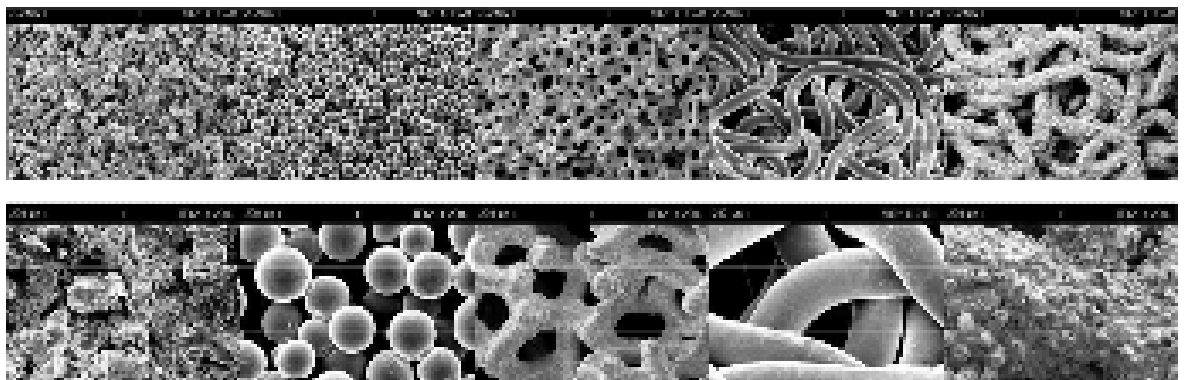


Figure 1.7 Topographical and chemical surfaces of uncemented hip implants adapted from <http://www.zimmer.com>. Images A-E are 50x F-J 200x magnification. Images A and E show a plasma spray coat, B and F sintered beads, C and G trabecular metal, D and H fibre metal, E and I HA/TCP coated fibre metal (Zimmer, 2003b).

The *Mayo hip* prosthesis reduces the quantity of bone excised from the proximal femur and incorporates three topographies, a polished Ti alloy taper, circumferential corundumisation of the stem and the inclusion of fibre metal pads (figure 1.8a) (Zimmer, 2006). Combination with chemical enhancement using a regionally applied Calcicoat* of a HA/TCP composite (figure 1.8B) is available (Zimmer, 1999).



Figure 1.8 The *Mayo Conservative* hip prosthesis adapted from <http://www.zimmer.com>. The stem taper has been highly polished, the stem has been corundumised proximally, and a fibre metal pad has been included to maximize osseointegration (Zimmer, 2006). A HA/TCP coating may also be used, images 'a' without enhanced chemistry and image 'b' with calcicoat

Bone implant integration is less than 25 % despite good bone to implant contact (figure 1.9). Appositional bone index (ABI) and ingrowth are becoming an increasingly common addition to survivorship in the publication of the results of uncemented prostheses. In 1991 Bloebaum et al described a 22 % ingrowth despite a 67 % ABI (the percentage of bone in direct contact with the porous surface) and in association with cancellous structured Ti (CSTi) and a 9 % ABI and 0 % ingrowth with CoCr beads surfaces on a tibial baseplate (Bloebaum et al., 1991). The same author published an 84 % ABI and 12 % ingrowth on an acetabular shell and a 73 % ABI and 6 % ingrowth on a tibial baseplate in 1997 (Bloebaum et al., 1997).

Bone Ingrowth / Biologic Fixation Comparison


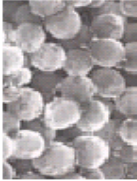
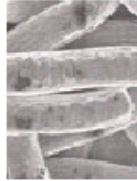

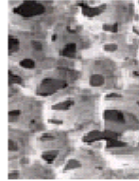
					
	CSTi	CoCr Beads	Ti Fiber Mesh	Plasma Spray	Trabecular Metal*
Manufacturer	Centerpulse	Howmedics Osteonics J&J Depuy	Zimmer	Biomet	Zimmer
Pore Size	400 - 600 μ m	variable	-	variable	300 μ m
Pore Volume	50 - 60%	35%	68%	variable	70%
Coating Material	Ti	CoCr	Ti	Ti	Ta
Retrieval Results					
% - Ingrowth Tibial Baseplates	6 - 22% ^{4,9}	6 - 9% ^{4,15}	9.5% ¹⁶	NA	NA
ABI Tibial Baseplates	73% ⁹	36% ¹⁵	27% ¹⁶	NA	NA
% - Ingrowth Acetabular Shells	12% ¹	0 - 10% ¹⁷	12% ¹⁸	NA	NA
ABI Acetabular Shells	84% ¹	NA	0-55% ¹⁸	NA	NA
Clinical Advantages and Features					
Optimal Pore Size	■				■
Optimal Pore Volume	■		■		■
Bone Ingrowth Coating	■	■	■		■
Micro-Surface Texture	■			■	■
Bimetal (Ti coating on CoCr)	■			■	
Interconnected Pores	■	■	■		■
Coating does not Disassociate	■				■*

Figure 1.9 A comparison of bone ingrowth and biological fixation of implants obtained from (Zimmer, 2003a). The bone ingrowth levels on these surfaces are disappointing (0-22 %) despite bone apposition up to 84 %.

1.6 Tissue responses to surface modification

1.6.1 Cellular responses to surface modification

Surface chemistry and topography regulate a diversity of cellular behaviour; including cell adhesion, spreading, proliferation, and differentiation (Hamilton and Brunette, 2007). Chemical, topographical and Young's modulus (material stiffness) changes (Dalby et al., 2007; Engler et al., 2006; Kilian et al., 2010; McBeath et al., 2004; Oh et al., 2009) have been shown to influence cell adhesion size, shape and number (Biggs et al., 2008), and change cytoskeletal arrangements (Dalby, 2009). Stem cells respond to chemical cues (Curran et al., 2006), stiffness in 2d and 3d culture (Wang et al., 2010) and topographical features (Dalby et al., 2007). Cells' interactions with islands of topography, and islands of chemistry may be produced by similar mechanisms (Dalby et al., 2002b).

Biomimetic materials are developed using inspiration from nature. Chemistry, stiffness and topography influence MSCs and this can be biomimetic. The material may be made of the same components such as laminin in extracellular matrix or HA in bone. By growing cells on materials of the desired stiffness cells can also be influenced towards the development of a desired tissue. Hydrogels with a low Young's modulus, similar to the muscular surfaces upon which they commonly lie, are used to culture neurons whereas materials with a high Young's modulus such as Ti in trabecular metal are used to culture bone. The biomimetic effects may also relate to the shape or topography of the material. Adding biomimetic levels of disorder (i.e. biological standard deviation) can further trigger an appropriate cell response (Dalby, 2009).

Nature does not exhibit the exact replication associated with current manufacturing techniques. A normal distribution variation is seen in virtually all measurements taken, for example macroscopically from height to weight and microscopically in terms of the exactitudes of fiber size and orientation in the extracellular matrix. In this work the ± 50 nm displacement of the nanopits aims to replicate this natural variation.

The influence of material topography at a scale below that of cell size has a greater effect on cell development than larger features (Rea et al., 2004). An understanding of the influence of micrometric topography is eased by an appreciation of the sizes of the cells and extracellular matrices. Osteoclasts and their associated resorption pits are approximately $40\text{ }\mu\text{m}$ in diameter. ECM components include individual fibril elements and fibril bundles in tendon tissue these range from 15 to $400\text{ }\mu\text{m}$ in diameter (Dalby et al., 2003). The topography of collagen fibres, with repeated 66 nanometer (nm) banding, and nanotopography from neighbouring cells both appear to effect cellular responses (Curtis and Wilkinson, 1999). It has become well documented that many cell types react strongly to micrometric topography. Extensive characterization of the associated morphological changes has been undertaken (Dalby et al., 2002b).

The filopodia of osteoprogenitor cells, which probe the surfaces for suitable adhesion sites, are in the range of 100 nm in diameter and favour submicron-scale topography (Zhao et al., 2006). In the light of this knowledge microtechnology is evolving into nanotechnology. There is increasing evidence that cells respond to nanometric cues *in vitro* (Dalby et al., 2002b). Reactions to nanometric surface features, below 20 nm in dimension, have been documented (Dalby et al., 2007; Maclaine et al., 2012; McNamara et al., 2011; Sjostrom et al., 2009a; Sjostrom et al., 2009b). MSCs have been stimulated to produce bone *in vitro* (Dalby et al., 2007), using 14nm high nanoislands HOBs have been stimulated to produce the osteoblast specific matrix protein, OCN, on PCL (Maclaine et al., 2012) and MSCs quiescent on planar Ti have undergone transition to an active phenotype with bone matrix nodule formation after 21 days using 15nm nanopillars (McNamara et al., 2011; Sjostrom et al., 2009a).

Nanotechnology aims to create and use structures and systems in the size range of 1-500 nm. This size range incorporates the atomic, molecular, and macromolecular length scales (Biggs et al., 2010). Nanoscale changes in topography have been shown to alter the differentiation of MSCs (Dalby et al., 2007; Wilkinson et al., 2011). Osteoconversion of MSCs has been achieved using a ± 50 nm level of disorder, applied to a pattern of nanopits (Dalby, 2009). A surface disordered at the nanoscale level has, in the absence of osteogenic media, been shown to stimulate MSCs to produce bone mineral on a surface comprised of poly-methylmethacrylate (PMMA), the main constituent of bone cement (Dalby et al., 2007). PMMA is not otherwise noted for its osteogenic properties and is more regularly considered with respect to osteolysis and aseptic loosening of implants.

A combination of nanotopographical features with micrometric surface features is under investigation. A complex patterning of submicron topographies has been manufactured within 30 μ m pits. The regularly spaced pits were produced by photolithography on otherwise smooth Titanium disks. The internal aspect of the pits had a variety of topographies engraved from smooth (40-60 nm), to porous

anodized (400 nm) and acid etched (700 nm). A combination of sand-blasting and acid etching (SLA) created an alternative pattern of comparatively shallow, irregularly placed craters of 10-100 μm diameter. Osteoblast-like (MG63) cells cultured on these surfaces showed differing morphology, with a continuous monolayer on the smooth surfaces and an elongated morphology on the acid etched surfaces (anchoring in adjacent cavities). The porous anodized Ti exhibited a combination of the two morphologies. The cells on the acid etched and SLA surfaces were lower in number, more differentiated in phenotype, and with increased OCN, prostaglandin E2 (PGE2), and TGF β 1 expression. Differences were noted in the results from the regular acid etched topography and the irregular SLA topography (Zhao et al., 2006).

Research, combining chemical and topographical work, revealed that the effect of HAPEX on human osteoblasts (HOBs) was enhanced by the addition of micrometric topography. The cells attached more rapidly and in greater numbers to the optimized surface (Dalby et al., 2002a). The development, application and use of new osteogenic compounds (Kantawong et al., 2010) in addition to differing presentation of existing chemistries, such as the nanoparticulate coating of HA to microstructured Ti (Nishimura et al., 2007), continues.

1.6.2 Intracellular responses to surface modifications

Alterations in gene and protein expression can occur within minutes of a cell adhering to a surface. Focal adhesion complexes mediate the phosphorylation of several intracellular signalling proteins (e.g. focal adhesion kinase, FAK). The phosphorylation of proteins at focal adhesions (the bridge between the extracellular matrix and the cytoskeleton) creates docking sites for the activation of the cytosolic protein kinases/phosphatases involved in migration, cytoskeletal organization, gene expression, and cell cycle progression (Hamilton and Brunette, 2007). An example is extracellular-signal related kinase 1/2 (ERK1/2). This key signalling hub is stimulated by e.g. FAK activation and it controls cell growth (Biggs et al., 2009). For MSCs, if ERK1/2 is not stimulated the cells will become post-mitotic and the transcription factor peroxisome proliferator-activated receptor gamma (PPARG) will promote adipogenesis

(adipocytes and poorly adhered, round cells) (Biggs et al., 2009). If medium ERK activation is stimulated proliferation and fibrogenesis will occur. If ERK is heavily phosphorylated it will negatively feed back on itself to slow growth and e.g. RUNX2 will be phosphorylated promoting osteogenesis (hence osteoblasts are large cells with large adhesions) (Biggs et al., 2009).

Morphological and gene expression differences have been noted with changes in the *in vitro* environment presented to stem cells (including 2 dimensional (2d) culture versus 3 dimensional (3d) scaffolds). Culture of mouse embryonic stem cells in porous tantalum and on solid substrates revealed the exclusive expression of several genes following 3d culture, including the gene encoding BMP 4 (Liu et al., 2006).

An *in vitro* study of chemical vapour deposit (CVD) nanopatterned diamond features suggested that features in the range of 30-100 nm were more supportive of osteoblastic functions than features approaching 100-600 nm in size. Feature clustering may have contributed to the effect (Webster et al., 2009). CVD can nanopattern bulk areas of material. Defined pillar-like titania nanofeatures manufactured using through-mask anodisation, at a height of 15 nm can be particularly effective at promoting the differentiation of MSCs into osteoblasts (McNamara et al., 2011; McNamara LE, Manuscript in Preparation; Sjostrom et al., 2009a).

Culture of calvarial osteoblasts in differentiation media, on grit blasted Ti with and without hydrogen fluoride, revealed an *in vitro* RUNX2 (2-6 fold) increase, OSX (0-3 fold) increase, BSP at days 1-14 (1-8 fold) increase (maximal at day 3). BSP expression was reduced by day 14 (Guo et al., 2007). Fluoride-modified rough etched Ti surfaces have been associated with an increase in RUNX2 expression by human embryonic palatal mesenchymal cells at 7 days (Isa et al., 2006).

MSC differentiation can be controlled to favour differentiation into osteoblasts through low levels of distortional strain and interstitial fluid flow (Huiskes et al., 1997), a principle important in the development of 3d scaffolds seeded with stem cells and cultured to produce autologous osteochondral grafts.

1.7 My hypotheses and the progression to protocol development

The effects of nanotopography on MSCs and osteoblasts have been discussed. The aim of this research is to investigate the possibility of using PCL in combination with nanotopography as a substrate for expansion of autogenous bone graft. I plan to test the hypothesis that both NSQ50 and nanoisland topography will support osteogenesis on PCL and that the addition of HA into the PCL will enhance the osteogenic effects.

The research outlined in chapter 4 using nanoisland topographies using HOBs obtained from Promocell GmbH (Germany) was undertaken prior to my development of techniques to isolate HBMCs and the research into the effects of nanopit topographies on these cells. The research was performed in this way in order to confirm or refute pilot studies undertaken by a colleague (Miss Gadhari) and to hone my own tissue culture, immunofluorescence and qPCR techniques. This part of my research has also led to experience in publication of manuscripts {Maclaine, 2012 #162}.

The experiments that followed were undertaken in order to develop the protocols for HBMC isolation and reduce the need for external and expensive cell acquisition. Concurrently experiments examined dual-sided culture and the effects of the NSQ50 topography. Human bone marrow was harvested from hip arthroplasty patients, the mesenchymal stem cells culture expanded and used for cellular analysis of substrate bioactivity. The cell line specificity and osteogenic behaviour was demonstrated through immunohistochemistry, confirmed by real-time PCR and quantitative PCR. Mineralisation was demonstrated using alizarin red staining. Through the use of the HBMCs for definitive research I hoped to show the protocols from shim production to bone marrow harvesting and dual sided cell culture to be reproducible and potentially applicable to economical larger scale production.

Chapter 2 Protocol Optimisation: Materials and Methods

2.1 Introduction to materials and methods

The methods, pilot study results and discussion detailed (chapter 2.2-2.4) provide an understanding of the thoughts and processes that led to the definitive protocol used to delineate the effect of nanotopography on HBMC culture. The process was gradual. The salient features are detailed with a discussion (chapter 2.4) following a description of the pilot study results (chapter 2.3). Three nanotopographies (nanopits (NSQ50) and nanoislands (14 nm and 18 nm high)) were manufactured using two different techniques. Each technique is outlined. The production pathway from shim to substrate was common to all topographies varying solely with respect to the single or dual-sided nature of patterning.

Acellular analysis of substrates was undertaken with both the planar and patterned surfaces being scrutinized using scanning electron microscopy (SEM) and atomic force microscopy (AFM). Polycaprolactone (PCL) and nanopattern degradation was determined after a 28-day period of exposure to air, simulated body fluid (SBF) and media. SBF has ion concentrations approximately equal to human blood plasma. Cellular analysis of substrates was undertaken using a combination of light microscopy, immunofluorescence microscopy, gel and quantitative PCR. The acquisition and culture of HBMCs from local sources is of increasing interest to the Centre for Cell Engineering, at Glasgow University, and was newly undertaken (2.2-2.4).

Single sided cell culture upon the uppermost surface of substrates is common practice and procedures universally accepted (Kantawong et al., 2010; Kilian et al., 2010; McMurray et al., 2011; McNamara et al., 2011). A significant amount of work has enabled cell culture on the surface of biomaterials, within gels, and within 3d constructs (Liu et al., 2006; Wang et al., 2010). Research has focused on nutrient flow to the centre of such scaffolds (Huiskes et al., 1997). To our knowledge there has been no attempt to culture cells on both surfaces of planar and embossed substrates. I developed this new technique alongside my research into the effects of nanotopography on HBMCs. The four methods of seeding and cell culture trialled in the development of my dual-culture technique are described (2.2-2.4).

Osteogenic media remains the gold standard to which the osteogenic properties of a substrate, culture media or technique are commonly compared (Dalby et al., 2007; Jorgensen et al., 2004; Maclaine et al., 2012; Yang et al., 2003). Autograft is the 'gold standard' graft to which all other bone grafts and their substitutes are compared (Khan et al., 2012). HA and BMP are clinically utilised alternatives to the *in vitro* usage of osteogenic media (Petit, 1999; Termaat et al., 2005). This research has combined these *in vivo* and *in vitro* gold standards in an analysis of the properties of nanopatterned PCL.

The pilot studies relating to this novel work are detailed (chapters 2.2-2.4) and my definitive results are shown in chapters 3 and 4. Outlined in this chapter is a background to the materials, cell lines and techniques used during the development of the definitive protocols. The honing of substrate manufacture, cell acquisition, cell culture and cellular analysis techniques will be detailed with an outline and discussion of the preliminary results. Unless otherwise indicated Sigma-Aldrich (UK) supplied the reagents and Vector labs, UK supplied the immunostains. Details of the media and reagents used can be found in the appendix.

2.1.1 Nanotopography

By default or design orthopaedic implants have a surface chemistry and topography. In this research I am harnessing the power of topography and examining its effects on HBMCs and HOBs. Nanoscale topographical research over the last decade has fallen into two camps. Highly ordered topography is fabricated down to 10 nm with high precision (Vieu C, 2000). Random nanoscale roughness is associated with surface polishing, blasting, and anodisation (Anselme et al., 2000). High-order surfaces tend to be low-adhesion (Dalby et al., 2004a; Gallagher et al., 2002) whilst the results from roughened surfaces vary due to a lack of reproducibility i.e. surfaces with two similar Ra values can look very different. Recent evidence revealed that controlled disorder is critical to inducing the osteoblastic phenotype (Dalby et al., 2007).

The main topography of focus for my thesis, the NSQ50 topography, has been shown to induce similar levels of MSC differentiation to the use of osteogenic media (Dalby et al., 2007). NSQ50 topography uses a square pattern of pits (120 nm diameter, 100 nm depth and 300 nm centre-centre spacing) modified by the addition of randomly calculated ± 50 nm displacement in X and Y (Dalby et al., 2007). I will also explore a new bottom-up fabrication methodology. Most bottom-up methods, such as polymer phase separation (Affrossman et al., 2000; Affrossman and Stamm, 2000), can be used to manufacture nanoscale surfaces (Dalby et al., 2002a; Dalby et al., 2006b; Dalby et al., 2002b) but the order cannot be easily controlled. The use of block co-polymers has changed this (Cheng JY, 2002; Glass R, 2004; J. Y. Cheng and Vancso, 2002; Krishnamoorthy et al., 2006). Tethering phase-separating polymer blocks to each other to give (inverse) micelles can lead to surfaces with good (but not perfect) order, similar to the NSQ50.

Three patterns incorporating nanodisorder manufactured using electron beam lithography (EBL) (chapter 3.1) and block co-polymer phase separation (chapters 4.1-4.2) are represented in my thesis. EBL has been used in order to produce a specific pattern of nanopits (NSQ50) (Dalby et al., 2004a; Dalby et al., 2007) and block co-polymer phase separation has been used to produce two sizes of nanoislands with good, but not perfect, order (Maclaine et al., 2012). The initial fabrication step differed with the type of topography generated and is detailed in chapter 3 for NSQ50 and in chapter 4 with respect to the nanoisland topographies. The nickel plating and embossing of PCL was common to all topographies (chapter 2.2.2).

2.1.2 Materials

The substrates used in this research were formed from PCL, a biodegradable polymer (12-24 month degradation time) in clinical usage (food and drug administration (FDA) approved) (Gadegaard et al., 2003). The thermopolymer has a convenient melting point of 74°C rendering it readily patternable through the use of hot-embossing (McMurray et al., 2011; Thoms et al., 2003). Comparison of a variety of topographical surfaces to osteogenic media has been

of long-standing import in the assessment of a substrate's osteogenicity (MacLaine et al., 2012). The media consisting of basal media with the addition of dexamethasone and ascorbic acid can be used *in vitro* but is not used in clinical practice. In this new research I have created a composite of HA and PCL (HAPCL) to enable a comparison to be made between the effects of topography on osteogenesis with the *in vivo* 'gold standards' of HA and BMP as well as osteogenic media. The presence of HA in the PCL has been analysed in both planar and patterned substrates.

HA and BMP are both used *in vivo* to enhance bone production. As previously mentioned HA application to femoral stems, in the presence of roughened topography, is commonplace (chapter 1.5.4). HA coats have been applied to multiple orthopaedic and dental devices including external fixator pins. HA containing composites have found clinical usage, for example a mixture of 20 % HA and 80 % β -TCP has been used in both spinal (Fujibayashi et al., 2001; Kasai et al., 2003; Moro-Barrero et al., 2007) and hip procedures (Stevens and George, 2005). HAPEX™, an early bioactive composite of polyethylene and HA has been used successfully in the repair of orbital floor fractures and in middle ear implants (Tanner, 1994). BMP has been used to enhance union rates in spinal fusion surgery, in fracture healing *de novo*, and following fracture non-union (Chen et al., 2004).

BMP

BMP was the factor contained within demineralised bone matrix deemed responsible for induction of new bone formation when implanted in muscular tissue (Urist, 1965). Incubation of a clonal myoblastic cell line with BMP2 for 6 days inhibited troponin and myosin formation and resulted in the formation of numerous ALP positive cells. At concentrations above 100 ng/ml there was a dose dependent result on ALP and OCN production, i.e. osteogenesis (Katagiri et al., 1994). The effect was shown for 6 days, but on removal of the stimulus the myogenic phenotype returned (Katagiri et al., 1994). A typical sequence of events can be observed leading to the induction of endochondral bone formation by BMPs (figure 2.1). Monocyte and mesenchymal cell recruitment and

proliferation precede differentiation into chondrocytes and calcification of the cartilage matrix. Vascular invasion is associated with osteoblast differentiation and bone formation. Osteoclastic remodelling of the newly formed bone is finally undertaken.

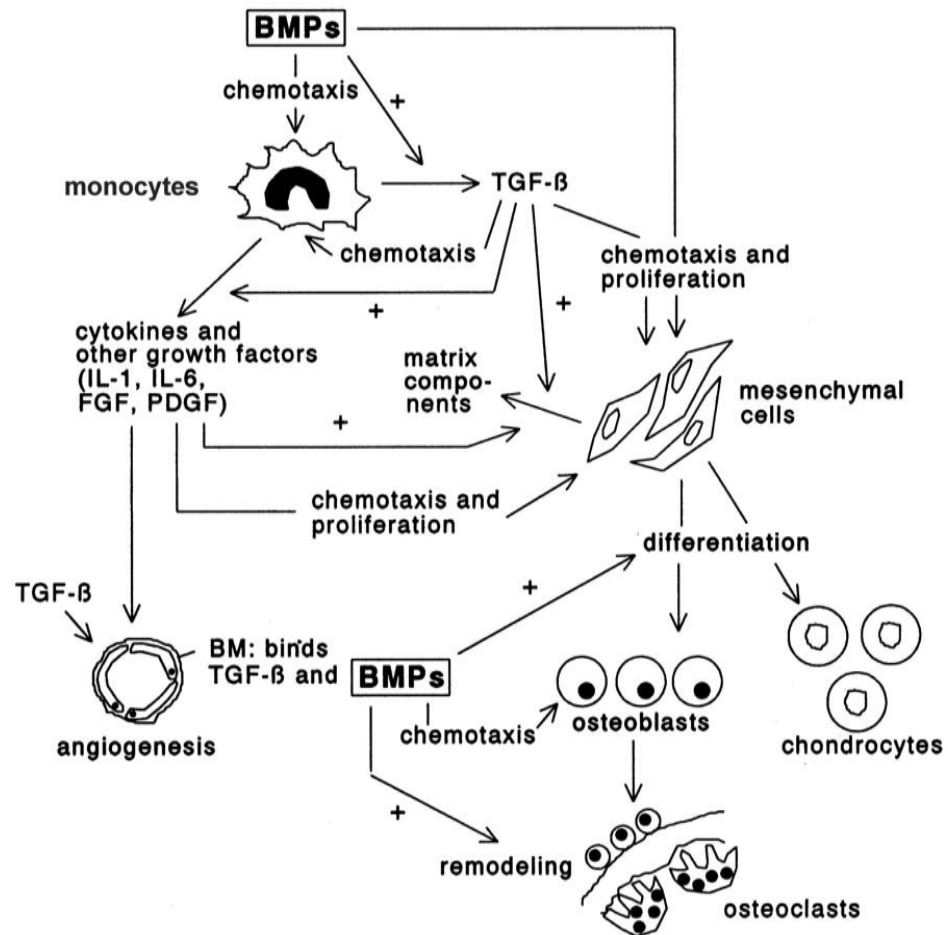


Figure 2.1 The mechanisms of action of BMPs in bone repair. BMPs are related to chemotaxis of monocytes and a release of TGF- β enhancing proliferation of MSCs, the production of matrix components and the release of cytokines (interleukin-1 (IL-1) and interleukin-6 (IL-6) and other growth factors FGF and platelet-derived growth factor (PDGF)). The BM (basement membrane) binds TGF- β and BMPs leading to osteoblast recruitment and differentiation and osteoclastic remodeling. Reproduced from Bone Morphogenic Proteins. (Termaat et al., 2005).

2.1.3 Cell lines

A number of cell lines have been used to understand the cellular behaviour of the skeletal system in this thesis including Htert fibroblasts, osteoprogenitor cells isolated from human bone marrow and HOBs. Htert, a human telomerase reverse transcriptase immortalised cell line, was readily available within the laboratory and provided an inexpensive number of cells upon which to trial ideas during protocol development. These cells (obtained from ATCC, USA) are used in the introduction of students to tissue culture due to their ready adherence, rapid cell division (1:2 to 1:3 twice weekly), hardiness and phenotype maintenance through 15 doublings.

As aforementioned following the acquisition of generic tissue culture experience I used primary HOBs were obtained from PromoCell GmbH (Germany) and undertook the assessment of the nanoisland topography detailed in chapter 4. Subsequently I isolated cells from bone marrow and from cancellous bone fragments (obtained at the time of hip arthroplasty). The cells obtained from the cancellous bone fragments were not fully characterised, and therefore solely used as a disposable cell line during pilot studies in the latter stages of protocol optimisation (chapter 2). Responsible for the synthesis of bone matrix, and in certain circumstances matrix mineralization, HOBs have the disadvantages of being relatively slow to proliferate. The proliferation of HOBs ceases with increasing differentiation and mineralization and therefore these cells were not used in the definitive experiments (chapter3).

Human bone marrow represents a readily harvestable and locally available source of stem cells, progenitors and mature cells (collectively referred to as HBMCs hereafter) (Caterson et al., 2002). Obtained through the extraction of the mononuclear cell fraction (Caterson et al., 2002) the HBMCs used in my research have been obtained from bone marrow sourced from arthroplasty patients, a demographic similar to that for whom a paucity of bone graft is a problem. The heterogeneous nature of the cells harvested cell is representative of the cell population encountered by the final product (culture expanded bone graft). In addition to their use within my definitive research into dual sided cell culture

and the NSQ50 nanopit topography I also provided HBMCs for use by other students and subsequently teaching into their isolation.

2.1.4 Background to experimental techniques

My assessment of the substrates involved acellular and cellular analysis. To analyse the cellular reaction to the substrates I have applied techniques including the use of light and immunofluorescence microscopy and cell fixation in association with the application of cell stains. I used SEM and AFM for the delineation of substrate topography and degradation characteristics.

Culture of osteogenic cells on Titanium has yielded results that illustrate the need for temporal analysis of gene expression and protein production in mineralising cultures (Ong et al., 1997). Messenger ribonucleic acid (mRNA) extracted from cells can be qualitatively and quantitatively analysed using reverse transcription (RT) and polymerase chain reactions (PCR). I have temporally analysed the effects of the topographies using both microscopy and PCR.

Light microscopy

The passage of visible light through or reflection by a sample enables imaging of dark or strongly refractive objects. Resolution of 0.2 μm is imposed due to diffraction of light (Croft, 2006). Contrast within images is commonly enhanced using dyes such as Coomassie blue (a nonspecific stain for proteins) and alizarin red. Alizarin red is an early stage marker of matrix mineralization, day 14 of *in vitro* culture (Caterson et al., 2002).

Immunofluorescent microscopy

Illumination with a specific high energy light results in the emission of fluorescence, a lower frequency light that differs in wavelength from the excitation light. In the absence of autofluorescence the use of antibodies in combination with a fluorophore (such as Rhodamine or Fluorescein

isothiocyanate (FITC)) may be undertaken. Rhodamine phalloidin (TRITC) staining of the cytoskeleton may be combined with DAPI staining of deoxyribonucleic acid (DNA) and fluorescein staining of OPN or OCN. The peak excitation and emission wavelengths of TRITC and FITC are 547 nm & 572 nm and 495 nm & 521 nm respectively. DAPI shows a strong blue fluorescence (wavelength 455 nm) when bound to the Adenine=Thymine (A=T) rich repeats of chromosomes and excited by ultraviolet light (wavelength 345 nm).

Immunofluorescent staining may be direct or indirect. Direct staining (figure 2.2) involves the association of a target (proteins in figure 2.2A and B) to a fluorescence-labelled antibody (anti-A in figure 2.2). Indirect staining involves the attachment of a primary antibody (for example rabbit anti-A in figure 2.2) to a target (A) before becoming the target for a fluorescence-labelled antibody (goat anti-rabbit in figure 2.2B).

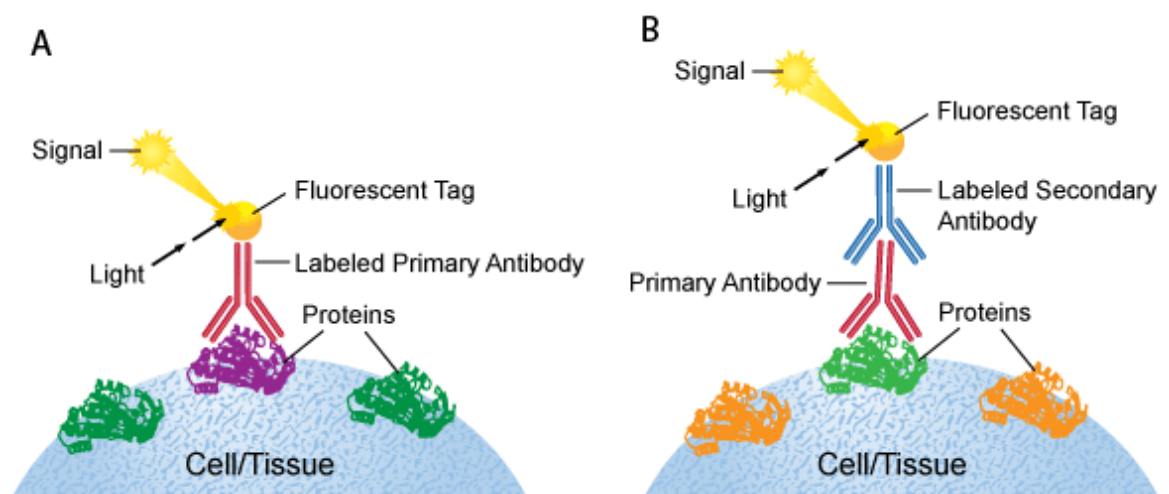


Figure 2.2 Direct and indirect immunohistochemical staining. Image A shows direct immunohistochemical staining using a labelled antibody binding directly to the antigen being stained for. Image B shows the indirect method using an antibody against the antigen being probed for, and a second, labelled, antibody against the first. Adapted from (Leinco, 2013).

AFM (Atomic Force Microscopy)

Binnig, Quate and Gerber invented AFM, in 1985 (Eaton and West, 2010). Certain modes of AFM, such as that used in my research, utilise a laser beam deflection system. On ‘tapping mode’ a stiff cantilever oscillates close to the sample and the tip intermittently taps or touches the surface. The dragging or lateral forces associated with the contact mode were thus limited. The measurement taken is the deflection of the cantilever. I have included AFM and SEM images and cross-sectional analysis of the nanoisland topography (chapter 2.3.1).

SEM (Scanning Electron Microscopy)

SEM was developed between 1935 and 1965 (Croft, 2006). Surfaces are imaged through an analysis of the interaction of the atoms of a material surface with a high-energy beam of electrons. The resolution of SEM is between <1 nm and 20 nm (Croft, 2006). 3d data can be gathered using SEM. In this research the SEM has been used to analyse surface topography and obtain the surface roughness measurements used in my research (chapter 2.3.1).

Phenotype identification through analysis of gene expression

Tissues may be classified according to an analysis of gene expression. Identification and quantification of mRNA produced is undertaken using a process of RT in combination with PCR plus gel electrophoresis (real time (rtPCR) or gel PCR) or quantitative (qPCR).

RT (Reverse Transcription)

RT creates single-stranded DNA from an mRNA template (figure 2.3). Ribonucleic acid (RNA)-dependent DNA polymerase transcribes the mRNA producing complementary DNA (cDNA). Reverse transcriptase degrades the RNA in the RNA-DNA hybrids producing cDNA for use in PCR.

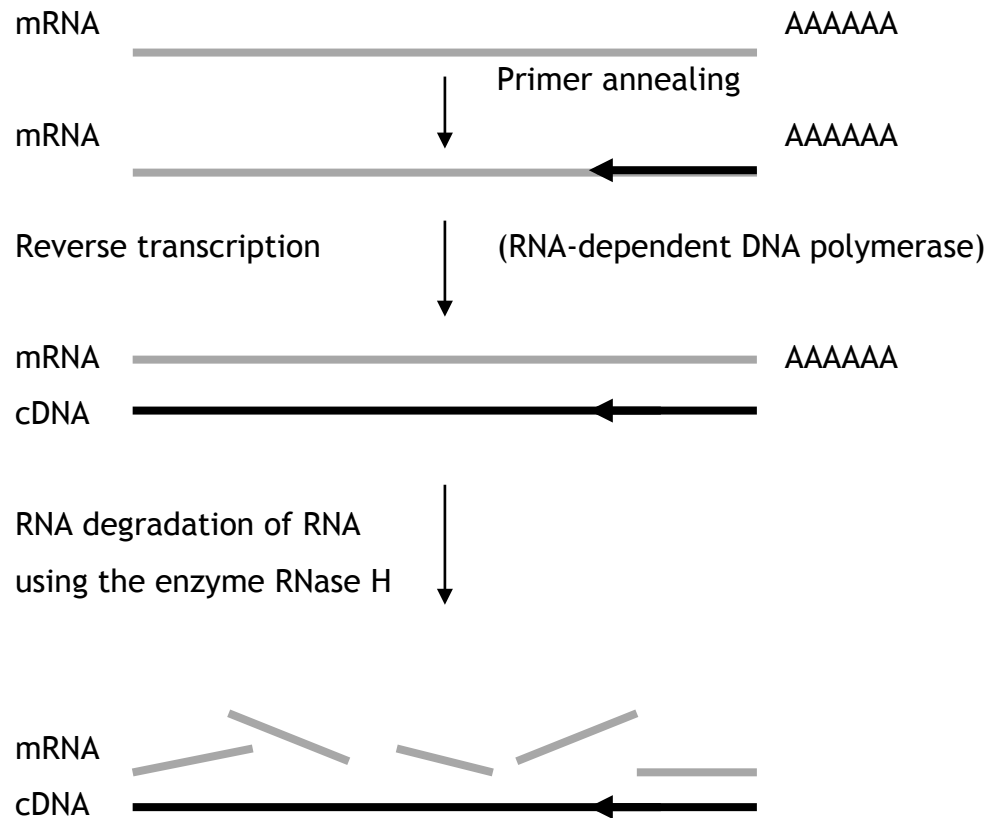
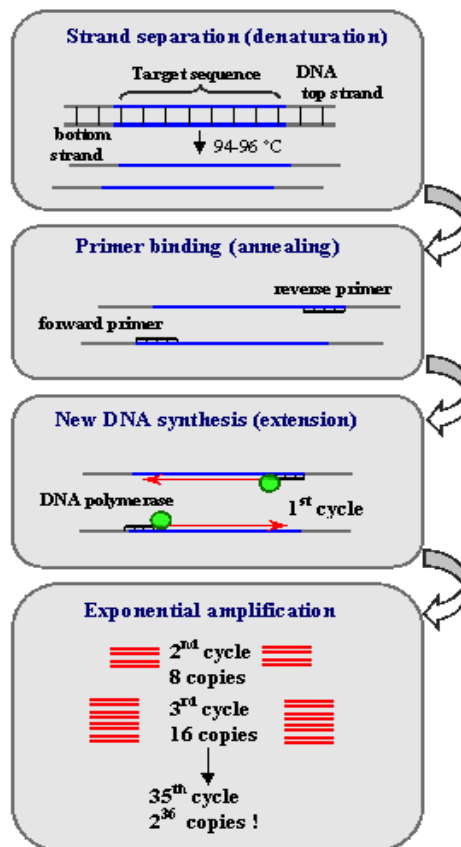


Figure 2.3 RT (adapted from the Quantitect reverse transcription handbook) (Qiagen, 2009). The three component steps of RT using the Quantitect RT kit include primer annealing, RT and RNA degradation.

PCR (Polymerase Chain Reaction)

PCR generates sufficient genetic material to investigate the genetic functions of the cells harvested (figure 2.4). Thermal cycling enables the separation of the two stranded DNA and enzymatic DNA replication. A DNA polymerase enzyme (such as Thermostable DNA (Taq) polymerase) assembles new strands of DNA from nucleotides present in the solution through the use of single-stranded DNA templates. DNA oligonucleotides (primers) are required for the initiation of DNA synthesis. Progression of the reaction is brought about when the products of the first reaction become substrates for the next.



High temperature applied to the double stranded DNA separates the strands.

The enzyme Taq DNA polymerase (in this case) generates new strands of DNA from the template starting at the forward and reverse primers. Primers (short pieces of single stranded DNA) are complementary to the target sequence.

Figure 2.4 PCR (Adapted from the National centre for biotechnology information (NCBI)). PCR involves cycles of DNA strand separation, annealing (binding of forward and reverse primers to the 2 DNA strands) and synthesis of new DNA using DNA polymerase (NCBI, 2013).

DNA amplification occurs exponentially until the reaction is limited. Limiting factors are: the presence of inhibitors, the running out of reagent, the accumulation of pyrophosphate molecules, or self-annealing of the product.

Real time PCR

RtPCR utilizes gel electrophoresis to delineate the DNA products of PCR. Comparison of the DNA products with ladders incorporating known products indirectly identifies the mRNA harvested from the original cells or tissue. An approximation of quantity can be conferred from the extent of fluorescence of attached markers in each band.

qPCR (Quantitative PCR)

Real-time monitoring of DNA amplification, introduced by Higuchi et al in 1993, utilizes the linear relationship between the quantity of target DNA obtained from an RT reaction and the product generated during the exponential phase of PCR. A probe is attached to the DNA down-stream from the primer (figure 2.5). Fluorescence is emitted when the probe is reached by the DNA polymerase enzyme, degraded and separated from the DNA and from its quencher. A measurement of the fluorescence emitted provides a quantification of the DNA being replicated at each stage. Annealing of the primer and probe to the DNA strand brings the quencher back into proximity with the reporter fluorophore and the fluorescence stops (figure 2.5).

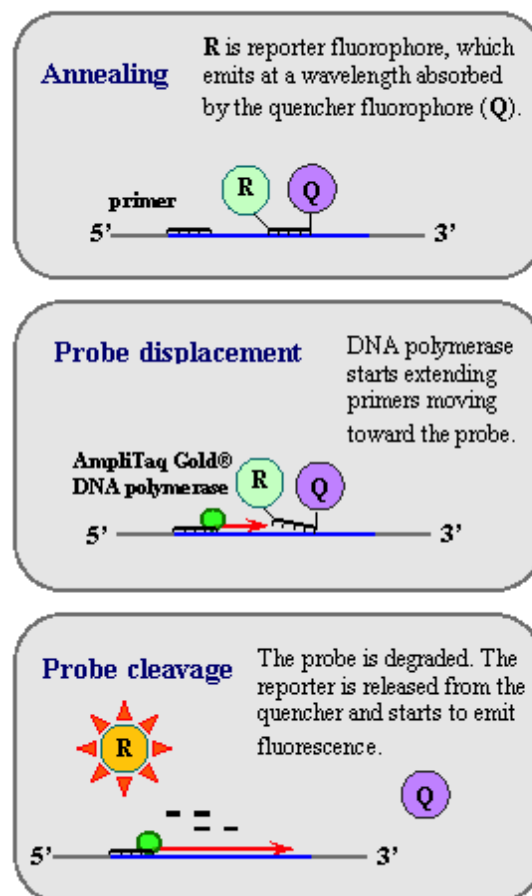


Figure 2.5 Real time qPCR The real-time aspect of QPCR (Image from (NCBI, 2013)). The quencher absorbs the fluorophore emission until the probe is degraded from the DNA at the end of each replication at which point the emission is detected and measured.

Quantification is undertaken as a calculation of the number of cycles (cycle threshold (CT)) required in reaching the exponential phase of the reaction (figure 2.6). The lower the amount of the target mRNA extracted from the original sample, converted to cDNA in the RT reaction, and entering the qPCR reaction, the greater the number of cycles required to reach the CT. For comparative purposes similar total quantities of mRNA are used in the control and target assays. The quantity of target DNA obtained from the experimental tissues or cells relative to the quantity of DNA from a housekeeper gene is compared to that obtained from the control tissues or cells. A plateau effect occurs when amplification ceases (figure 2.6).

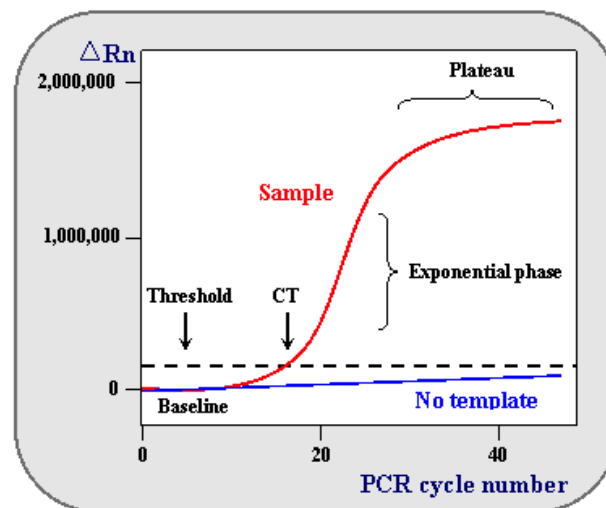


Figure 2.6 A model 'real time' qPCR plot (Adapted from the National centre for biotechnology information (NCBI, 2013)). Thermal cycling produces an exponential increase in DNA until a plateau phase is reached. Limiting factors include quantity of available reagent and enzyme, and the presence of reaction inhibitors.

2.1.5 Gene expression and cell phenotype

Cells express proteins as a result of up or down regulation of genes within their DNA. These genes can be controlled in a number of ways including the use of transcription and growth factors. Cells consistently express some genes irrespective of phenotype. These housekeeping genes, including GAPDH and 18S, are responsible for basic cell functions and are commonly used for comparative purposes in assays of gene expression.

When they start to differentiate into osteoblasts, Osteoprogenitors express a range of genetic markers, including OSX, COL1, Osteonectin, OPN and OCN (Table 2.1). Markers have been identified for cells of other mesenchymal phenotypes including cartilage, muscle, fat, and neural tissue (Table 2.1). I analysed multiple gene products in my determination of the effect of the nanotopographies on HOBs and HBMCs.

BMPR2	Expressed by multiple tissues, involved in up-regulation of bone mineralisation.
RUNX2	Expressed by immature osteoprogenitors, it upregulates osteogenesis.
Osteonectin	Required for calcification of collagen in bone and involved in ECM synthesis.
OPN	Expressed by fibroblasts, preosteoblasts, osteoblasts, osteocytes, hypertrophic chondrocytes, dendritic cells, skeletal muscle cells and some bone marrow cells. Synthesis of osteopontin is stimulated by calcitriol (1,25-dihydroxy-vitamin D ₃).
OCN	Solely secreted by Osteoblasts.
SOX9	Marker of chondrocyte differentiation.
MYOD1	Marker of myogenic differentiation, one of the earliest markers of myogenic commitment.
PPARG	Marker of and regulator of adipocytes.
TUBB3	Marker for neural cells, primarily expressed in neurons and responsible for microtubule formation.
GAPDH	Responsible for the protein involved in the catalysis of the 6 th step of glycolysis, amongst other functions.
18S	Responsible for ribosomal RNA, important random target in PCR.

Table 2.1 Gene expression and cell phenotype. Gene products may predominate in osteogenesis, be markers for alternative mesenchymal tissues or common to tissues of multiple lineages.

2.2 Methods

Ethics approval obtained by Mr Meek in 2004 was sufficient to enable bone marrow aspiration from living donors at the time of total hip arthroplasty, HBMC isolation and use for this research. The ethics agreement number was 04/S0702/22. In addition each patient was consented for the retention and use of residual tissue for *in vitro* research. Although this consent forms an integral part of the routine informed consent process undertaken prior to total hip arthroplasty, a supplementary form was also used. Nursing and medical staff obtained consent at the time of procedural consent. All those in contact with the bone marrow had been previously immunised against Hepatitis B.

2.2.1 Shim manufacture

Samples were fabricated using a three-step process. Shim production using either EBL (NSQ50) (Gadegaard et al., 2003) or the block co-polymer technique (nanoislands) (MacLaine et al., 2012) was followed by nickel die fabrication and thumb embossing. The details with respect to the shim production of the nanopits and nanoislands were topography specific (chapters 3 and 4).

2.2.2 Preparation of PCL substrates

PCL beads (molecular number (Mn) 60000) were soaked in 99 % methanol for 1 h prior to removal of the supernatant and air-drying in a fume cupboard for 24 h.

Single bead melts

PCL beads were placed onto a heat resistant glass sheet at 2 cm intervals and heated (74 degrees centigrade (°C)) until they resembled water droplets (defined as a wet melt).

PCL sheets

A petri dish containing dried PCL beads was emptied onto the centre of a heat resistant glass sheet. A second sheet applied to the top and was held in place with Bulldog clips. The beads were melted (74°C) until the molten PCL neared the glass sheet edges. Cooling at room temperature preceded clip removal. PCL sheets were stored between glass plates.

HAPCL sheets

HAPCL 20 % by weight was made by melt mixing HA powder into PCL. The weight of a PCL sheet was measured and an appropriate quantity of spray dried HA with a particle size 4 μm and surface area of 10 m^2/g was used. Aliquots of HA were sequentially added to a molten PCL sheet. The HA was mixed into the molten PCL in a method similar to cement mixing by builders, using a microscope slide the molten PCL gathered into the middle of the glass sheet upon which it was melted and spread repeatedly until the PCL solidified, at which time it was remelted and further HA was added. Increasingly concentrated HAPCL sheets were formed by repeating the process until the composite was macroscopically homogeneous.

Planar substrates

An ethanol washed air-dried shim or glass microscope slide was warmed to 74°C on a copper heat sink. 1 cm^2 planar substrates were manufactured as follows and used as controls in experiments involving the NSQ50 topography. Three bead melts were placed onto the slide and when wet melt was achieved (and the surface of the bead reflected light evenly) a further warmed glass slide was placed on top. The slides were placed on a heat resistant surface and thumb pressure applied such that 1.3 cm diameter PCL substrates were formed. Using a scalpel and forceps, 1 cm^2 square substrates were cut out and placed in petri dishes.

Planar substrates were manufactured by cutting 2.5 cm x 2.5 cm squares of PCL sheet and placing onto a warmed microscope slide (74°C) to melt. On wet melt a further warmed glass slide was placed on top. The slides were placed on a heat resistant surface and thumb pressure applied. 2.5 cm x 2.5 cm square substrates were cut out and stored for use as controls in experiments involving the nanoisland topography.

Single sided substrates

PCL sheets were cut into squares of a size appropriate to the shim (2.5 cm x 2.5 cm square for the nanoislands and 1 cm x 1 cm for the NSQ50). A PCL square was placed onto a warmed shim and on wet melting a warmed glass slide placed on top. The shim and slide were placed on a heat resistant surface and thumb pressure applied such that the PCL entirely covered the nanotopography. An absence of macroscopic air bubbles was ensured prior to accepting an embossed PCL substrate. When cooled the slide and shim were separated and the PCL trimmed to the area of topography. A small impression was made on the embossed surface and the substrates stored embossed surface uppermost.

Dual embossed substrates

Two shims were used in the manufacture of dual embossed surfaces. When cooled the shims were separated, and the PCL trimmed to the area of topography. Confirmation that both sides were covered with topography was undertaken and the substrates placed vertically in a well plate.

Substrate sterilisation

Each substrate was soaked in ethanol for 1 h. Substrates were air-dried vertical in well plates within a level 2 fume hood prior to soaking sequentially in hepes saline (HS) (twice) and media (twice) for periods each of five min.

2.2.3 Acellular analysis of substrates using SEM and AFM

Surface analysis of planar and nanoembossed substrates was undertaken using SEM and AFM (nanoscope III). SEM (S4700 at 10 kilovolts in backscatter mode) provided images of the substrate surfaces and AFM a means to measure surface roughness. The effect of 28 days exposure to media, air and SBF on the surface characteristics of NSQ50 and planar substrates was undertaken using AFM.

Acellular analysis of substrate degradation

Substrates were prepared and sterilised (chapter 2.2.2) prior to vertical placement in 48 well plates. Two samples (of each type) were left exposed to air, or had 1.4 ml of either modified Dulbeccos Modified Eagles medium (DMEM) or simulated body fluid (SBF) added. The constituents of SBF are detailed in the appendix. In addition two planar samples had 1.4 ml osteogenic media added. The well plates were incubated under standard conditions for 28 days acellular culture. AFM was performed on each substrate.

2.2.4 HBMC acquisition

Bone marrow aspiration

Consent obtained from patients undergoing THR procedures was extended to include the acquisition of bone tissue for research purposes. Bone marrow was aspirated at the time of THR procedures. After cutting the femoral neck, the exposed surface was washed with normal saline. 20 ml of bone marrow was aspirated using a catheter tipped syringe at the time of femoral canal rasping. The bone marrow aspirate was placed into 40 ml of transfer media (appendix). Cancellous bone fragments obtained by milling the excised femoral head and by curetting and rasping the femoral canal were added to a further container of transfer media. Samples were immediately transferred to the laboratory and the processing was undertaken within 24 h.

Mononuclear cell separation

The transfer media and the bone marrow aspirate were transferred to universal containers and centrifuged at 300 g for 10 min, or until the supernatant cleared. The cell pellet was re-suspended in 20 ml of basal media (modified DMEM) and the cells washed twice by centrifugation at 300 g for 10 min. The bone marrow supernatant was discarded and the cell pellet re-suspended in 20 ml of basal media.

10 ml aliquots of the cell suspension were layered onto 5 ml aliquots of Ficoll-paque (1.077 gram/decilitre (g/dl)) (GE healthcare bio-sciences AB, Uppsala,

Sweden) in universal containers. Residual blood clots were avoided during aspiration of the suspended cells. Centrifugation was undertaken at 450 g for 35 min followed by 376 g for 10 min.

The supernatant media layer was aspirated and discarded (Figure 2.7). The mononuclear cells were aspirated along with the Ficoll/media interface. The aspirate (approximately 2.5 ml) was placed into two universal containers. The cells were washed twice with 10 ml aliquots of basal media, and centrifuged prior to resuspension in 12 ml of basal media. The cell suspension was placed into two 25 cm² flasks.

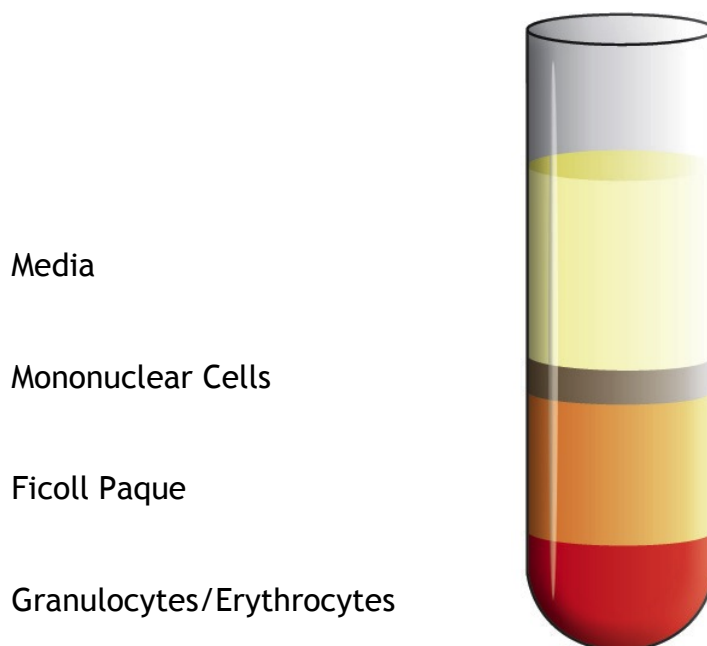


Figure 2.7 Cell separation using a Ficoll gradient. The mononuclear cells lie at the interface between the media and the Ficoll-Paque.

HBMC separation by adhesion to cell culture plastic

Cell culture was undertaken in modified DMEM for 5 days prior to the first media change. After 5 days the media were changed. The culture fluid collected underwent centrifugation and a pellet containing the non-adherent cells was re-suspended in 6 ml media and placed into a further 25 cm² flask. Incubation continued with 50 % media changes triweekly for 1 month or until 70-80 % confluence was reached.

HBMC harvesting from cell culture flasks

On harvesting, the media were aspirated and the adherent cells (HBMCs) washed with 4 ml versene (V). 4 ml trypsin-versene (TV) was added and incubation undertaken for 5-10 min or until cell detachment was noted. The cell suspension was aspirated by pipetting and placed into a universal container. An equal volume of medium was added to each flask and a cell scraper used prior to further aspiration and addition to the universal container. The resultant cell/TV/media suspension was centrifuged at 300 g for 10 min. The pelleted HBMCs were washed in 6 ml of media with re-centrifugation (300 g for 10 min) and either utilized for experiments, or culture expanded at 20×10^4 cells/ 75 cm² flask.

Cell Counting

HBMC were counted using a modified Fed-Fuchs Rosenthal haemocytometer. The total volume of 1 large square was 0.2 mm³. The average number of cells per large square multiplied by 0.5 equalled the cell concentration $\times 10^4$ per ml.

HBMC harvesting from bone fragments

Washed bone fragments were treated with collagenase (36.5 mg of collagenase was added to 50 ml of basal media in an unvented 75 cm² flask). 50 ml of filtered carbon dioxide (CO₂) was added and the flask placed on a shaker platform in a hot room at 37°C for 3-4 h. The flasks were turned hourly. Washing was undertaken using 750 ml of sterile phosphate buffered saline (PBS) and the bone fragments placed in four 75 cm² flasks with 25 ml of basal media and 50 ml of filtered CO₂. An unvented lid was used and media flow induced by placing the flasks on a shaker platform.

After 28 days in culture the media were aspirated, the bone fragments washed with PBS, and sufficient TV added to cover the bone fragments. Incubation was undertaken until cell detachment was noted. The cell suspension was aspirated and an equal volume of media added. The cells were then pelleted and washed in media using the centrifugation method described above. Re-suspended cells

were cultured in 6 ml basal media in vented 25 cm² flasks under standard conditions. Media covered the bone fragments, CO₂ was added and they were cultured in unvented flasks. The flasks were placed in the hot room and 50 % media changes undertaken bi-weekly. The harvesting process was repeated 4 times at monthly intervals prior to the bone fragments being discarded.

2.2.5 Cell Culture

HOBs and HBMCs were harvested at passage 1 or 2. Cells from the different flasks were combined to provide a standard cell mix that was either used for a single sided experiment or split with half being returned to the flask for re-harvesting the next day for dual sided culture. An HBMC pellet was generated by centrifugation at 300 g for 4 min. The HBMCs were washed using media and centrifuged at 300 g for 4 min. The HBMC pellet was re-suspended in media and the cells counted.

Multiple different methods of seeding and cell culture were trialled. The seeding and culture protocols varied with the number of sides seeded. The well plates and volume of media used varied with the size of the substrates. Planar and embossed substrates were treated the same way within each experiment or set of experiments. The protocols were as follows unless otherwise stated (see chapter 4). The well plates were incubated for a predetermined time period and 50 % media changes undertaken tri-weekly. The cells were subsequently stained *in situ* or harvested for use in rtPCR or qPCR.

Initially a Cellon rotatory bioreactor was used for dual sided culture with cells being seeded directly within the bioreactor or cultured on the substrates for a few days prior to placing in the bioreactor (figure 2.8). A variety of bioreactor settings were used. Dual sided cell seeding was subsequently followed by culture within well plates with and without substrate turning, suspension on sterile sutures (figure 2.9) and vertical placement in a 48 well plate (figure 2.10).



Figure 2.8 Rotatory bioreactor. The 4 circular nanopit embossed substrates are shown (arrow) in a gravity dependent position following switching off the rotation.

Single sided cell seeding

A PCL substrate was placed in each well of an appropriately sized well plate. The exactitudes of cell seeding are as follows unless otherwise indicated (as in chapter 4). 2.5×10^4 cells were seeded in $65 \mu\text{l}$ of media per cm^2 substrate. Cells were left to adhere (covered) for 30 min prior to the addition of 1 ml of either basal or osteogenic media. Care was taken to minimise disruption of the initial fluid at this stage.

Dual sided cell culture

The initial seeding of substrates was undertaken as above and after 24 h culture the substrates were turned over using two sterile forceps. Care was taken to minimise disruption of the adhered cells and maintain sterility. A further 2.5×10^4 cells were pipetted onto the centre of each substrate and left undisturbed for 30 min to adhere. The well plates were subsequently incubated for 18 h.

The turning technique involved turning substrates over at 24 h intervals. Developed using sterile surgical instruments, the suspension technique involved the aseptic threading of substrates (green arrow) onto sterile suture material (red arrow) and their suspension within media in 12 well plates (figure 2.9). The angle of suspension varied slightly but both sides of the substrate had access to media (blue).

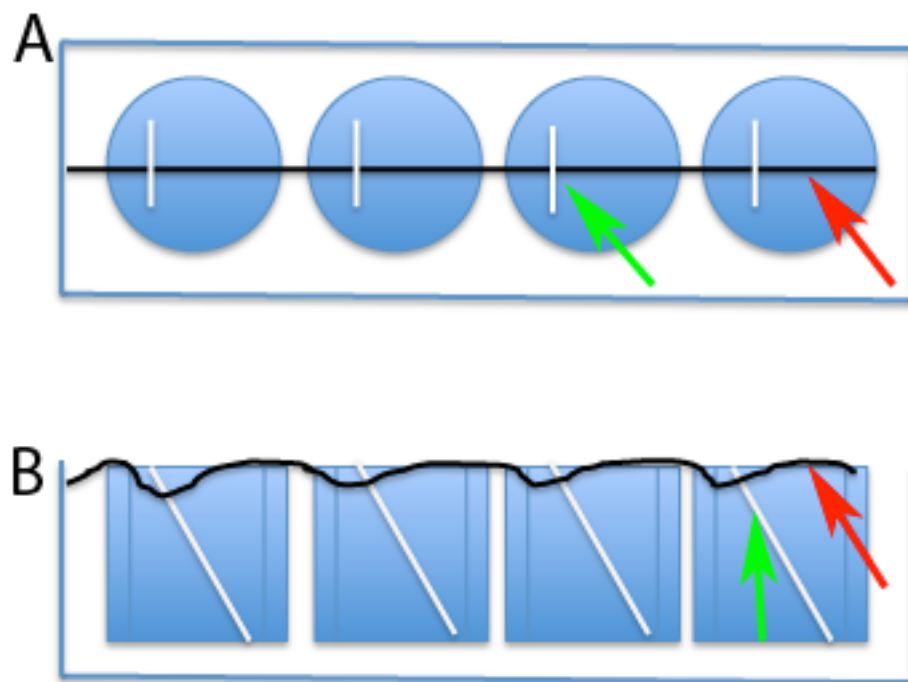


Figure 2.9 The suspension culture technique. The 1 cm² substrates can be seen orientated in a near vertical position in this 24 well plate. Green arrows show the substrates through which the suture thread (red arrows) has been passed. The media (blue) was able to contact both surfaces of the substrates. Diagram A shows the plate from above and B the plate from the side.

I developed the vertical culture technique (figure 2.10) during pilot studies undertaken as follows: 400 µl of fresh media was placed into the wells of a 48 well plate. The substrates were aseptically transferred and placed vertically into corresponding wells of a 48 well plate. One ml of media was transferred with each substrate.

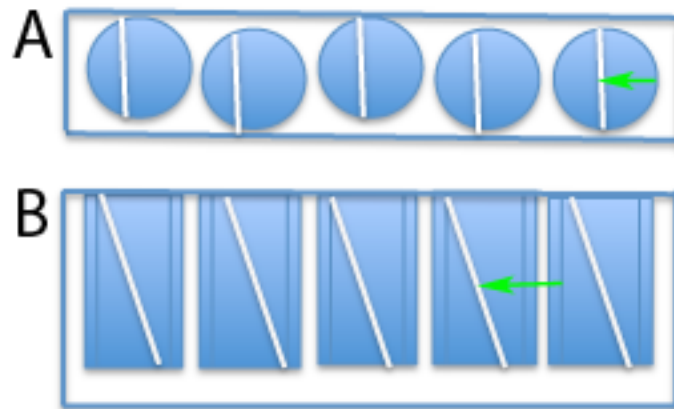


Figure 2.10 The vertical culture technique. The 1 cm² substrates (green arrows) can be seen orientated in a near vertical position in this 48 well plate. The media (blue) was able to contact both surfaces of the substrates. The substrate position was supported by walls of the culture wells of the 48 well plate. Diagram A shows the plate from above and B the plate from the side.

It should be noted that whilst the substrates in some samples were truly vertical, the term ‘vertical culture’ denotes the method of culture chosen (to facilitate media access to both substrate surfaces) and substrates were not truly set at 90° to the horizontal in all cases. Cell culture was undertaken in 1.4 ml of media for the appropriate number of days. Samples were turned vertically by 180° at weekly intervals and 50 % media changes undertaken tri-weekly.

Cell media

Planar PCL samples, nanoembossed samples and nanoembossed HAPCL samples were cultured in modified DMEM unless otherwise stated. Where indicated osteogenic media (modified DMEM with Dexamethasone (10 nM) and L-ascorbic acid (150 g ml⁻¹)) was used in combination with planar PCL substrates as an osteogenic control. 100 ng/ml of BMP was added to the culture flask 12 h prior to harvesting and the seeding of substrates. BMP exposure where indicated was temporary and cells exposed to BMP were cultured in modified DMEM for the remainder of the culture period.

2.2.6 Cell staining and imaging

Cell fixation

Cells on test materials were fixed using 4 % formaldehyde in PBS, with 1 % sucrose at 37°C for 15 min. Once fixed, the samples were washed with PBS. Two replicates of each substrate were used per stain per experiment.

Coomassie Blue Staining

Cell fixation was followed by application of microfiltered coomassie blue for 2 min and washing with filtered PBS until the solution ran clear. Substrates were mounted between 2 cover slides. Microscopy of both sides was undertaken using the Zeiss Axiovert 25 microscope.

Alizarin Red Staining.

Cells were fixed as above. The alizarin red 2 % by volume in H₂O was microfiltered immediately prior to its application to each substrate. Staining was undertaken for 60 min. Dipping in 70 % ethanol or Coomassie blue counterstain for 1-2 seconds (s) preceded washing with PBS. Substrates were placed between coverslips and viewed using the Zeiss Axiovert 25 microscope.

Immunostaining

Fixed samples were permeabilised with a buffered solution (pH 7.2) of 0.5 ml Triton X-100, 10.3 g sucrose, 0.292 g NaCl, 0.06 g MgCl₂, 0.476 g (4-(2-hydroxyethyl)-1-piperazine-ethanesulphonic acid) (HEPES) in 100ml PBS; at 4°C for 5 min. Non-specific binding sites were blocked with 1 g bovine serum albumin (BSA) in 100 ml PBS, at 37 °C for 5 min.

Substrates were incubated for one h with a 1:50 concentration of rhodamine phalloidin (Invitrogen, UK) and a primary antibody. All antibodies were used at 1:50 in 1 BSA / PBS. Each stage was preceded by washing in 0.5 % Tween 20/PBS (5 × 3 min). The appropriate (anti-mouse or anti-goat) biotinylated monoclonal horse antibody (Vector Laboratories, UK) at 1:50 was added for 1 h (37°C) prior

to washing and the addition of FITC conjugated streptavidin (Vector Laboratories, UK) at 1:50 4°C for 30 min. Substrates were mounted between cover slides using Vectorshield mountant for fluorescence (Vector Laboratories, UK) prior to viewing with a Zeiss Axiovert 200M microscope with a Zeiss Plan Neofluor 10x, 20x or 40x lens. The colour channels were superimposed in Adobe Photoshop (Adobe Systems Inc., USA). Antibodies for OCN, OPN, COL2a, MYOD, TUBB3, PPARG, and PSELECTIN were used (obtained from Autogen Bioclear (UK) and Santa Cruz Biotechnology (USA) (appendix)).

2.2.7 RNA extraction for qPCR

Direct and indirect cell lysis was trialled. Initially cells were harvested prior to cell lysis but during the latter stages of protocol development and in the definitive method the following direct lysis technique was used. RNA was extracted using Stratagene RNA Miniprep (Agilent technologies). The elution buffer was warmed to 60°C. The 70 % ethanol (made using 70 ml RNAase free water and 30 ml 99 % ethanol) was removed from the fridge. The quantities of reagent shown were used for 16 RNA samples, and appropriately reduced for 9 RNA samples. 6300 µl lysate buffer was mixed with 45 µl βmercaptoethanol (βME). The medium was removed and the substrates transferred to a 6 well plate (one 2.5 cm² nanoisland substrate or four 1 cm² NSQ50 dual sided substrates per well). 300 µl lysis buffer-βME mix was added to each well. A cell scraper was used and the fluid obtained pipetted into 1.5 ml eppendorf tubes. The wells were washed with a further 50 µl lysis buffer-βME mix and the fluid added to the eppendorf.

Cell lysates were passed three times through a 21 gauge (0.8 mm) needle, the tubes vortexed and the fluid pipetted onto prefilter spin cups. Filtration using an Eppendorf minispin centrifuge was undertaken at 13.4 r.p.m. for 5 min and preceded discard of the filter and addition of 350 µl 70 % ethanol to the filtrate. Vortexing for 5 s preceded fluid transfer into RNA binding cups (in fresh centrifuge tubes) and centrifugation for 60 s. Binding cups were washed with 600 µl low salt wash buffer and centrifugation for 60 s, the filtrate was discarded, the cup closed and centrifuged for a further 2 min. 900 µl DNase digestion buffer

was gently mixed with 90 µl RNase free DNase. 55 µl of the DNase digestion buffer - RNase free DNase mix was added to the matrix of each spin cup, the lids were closed and the cups incubated at 37°C for 15 min. Spin cups were sequentially washed with 600 µl high salt wash with 60 s centrifugation, 600 µl low salt wash with 60 s centrifugation, 300 µl low salt wash with 2 min centrifugation.

Each spin cup was placed into a 1.5 ml microcentrifuge tube. 30 µl warm elution buffer was added, incubation was undertaken at room temperature for 2 min and the microcentrifuge tube centrifuged for 1 min. Unless otherwise stated this process was repeated with a further 20 µl warm elution buffer. The RNA obtained was quantified using a nanodrop 1000 and stored at -80°C.

2.2.8 PCR

The three best RNA samples (based upon concentration and purity (260/280 ratio) were chosen for each qPCR experiment. An equal quantity of RNA was added to each 0.2 ml thin walled tube and the volume made up to 24 µl using RNAase free water. 4 µl of genomic DNA (gDNA) wipeout buffer was added to each tube and the tubes agitated, centrifuged for a few seconds and placed in the thermocycler (setting 42°C for 2 min cooling to 4°C thereafter). 12 µl of master mix was added to each tube prior to placement in the thermocycler and incubation (setting 42°C for 15 min, 95°C for 3 min and cooling to 4°C). The cDNA was stored at -80°C until required.

QPCR was common to all topographies tested. SYBR green and Taqman kits were trialled. The Taqman protocol detailed below was the final modification developed with the alterations detailed in the discussion (chapter 2.4). The Taqman gene expression assay protocol was followed for standard rate qPCR and a 7500 Fast Real-Time PCR system (Applied Biosystems) used.

45x master mixes were made for each primer-probe and 59.4 µl of master mix added to each 0.2 ml tube. 6.6 µl of cDNA was added prior to agitating the tubes

and centrifuging for 15 s. 20 μ l was added to each well in the reaction plate prior to its centrifugation at 3600 g for 15 s using an Eppendorf centrifuge 5804R. Two plates were set up simultaneously using GAPDH and 4 genes of interest. Negative controls were used for each mastermix. Genes analysed were RUNX2, BGLAP (OCN), SOX9, PPARG, and GAPDH.

The run details for the Taqman qPCR were as follows 50°C 2 min, 95°C 10 min, 40 cycles (95°C 15 s, 60°C 1 min). The thresholds were manually set at the midpoint of the straight region of each log curve and checked against the position on the linear curve. The melt and amplification curves of each well were analysed for evidence of impurities. The individual CT values were exported to Excel (Microsoft Corporation, USA) and used for calculations to normalise gene expression against GAPDH, and compare against the planar control surface. The delta CT for each substrate and replicate was calculated (CT gene tested-CT endogenous control). Relative quantification (RQ) was then calculated using the delta-delta Ct (change in CT of the sample-change in CT of the planar substrate). The RQ represents the fold increase or decrease in gene expression in comparison to the planar PCL substrates. Statistical analysis was undertaken in Excel using T-test and analysis of variance (ANOVA).

2.3 Results

The most influential of the results obtained during the pilot studies and the developmental process are discussed within this chapter. The findings of the acellular analysis of substrates using AFM and SEM of planar and nanoembossed surfaces are presented (chapter 2.3.1) in addition to those obtained from the analysis of substrate degradation over 28 days (chapter 2.3.2), the yields of HBMCs from bone marrow and bone spicules are outlined (chapter 2.3.3).

The results obtained using light microscopy after cell culture within the rotatory bioreactors, in well plates using a variety of turning regimens and those following suspension and vertical culture are included and show the progression towards the definitive dual sided culture protocol. The light and

immunofluorescence microscopy of cells following dual sided vertical culture are detailed, and those obtained from rtPCR and qPCR are outlined. The definitive results obtained from the single and dual sided culture of HBMC on NSQ50 nanopit topography can be found in chapter 3 and those relating to the nanoisland topographies in chapter 4.

2.3.1 Acellular substrate analysis

SEM analysis of the dual embossed nanopit (NSQ50) substrates

SEM of the dual embossed substrates revealed successful reproduction of the controlled disorder of nanopits in this topography using the hot embossing technique (chapter 2.2.2). The pattern was reproduced on two sides of each substrate and there was a clear demarcation between the embossed and planar regions (figure 2.11A-D).

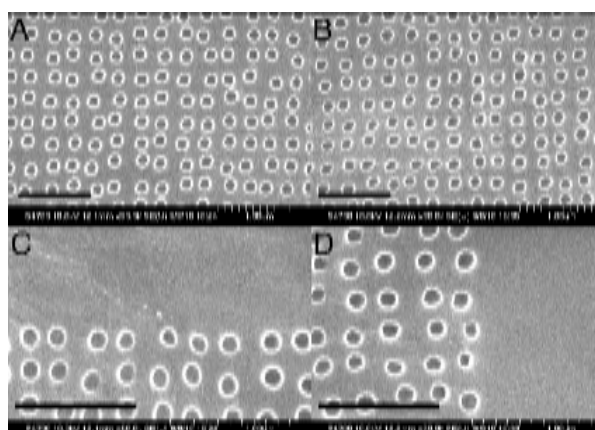


Figure 2.11 SEM images of the NSQ50 nanoembossed substrates. Image A shows The NSQ 50 embossed region of a substrate and image B the other side of the same substrate. Images C and D include a junction between the NSQ50 nanoembossed and planar regions. Two magnifications are shown in this figure and the scale lines in each image represent 1 μm .

AFM analysis of the dual embossed nanopit (NSQ50) substrates

AFM images revealed successful reproduction of the nanopit topography with its associated controlled disorder of pit placement on the PCL and HAPCL (figure 2.14 images B and D). The surface roughness (RMS) of planar HAPCL (RMS 15.6

nm \pm 3.2) was greater than planar PCL (RMS 11.0 nm \pm 6.5). The surface roughness of nano-embossed HAPCL (RMS 25.8 nm \pm 1.5) was greater than the nanoembossed PCL (RMS 11.4 nm \pm 1.5).

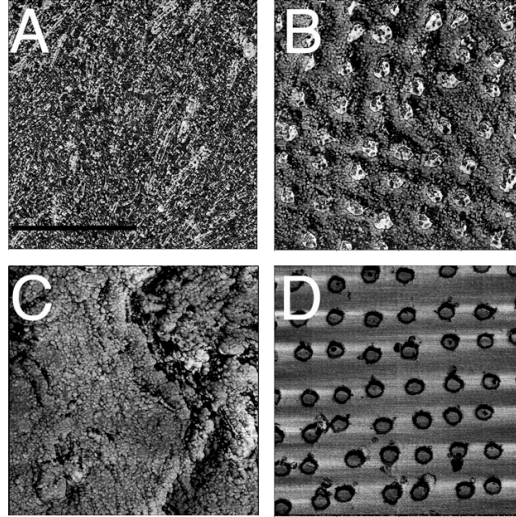


Figure 2.12 AFM images of Planar and NSQ50 embossed PCL and HAPCL. These images taken after 28 days exposure to air under standard incubator conditions show a difference in appearance between the planar PCL (image A), planar HAPCL (image C) and nanoembossed PCL and HAPCL (images B and D respectively) substrates. The controlled disorder of the nanopits is apparent. A 2 μ m scan size was used. Scale bar 1 μ m.

2.3.2 Acellular assessment of substrate degradation

AFM images taken after a 28-day period of exposure to air, media and SBF (under standard incubator conditions) revealed changes in the appearances the planar and nanoembossed topographies (figures 2.12-2.14). The NSQ50 topography appears much clearer following exposure to SBF (figure 2.13) in comparison to basal media (containing FBS) (figure 2.14). It is postulated that protein deposition on the substrates may be the cause for the smaller appearances of the nanopits seen on images 2.14B and D, in comparison to those on figures 2.12 and 2.13, images B and D.

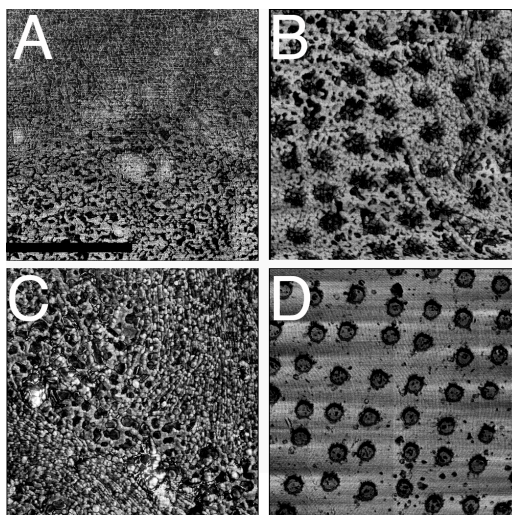


Figure 2.13 AFM images after a 28-day period of exposure to SBF. The random topography of the planar PCL (image A) and planar HAPCL (image C) after this period of time and the controlled disorder of the NSQ50 PCL and HAPCL (images B and D respectively) substrates are shown. Scale bar 1 μm .

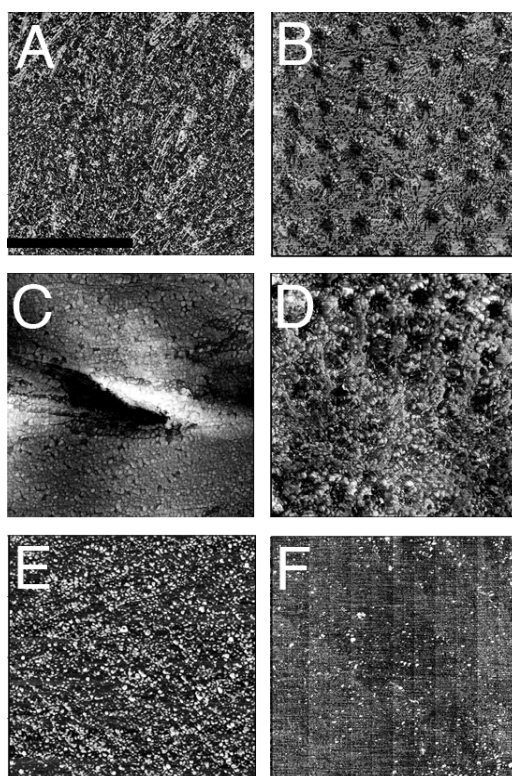


Figure 2.14 AFM images after a 28-day period of exposure to media. The random topography of the planar surfaces (images A, C, E and F) after this period of time and the controlled disorder of the NSQ50 topography (images B and D) are appreciable on both the PCL and the HAPCL. The images were taken as follows: image A planar PCL, image B NSQ PCL, image C planar HAPCL, image D NSQ50 HAPCL, image E planar PCL exposed to BMP and image F planar PCL kept in osteogenic media. Scale bar 1 μm .

RMS values were obtained using AFM (figure 2.15). The differences in RMS were compared by topography type and between substrates using single factor ANOVA. After 28 days exposure to basal media (containing FBS) the differences between topography/substrate types were statistically significant ($p < 0.05$). The RMS of NSQ50 PCL was statistically significantly different ($p < 0.05$) after 28 day exposure to each condition (air, media and SBF). 28 day exposure to media was associated with a reduction in the RMS of the NSQ50 surface that may be due to protein deposition on the substrate surface.

The RMS value of the planar substrate exposed to BMP containing media for 24 h and then air for 27 days had a surface roughness ($8.3 \text{ nm} \pm 4.3$) between that of planar PCL exposed to air ($11.0 \text{ nm} \pm 6.5$) and that kept in media ($6.4 \text{ nm} \pm 5.2$) for this period.

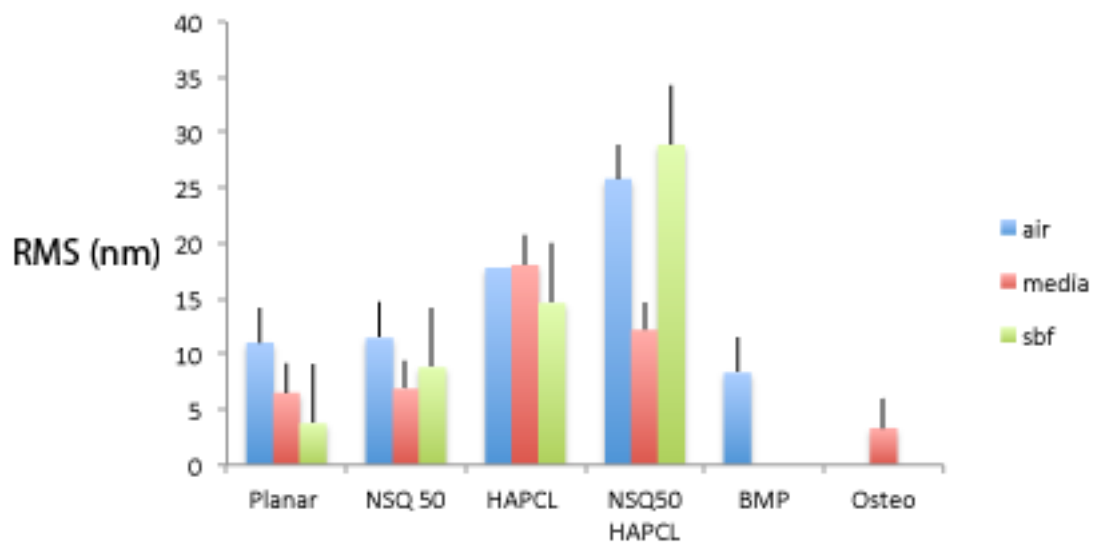


Figure 2.15 Surface roughness of PCL and HAPCL substrates after 28 days exposure to air, media and SBF. The average RMS of substrates ranged between 3 and 30 nm. Standard error bars are shown (number of repeats (n)=1-5).

2.3.3 HBMC acquisition

Bone marrow harvests, cell separation and HBMC culture, using my modification of the technique described by (Caterson et al., 2002), was successful and resulted in multiple yields. The spherical HBMC imaged at two days (figure 2.16A) are spread and proliferating by 28 days (figure 2.16B). A typical yield from one bone marrow aspirate was 60×10^4 cells at 28 days. Transfer into two 75 cm² flasks at 80 % confluence increased the yield to 172×10^4 and 230×10^4 cells at 8 and 9 weeks culture respectively. Cell culture from bone spicules was successful and the cells obtained were used in latter protocol development experiments. Images taken at 38 and 56 days are shown in figure 2.16 images C and D.

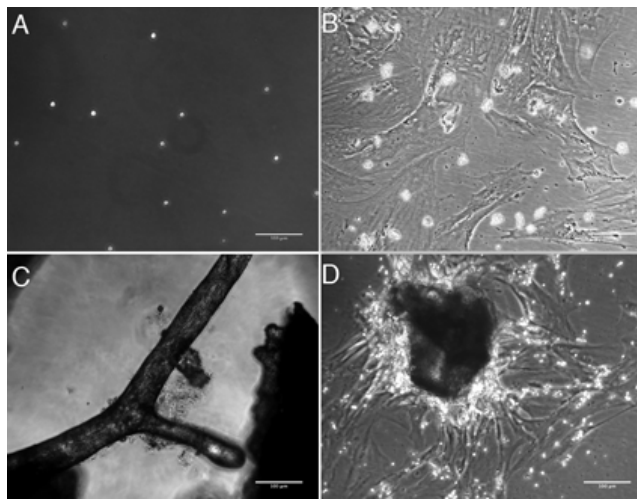


Figure 2.16 HBMC from bone marrow and fragments. HBMC cultured from human bone marrow aspirate (after separation using the Ficoll gradient) spherical at 2 days (A) have proliferated and spread by 28 days (B). Images C and D show cells growing from a bone spicule at 38 days and radially from a cancellous bone fragment at 56 days. Scale bars 100 μ m. No staining was used.

Multiple bone marrow samples were processed during this research. Qualitative assessment of this suggested that yields obtained from aspiration of bone marrow released by rasping the femoral canal resulted in greater initial yields (at the time of separation by adherence to plastic) than the bone marrow obtained by aspiration from the cut femoral neck using a syringe and 19 gauge (1.1 mm) white needle. The yield of cells from hand cut bone chips were greater than that obtained from acetabular reamings.

2.3.4 Single sided cell culture

My initial pilot studies used HTERT fibroblasts and a single sided culture protocol to allow for rapid seeding observations. The difficulties encountered during the dual sided culture within the rotatory bioreactor (chapter 2.3.5) led to the expansion of my pilot studies to include cell adhesion time, plasma treatment of PCL, the choice of PCL, and its soaking in methanol prior to use.

Cell culture on planar and nanoembossed PCL substrates (piloted using the HTERT cell line and a seeding density of 2.5×10^4) revealed cell adherence after 30 min (figure 2.17). The Coomassie blue stain used was associated with a degree of background colouration on light microscopy (figure 2.17A). The HTERT were clearly visualised on seeded samples. A profound increase in confluence was noted at four days on the 14 nm nanoisland substrates (figure 2.17D).

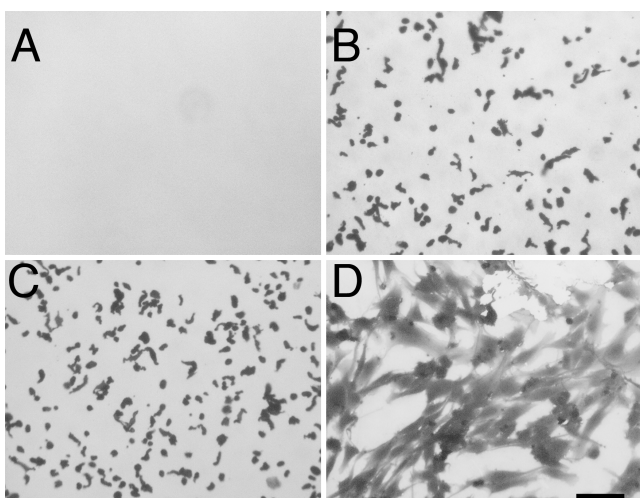


Figure 2.17 Coomassie blue staining of HTERT at 30 min and 4 days. Image A shows background staining of PCL with Coomassie blue on an unseeded surface. Image B shows HTERT 30 min after seeding on planar PCL, and image C on 14 nm nanoisland embossed PCL. Image D shows the confluence of the HTERT after 4 days static culture on the 14 nm nanoisland topography. Scale bar 100 μm .

Comparisons of HTERT adherence on PCL with and without prior plasma treatment using different seeding densities revealed greatest confluence after 15 s plasma treatment and after seeding at a density of 10×10^4 /ml (figure 2.18D). Plasma treatment was subsequently noted to alter the topography of the PCL when assessed using AFM.

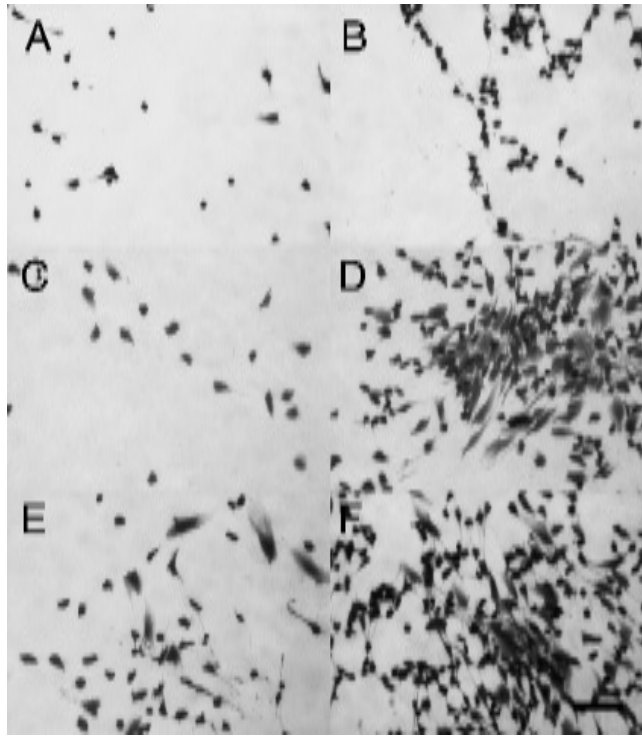


Figure 2.18 Coomassie blue images of HTERT using varied seeding densities and plasma treatment of the substrates. HTERT seeded at 5×10^4 /ml were associated with a lower cell density (images A, C and E), than when seeded at 10×10^4 /ml cells (images B, D and F). Plasma treatment of 5 s (images C and D) and 15 s (images E and F) was associated with markedly increased cell number and cell spreading of these planar substrates at 5 days in comparison to the control (A and B). Scale bar 100 μ m.

2.3.5 Cell culture on dual sided substrates

Simple turning regimens were piloted in addition to culture in the rotary bioreactor and the suspension/vertical culture techniques (chapter 2.2.5).

Static culture

Dual sided seeding of HTERT (chapter 2.3.4) in association with horizontal culture in a well plate (for 5 days) was associated with marked variation in cell confluence across the upper and lower substrate surfaces. Cell location was also dependent on the position with respect to the central or peripheral location visualised on the surfaces resting on the well floor.

HTERT cultured on the uppermost surface of nanoembossed PCL were significantly more confluent by 5 days as illustrated by figures 2.19B (peripheral) and D (central). HTERT cultured on the undersurface of the nanoembossed (NSQ50) PCL facilitated cell survival and cell spreading solely at the periphery (fig 2.19A) whereas the staining on the central region of the lowermost surface appeared more like cell debris with no evidence of cell spreading or cell division (fig 2.19C) (resting on the well floor).

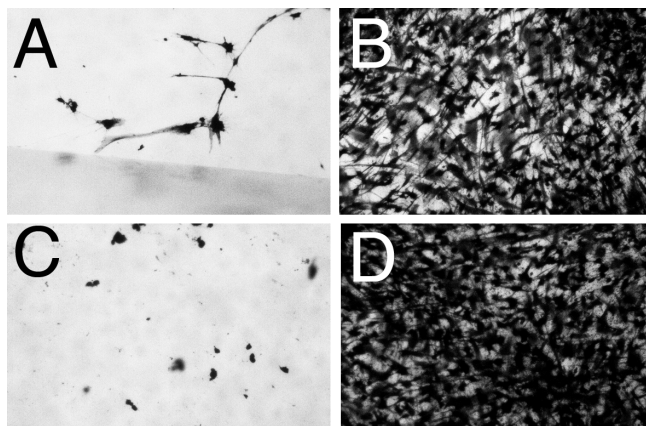


Figure 2.19 Dual sided culture of HTERT on nanoembossed PCL. HTERT confluence in the central and peripheral regions of the nanopit (NSQ50) embossed PCL at 5 days is evident on the uppermost surface following Coomassie blue staining. HTERT were significantly less confluent on the periphery of the lower most surface (A) and staining centrally gave the appearances of debris only (C). Scale bar 100 μm .

Rotatory bioreactor and static culture with turning over of substrates

During the first pilot study the rotation rate was set to optimize separation of the substrates.

Coomassie blue staining of MSCs seeded onto planar substrates and cultured for 48 and 56 h showed the cells to be attached and well spread (figure 2.20A and B). Planar PCL seeded in a similar fashion, placed in the bioreactor (chapter 2.2.5) and imaged at 48 and 56 h respectively revealed coomassie blue staining of protein or cell debris that appeared residual in nature (figure 2.20C and D). The cell spreading and increased cell confluence associated with the static culture plus turning (with turning over at 24 h intervals) was not present after culture within the rotatory bioreactor despite a low revolution rate (7.3 rotations per minute (r.p.m.) and minimisation of contact between substrates. Comparison of figure 2.19A and B with figure 2.20A and C suggests that the phenomenon of reduced cell survival in the lowermost central region of a dual sided PCL surface is overcome by turning over of the substrate at 24 h intervals.

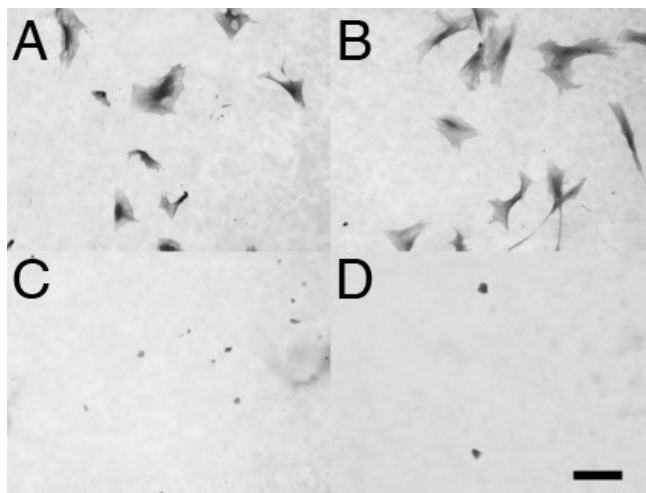


Figure 2.20 Static (with turning) and rotary bioreactor dual-sided culture of HBMCs. Coomassie blue staining of MSC after dual sided seeding with daily turning over in a well plate (images A and B) and continuous rotation in a bioreactor (images C and D) revealed well spread cells following the static culture and the suggestion of cell residue only on substrates cultured within the bioreactor. This was seen at both time points (images A and C taken after 48 h and B and D after 56 h). Scale bar 100 μ m.

Suspension Culture

Macroscopic imaging of samples (at day 21) revealed positive Coomassie blue staining on both surfaces of each substrate. Figure 2.21 illustrates, using scanned images, the aggregation of staining at the pole opposite to the suspension hole. This phenomenon was more pronounced on the planar sample (A) than the embossed surface (B) upon which the staining appeared more congruent. Macroscopic and microscopic analyses of Coomassie blue stained samples at 21 days revealed aggregation of HBMC in gravity dependent positions (figures 2.21 and 2.22). On both substrates cells were visible adjacent to suspension points, the holes made by the suture needle at the time of suspension on the sterile suture or ‘washing line’ (figure 2.21). On the planar surfaces the cells were primarily located and relatively confluent in gravity dependent regions (figure 2.21 and 2.22 C and D). In general on the embossed surfaces cells were more evenly spread over both surfaces (figure 2.22 H) although a few small areas of confluence were present (figure 2.22 G).

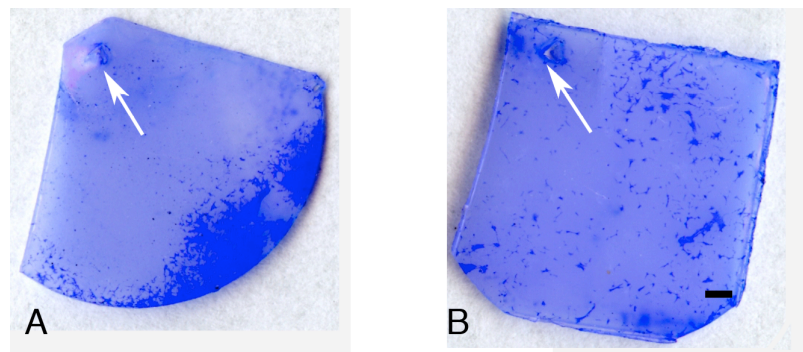


Figure 2.21 Macroscopic images obtained after suspension culture. These scanner images show the holes (white arrows) through which the suspending suture had been passed and cell spread 21 days after dual sided seeding (1.25×10^4 cells per side). Image A shows aggregation of cells in the lower gravity dependent regions on the planar control and image B a more even distribution on the embossed surface. Scale bar 10 mm.

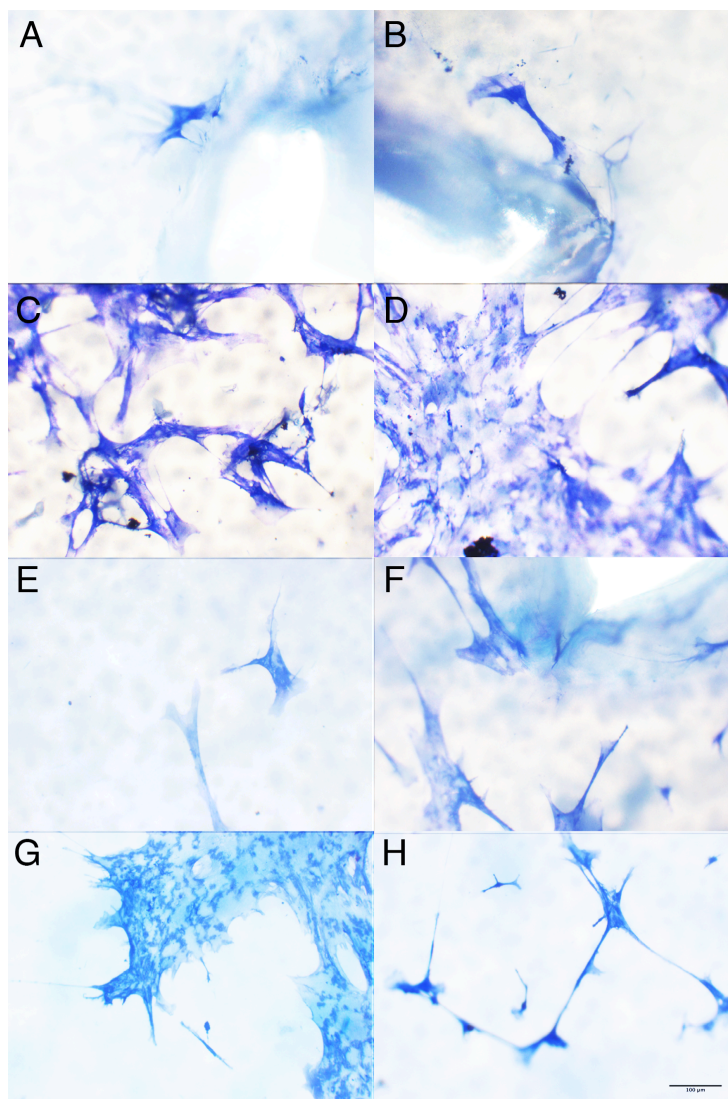


Figure 2.22 Coomassie blue staining following suspension culture. Images obtained at 21 days from one surface of a planar substrate, A (upper half) and C (lower half), are paired with images of the other surface, B (upper half) and D (lower half). Similarly images E and G from one surface of a nanoembossed substrate and F and H the other. Increased HBMC confluence at the lower or gravity dependent regions was more notable on planar substrates (images C and D) in comparison with the nanoembossed surfaces (images G and H). Image G shows that areas of confluence can be found in the lower regions of the nanoembossed substrates, overall these were not common. Scale bar 100 μm .

Temporal and cellular aspects of the substrate suspension technique

HOBs harvested at monthly intervals from bone fragments (chapter 2.2.4) and culture-expanded were used successfully in the temporal analysis of the gravity dependence. At seven days the tendency of HOBs to gather on the gravity dependent regions of the planar substrates was greater than on the NSQ50 substrates (figure 2.23).

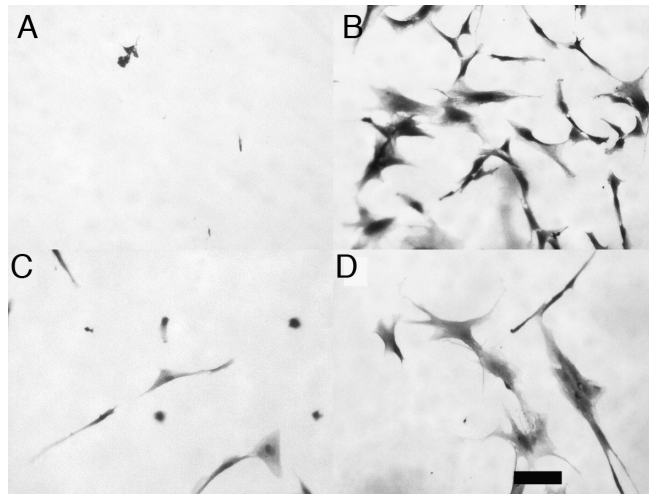


Figure 2.23 Coomassie blue images after 7 days. Cells are gathered on the lower (B) 1/3 of the planar substrate in comparison to the upper 1/3 (A). Greater numbers of HOBs remained in the upper 1/3 (C) of the nanoembossed substrate in comparison to the planar version (A). HOBs obtained from bone fragment culture were seeded at 2×10^4 per side following 5 s plasma treatments of the PCL.

At 14 days the tendency for cells to migrate downwards and aggregate in gravity dependent positions on the planar surfaces appeared enhanced. Significantly increased cell numbers were apparent (figure 2.24 image B) than had been at day 7 (figure 2.23B).

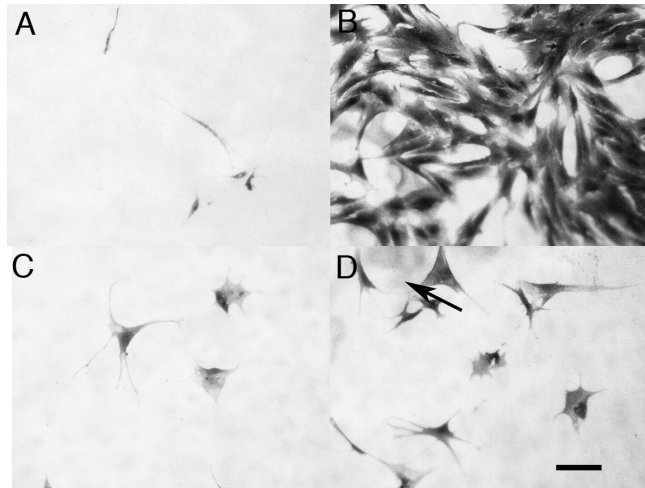


Figure 2.24 Coomassie blue images after 14 days. Coomassie blue images of HOBS cultured using the suspension technique show a gravity dependent position at 2 weeks, especially on the planar surface. Image B shows the propensity of HOBS on the lower half of the planar scaffold, with image A showing few remaining cells on the upper half. The HOBS were more widely spread on the NSQ50 scaffold as illustrated by images C and D. Show through of staining from cells on the contralateral side is shown in the upper left corner of image D (arrow).

Alizarin red staining

It was noted that staining with alizarin red (chapter 2.2.6) at early time points 7-21 days was associated with the identification of deposits which appeared indistinct from stained particles. A decision was taken to counter stain with Coomassie blue and the images obtained were the definitive images and are therefore shown in chapter 3. The deposits were successfully delineated using a combination of filtering the stain, and counterstaining for one min with Coomassie blue (figure 3.3). At 28 days counter stain was not required and cell morphology could be seen directly with alizarin red (figure 3.3).

Immunofluorescence staining

HOBS seeded on both sides at a seeding density of 1.25×10^4 cells per cm^2 substrate per side and were successfully stained using streptavidin for actin, fluorescein for OPN and OCN, and DAPI for nuclear material (chapter 2.2.6).

Immunofluorescence show-through from the other substrate surface created difficulties in the production of clear images. The streptavidin and fluorescein images have been superimposed (figures 2.25 and 2.26). Cells cultured on planar and NSQ50 substrates produced OPN (fig 2.25 images A, B and C). The protein distribution paralleled that of the cells. A moderate confluence was evident on the middle 1/3 of the embossed surfaces and high confluence on the lower 1/3 of the embossed and planar surfaces.

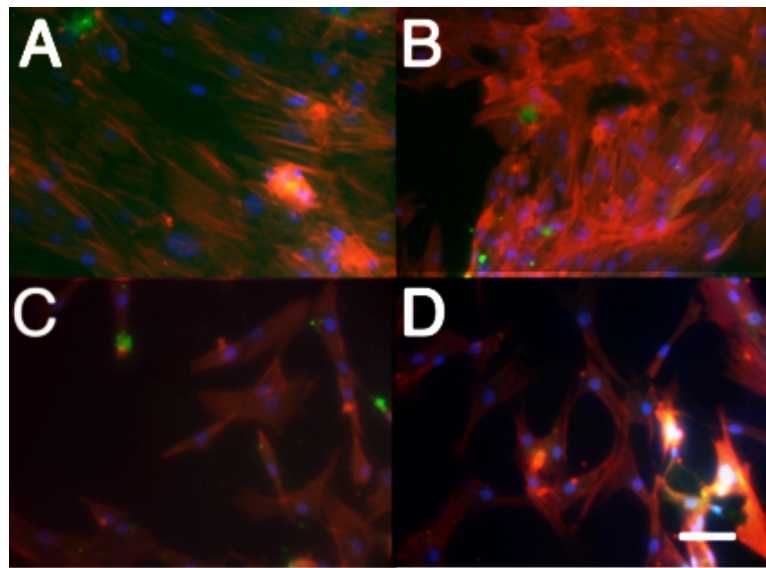


Figure 2.25 OPN immunofluorescence after 3 weeks. The greatest cell numbers were seen in image B, the lower half of the planar control following the three weeks suspension culture. The HOBS were more diffusely spread on the NSQ50 nanoembossed surfaces, although increased cell numbers were still seen in the lower half (image D) in comparison to the upper half (image C). OPN, evident as positive staining with fluorescein, was produced by HOBS on both substrates (images A, B and C). Actin red, OPN green and scale bar 100 μm .

The bone specific protein, OCN, was produced by HOBs on both the planar and NSQ50 substrates (figure 2.26 B and D). The protein distribution paralleled that of the cells, with a moderate confluence over the middle 1/3 of the embossed surfaces and high confluence in the lower 1/3 of the embossed surfaces and

planar controls. The interface between cells and no cells was much wider over the embossed surfaces, in comparison to the planar controls.

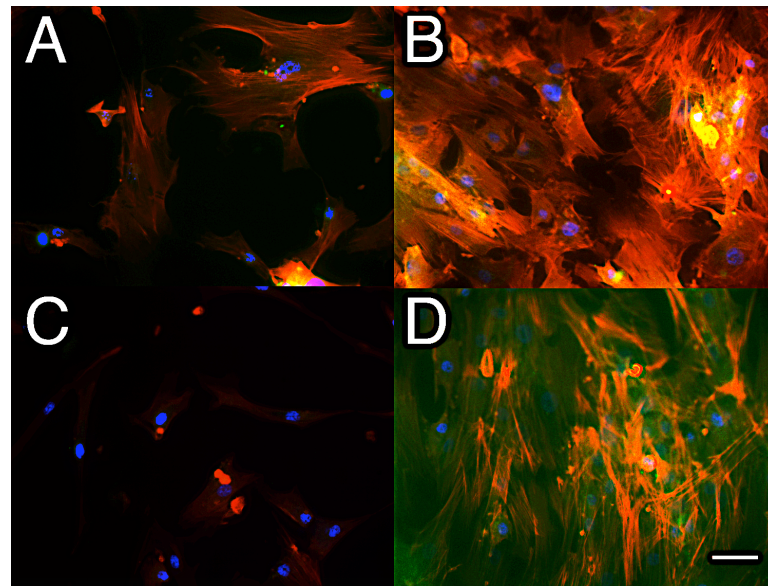


Figure 2.26 OCN immunofluorescence after 3 weeks. Greatest cell numbers are seen in image B, the lower half of the planar control. The cell spread on the NSQ50 (images C and D) was more diffuse, although an increased cell number is still seen in the lower half (image D) in comparison to the upper half (image C). Actin red, OCN green and scale bar 100 μm .

Some yeast infections were encountered during the period of investigation using suspension culture. My development of the alternative technique of vertical culture (without the need for suture material) was associated with an eradication of problematic yeast infections. In the final protocol substrates were turned over 180° (about the horizontal) at 7 day intervals.

2.3.6 RNA extraction optimization

Two methods of RNA extraction were trialled, direct cell lysis and the indirect method of cell harvesting prior to cell lysis. Calculations of the probable cell density at the times of harvest were used to calculate the mixture requirements (chapter 2.2.7) and revealed the necessity of maximizing the mRNA yield for each sample. Direct cell lysis was the method of choice in minimising the risk of

cell loss. Four dual sided substrates or six single sided substrates were required to produce sufficient mRNA in each extraction. Table 2.1 shows the RNA yield from 12 μl of RNA following 33 days single sided culture of two planar substrates. Table 2.2 shows the RNA yield following 28 days culture of four double-sided 1 cm^2 substrates. 11 μl of RNA was extracted.

The importance of mRNA integrity was highlighted by my pilot experiments and I decided to obtain four mRNA samples per substrate type and progress the optimal three to RT, facilitating the use of mRNA from an experiment in which 1 mRNA sample was suboptimal. The RNA yield, and integrity 260 and 280 values are tabulated in the appendix for each of the definitive qPCR experiments.

Coomassie blue staining of substrates following cell/mRNA harvesting revealed residual protein, following either agitation of the substrates or the use of TV alone. TV exposure for 10 min accompanied by agitating the substrates on the base of a well plate stopped this phenomenon.

Substrate	ng/ μl	ng RNA
HAPCL planar 1	1.63	19.6
HAPCL planar 2	3.98	44.2
BMP Rx 1	2.67	32.0
BMP Rx 2	2.90	34.8
Osteo 1	2.01	24.1
Osteo 2	0.48	5.76

Table 2.2 RNA yield at 33 days, single sided culture combining two planar substrates. 12 μl of RNA was extracted.

Substrate	ng/ μl
Planar PCL + DMEM	215.66
Embossed PCL + DMEM	207.70
Planar PCL + Osteogenic Media	132.98
Embossed HAPCL + DMEM	171.41

Table 2.3 RNA yield at 28 days, double sided culture of four substrates. 11 μl of RNA was extracted.

QPCR

The results of the qPCR are detailed in chapters 3 and 4. Initially SYBR green primers and probes and Taqman primer-probes were trialed and I noted that the results of the Taqman primer-probes were more consistent and therefore these were used throughout the definitive experiments.

2.4 Discussion

The definitive protocol was a product of the pilot studies and results outlined (chapter 2.3). This discussion highlights some of these results and my understanding of the probable causes behind the differences noted and the choices ultimately contributing to the definitive protocol. The development from pilot to definitive protocol formed a continuum up until the definitive results (chapter 3 and 4) were gathered. For reasons of clarity the results (chapter 2.3) are not presented in the temporal order according to which they were applied. The difficulties in seeding and cell culture in the rotatory bioreactor led to the cell attachment experiments.

2.4.1 Shim manufacture, substrate preparation and acellular analysis

PCL

Following the initial period of protocol development changes in the PCL available from the supplier resulted in difficulties in manufacturing homogeneous PCL sheets (without spaces and or air bubbles). The problems related to retention of the outer surface of the PCL beads on melting. Instead of a wet melt being achieved and thumb pressure creating homogeneous circular substrates, compression between two microscope slides created the appearance of a cracked shell with a macroscopically apparent topography of its own. Multiple different molecular weight PCLs were trialed and PCL with a number average molecular weight (M_n) of 60000 was chosen. I combined this PCL choice with soaking in methanol for 1 h and drying prior to processing. This combination produced a wet melt and homogeneous PCL sheets once more.

Hot embossing

Cold glass slides applied to a PCL wet melt was associated with uneven solidification of the PCL and a potentially uneven surface. I prevented this by warming the top slide prior to hot embossing and slow cooling on the metal fume hood surface.

PCL handling and sterilisation

PCL substrates were noted to scratch when stored in petri dishes and when handled. PCL samples were therefore moved using 21 gauge (0.8 mm) needle tips or forceps at the edge of each substrate and handling was minimised. Storage of PCL sheets was between the glass slides. I protected the integrity of experimental surfaces by storing dual embossed substrates vertically in well plates. Prolonged exposure of PCL to ethanol caused visible disruption of the PCL integrity. I limited substrate sterilisation to 1 h and this ceased. Washing substrates with HS without drying them first was associated with substrates floating and HS not mixing with the surface ethanol. Drying of the ethanol was noted to leave deposits on both petri dishes and substrates. I dried the substrates vertically and reduced both of these problems.

AFM images of all NSQ50 nanoembossed substrates reveal the presence of the nanopits. The clarity of the pattern on the substrates after 28 days exposure to air, FBS containing media and SBF was seen to vary. After 28 days exposure to basal media (containing FBS) the differences in RMS between topography/substrate types were statistically significant ($p < 0.05$). Differences in surface roughness attributable to surface topography and surface chemistry can be associated with different RMS values however 2 very different looking surfaces may have the same RMS value, this appears to be true when comparing my RMS values and the AFM and SEM images (figures 2.11 - 2.15). Embossing of the NSQ50 to the surface did not dramatically change the RMS measurement despite AFM and SEM images revealing the nanoembossed pattern. AFM analysis revealed that the roughness of planar and NSQ50 HAPCL was greater than the PCL equivalents.

The RMS of NSQ50 PCL was statistically significantly different ($p < 0.05$) after 28 day exposure to each condition (air, media and SBF). 28 day exposure to media was associated with a reduction in the RMS of the NSQ50 surface that may be due to protein deposition on the substrate surface. I believe that whilst RMS is universally used for topographical description it has limitations with respect to the detection of nanopits of this size.

2.4.2 Human bone marrow aspiration and HBMC acquisition

HBMC separation

Blood clots were associated with a reduced clarity of layering in the density gradients. Bone marrow samples were processed as early as possible, and I added the anticoagulant ethylenediaminetetraacetic acid (EDTA) to the transport media in order to minimise clot formation. Aspiration of clots was avoided. When layering onto the Ficoll-Paque I avoided mixing of the layers by slowly pipetting down the side of a near horizontal universal container. Aspiration of the supernatant media prior to collection of the media-Ficoll interface aided cell collection. The interface and up to 2.5 ml of associated Ficoll and media enabled harvesting of the visible cell layer.

HBMC adherence, culture and harvesting

I extended the initial period of three days prior to the first media change to five days. Cell adherence was noted from the supernatant media aspirated at three days. Alpha modified eagles medium (α MEM) was the medium of choice for HOBs when the initial experiments were undertaken (chapter 4) however laboratory policy changed and subsequent experiments were undertaken using modified DMEM using individual additives (such as nonessential amino acids).

HBMC harvesting using the recognised technique of flask irrigation with PBS followed by 4 min exposure to 4 ml TV was associated with minimal disruption of the adherent HBMCs. Irrigation with 4 ml Trypsin prior to incubation with 4 ml TV for 4 min maximised cell disruption. Microscopy following cell harvesting

revealed residual HBMC both adherent and non-adherent. Cell scrapers maximised cell detachment and using media to rinse flasks provided the media necessary to inhibit TV action during centrifugation and minimised loss of residual cells.

The paper by Tuli et al recommended a 20×10^4 cells per flask in order to maximise yield following HBMC culture (Tuli et al., 2003), whereas Sotiropoulou et al. recommended an initial plating of $38-75 \times 10^4$ cells per flask 75 cm^2 (Sotiropoulou et al., 2006). Trials of different flasks revealed increased adherence using thermolite (Thermo Fischer) flasks. This difference was greatest at the time of cell separation and therefore I used thermolite flasks at this stage and the standard 75 cm^2 flasks at the first passage.

HBMC yields were higher with an increased initial cell concentration. I noted that yields could be maximised by dividing the HBMC obtained from cell separation into two 25 cm^2 flasks for initial cell adherence and culture prior to combining into three 75 cm^2 flasks at the first passage. The yield after 1 passage was sufficient to facilitate an immunostaining or qPCR experiment.

Bone chips from the femoral head and rasping the femoral canal were associated with successful culture however those obtained from acetabular reamings were not. I suspect that the heat generated in acetabular reaming may be associated with cell death. Infection with fungi and or bacteria are noted in 1 in 3 bone donation samples on screening for clinical use (by communication with the National Health Service blood and transplant services). For this reason I doubled the dose of antibiotics and antifungals used in the transport medium. Harvesting from bone fragments was undertaken 4 times in accordance with the protocol described by Tuli et al (Tuli et al., 2003).

In view of the success of the HBMC acquisition and difficulties in ensuring or identifying fungal infection in bone fragment flasks following the pilot studies

HBMC became the cells of choice. I decided to use cells after passage 1 in order to minimise any potential for terminal differentiation prior to the experiments starting. Cell numbers were limited and qPCR was not possible on the same cell batch as the microscopy. The concept was tested with experiments that were repeated from bone marrow acquisition through to qualitative and quantitative results using multiple patient donors. HBMC culture using a mixture of different donors was not associated with cell detachment or cell death, however I chose not to use this technique for experiments in order to minimise the potential for discrepancies in the results.

2.4.3 Single and dual sided cell seeding and culture

Problems were found with cell culture within the rotatory bioreactor. Cell detachment was seen within the bioreactor even after successful seeding and initial culture in well plates. The cell detachment was not overcome by measures such as altering the speed of rotation or minimising the substrate number in each bioreactor. I decided therefore to investigate dual sided culture in well plates and experiments revealed that cell culture throughout the uppermost surface and at the periphery of the lowermost surface was possible using dual seeding and simple face-up culture techniques. Turning of substrates was successful in culturing cells on both surfaces but involved daily handling of substrates and I feared inoculation with infection and topography damage (cells had been noted to adhere to the topography around forceps marks).

Vertical culture using substrate suspension facilitated media access to both substrate surfaces and cell culture. I hypothesised that the increase in infection rate could be due to the threads passing over the wells and between substrates in addition to the use of HOBs from bone fragments. I developed vertical culture within smaller wells in order to remove the need for suture material. Gravity dependent positioning of the cells was noted after the first culture that was of 21 days duration. Further investigation revealed that turning over of substrates at weekly intervals minimised this and resulted in a more even spread across substrate surfaces.

The desire to maximise the number of substrate repeats and the number of control and test conditions possible for each experiment whilst only using cells from one bone marrow harvest rendered it necessary to develop a technique to maximise the cell density obtained from cell seeding. Following seeding with cells in a 1 ml suspension, cells were seen on light microscopy to adhere to the bottom of wells in addition to the surface of the substrate. I trialled a variety of cell suspension volumes and noted that a 65 μ l droplet of cells fully covered the surface of a 1 cm² substrate without seepage over the edge. After 30 min substrates were flooded with media for nutritional purposes.

Cell adhesion experiments revealed that cells were adherent within 30 min of seeding. However, I decided that in order to stabilise these adhesions 24 h would be left prior to turning over of the substrates to seed the second side and prior to placing in suspended or vertical culture. This technique was successful in producing cell attachment and cell culture without any cell detachment from the under-surface and facilitated the definitive dual sided culture experiments.

2.4.4 Coomassie blue and alizarin red staining

Coomassie blue staining facilitated all of my protocol developments. In the simplest experiments, Coomassie blue staining was combined with scanning of stained substrates to give a macroscopic appreciation of the cell spread. Coomassie blue and alizarin red staining resulted in the appearances of non-cell shaped deposits. I eliminated any doubt as to the origin of these by microfiltration immediately prior to use. Despite fixation (chapter 2.2.6) alizarin red resulted in detachment of the cell layer when irrigated with PBS. Dipping in Coomassie blue or ethanol prior to dipping in PBS stopped this. Co-staining with Coomassie blue facilitated a distinction between intra and extracellular calcium deposits at early time points and these were the images used as definitive figures in chapter 3 (figure 3.3).

Microscopy of both sides of stained substrates was limited by show through from the other surface. At low cell densities show through was seen whilst at higher cell densities problems were encountered with gaining adequate light passage through the samples. I limited the duration of Coomassie blue staining to reduce this.

2.4.5 Immunostaining and light microscopy

No problems were encountered with immunostaining and imaging the single-sided samples (results are seen in chapters 3 and 4). Dual sided samples stained for actin for periods greater than 7 days (at which time the cells were spread throughout the surfaces and increasing in density) were difficult to focus. It appeared that show through of fluorescence from the other side was again a problem. I diluted the antibody concentration and limited incubation to 1 h in order to minimise this. The immunostaining images were clearer when only the FITC staining was imaged and I kept records of both this and combination staining.

2.4.6 RNA harvesting, RT and qPCR

Calculations with regard to the number of substrates required to provide sufficient cells for RNA harvesting indicated that maximising the percentage yield was vital. The compromise I reached indicated that one 2.5 cm by 2.5 cm square or three 1 cm² substrates would provide sufficient RNA. A variety of methods of RNA extraction were used with different extraction kits. I observed that the yield following direct lysis was higher than that obtained from the two-stage indirect method in which cell lysis followed cell harvest. Direct experimental comparisons were not undertaken comparing the two techniques with the same HBMC population. The Stratagene kit was associated with a greater RNA yield than the Quantitect alternative. The Stratagene kit was thought from previous experience to be associated with less clogging of the cell column and higher RNA yields.

Following the loss of the results from one experiment purely as a consequence of one poor RNA sample, the numbers of each substrate were increased to allow RNA collection from four substrate groups per condition and the use of the optimal three for qPCR thereafter.

The difficulties experienced with the reproducibility of results within qPCR experiments were overcome in two ways. Taqman probes were associated with an increase in result consistency over the SYBR green alternative and I chose these for the definitive assays. The solutions were made up in bulk for each of the primer probes and the cDNA diluted into three wells for each. The three repeat option (as opposed to two repeat) was taken for all measurements. I undertook the greatest experiment sizes possible in order to maximise the number of genes tested for each control (GAPDH).

2.5 Conclusion

I have undertaken HBMC acquisition from the intra-operative bone marrow sampling through separation by Ficoll gradient and adherence to plastic to culture expansion and experimental use on test substrates. My careful optimisations and trials have led to established marrow isolation protocols now widely used in CCE. Robust data analysis of the cellular responses of NSQ50 and nanoislands, in comparison to osteogenic media, BMP2 exposure and HA inclusion within the PCL can be found in following chapters.

Chapter 3 Analysis of nanopit (NSQ50) embossed PCL

3.1 Introduction

In this chapter the effects of the NSQ50 topography on HBMCs are examined. The nanopits arranged in the near-square arrangement have been produced using EBL technology and reproduced in PCL and HAPCL (chapter 2.2). HA (used to enhance the stability of uncemented implants) has been shown to exhibit bonding osteogenesis after 10 days post implantation (Furlong and Osborn, 1991). BMP2 has found increasing interest for the management of bone defects, non-union fractures and spinal fusion (Chen et al., 2004). MSCs cultured *in vitro* using osteogenic (dexamethasone containing) media express those markers expressed by osteoblasts, the cells responsible for laying down bone matrix and mineral during bone formation *in vivo* (Birmingham et al., 2012).

The aim of the research within the following chapter is to culture HBMCs simply and reproducibly on two sides of PCL substrates and simultaneously use NSQ50 in order to quantify its potential osteogenic effect in comparison to the clinically used (BMP and HA) and *in vitro* alternatives (control conditions and osteogenic media).

3.2 Materials and methods

NSQ50 topography, produced through the use of EBL technology, was embossed onto PCL and HAPCL. Acellular analysis of the topography was undertaken with AFM and SEM (chapter 2.3). The cellular effect of the topography was studied using HBMCs in conjunction with immunocytochemistry, fluorescence microscopy and qPCR.

The NSQ50 shim was manufactured using EBL. In EBL an electron gun is used to “shoot” a beam of electrons (e-beam) in a specific direction. The emitter is heated to produce and excite electrons on the surface, following which application of a high voltage causes the excited electrons to accelerate towards a structure, or anode. By varying the voltage, the trajectory and the focus of the beam can be manipulated (Cheng, 2007). A system of lenses, within a vacuum,

has the ability to focus the electrons into a concentrated beam in a desired direction by a combination of electromagnetism and optics. Two electrostatically charged parallel plates result in an electric field capable of bending the beam in a desired direction (Cheng, 2007). After the beam is directed and concentrated by the optical column, it is focused on the surface. As with most lithography techniques, a substance covers the surface, a photoresist. High-energy electron bombardment causes bond breakage in the polymer and when the beam hits the surface, either an additive or subtractive reaction takes place. An additive writing method uses the electrons to induce a deposition of a compound on the surface. In the raster scan technique the e-beam is swept across the entire surface, pixel by pixel, with the beam being turned on and off according to the desired pattern. This method is easy to design and calibrate (Cheng, 2007).

In conventional EBL arrays of dots are designed as an array of circles. Our strategy was to effectively use a vector scan Leica EBPG5-HR beam writer as a raster scan tool. In this fast method the pattern is laid out as a rectangle and each shape is formed directly by a single exposure with a given spot size. Each shape is spaced by the beam step size (Gadegaard et al., 2003).

3.2.1 Shim manufacture

Nanopit topography (NSQ50)

Samples were made in a three-step process of electron beam lithography, nickel die fabrication and hot embossing. Silicon substrates were coated with ZEP 520A (a positive-tone resist) to a thickness of 100 nm. After the samples were baked for a few hours at 180°C they were exposed in a Leica LBPG 5-HR100 beamwriter at 50 kV. A 1 cm² area was efficiently patterned with 1-10 billion pits (Gadegaard et al., 2003). The spot size was 80 nm, resulting in pits with a diameter of 120 nm after embossing. The pitch between the pits was 300 nm. After exposure the samples were developed in *o*-xylene at 23°C for 60 s and rinsed in copious amounts of *iso*-2-propanol. Nickel dies were made directly from the patterned resist samples. A thin (50 nm) layer of Nickel-Vanadium (N-V) was sputter coated on the samples. This layer acted as an electrode in the

subsequent electroplating process. The dies were plated to a thickness of approximately 300 nm (Dalby et al., 2004a).

Polymeric replicas were made in PCL by hot embossing. Sheets of PCL were melted on a hot plate and the nickel die pressed by a thumb into it for about 10 s and then transferred to a water bath at room temperature to allow the sample to cool (Dalby et al., 2004a). Single and dual sided substrates were manufactured from PCL and HAPCL as has been described in (chapter 2.2.2).

3.2.2 Substrate conditions

All substrates were cultured in modified DMEM unless otherwise stated. Planar substrates were also cultured in osteogenic media. The use of planar PCL, NSQ50 PCL and osteogenic media was common to all experiments. Where indicated comparisons were also made to planar HAPCL, NSQ50 HAPCL and planar PCL using HBMCs with prior exposure to BMP2. BMP2 exposure was undertaken by adding 100 ng/ml of BMP2 to a 75 cm² flask of HBMCs 12 h prior to the cell harvest. The BMP2 containing media was removed at cell harvest.

3.2.3 Horizontal single sided culture for microscopy

HBMCs used were obtained from 2 source patients and concurrently culture expanded (chapter 2.2.4-2.2.5). HBMCs were cultured on planar PCL in DMEM and in osteogenic media. Comparisons were made to HBMCs cultured on NSQ50 PCL substrates, cultured on planar HAPCL substrates, and cultured following BMP2 exposure. Media changes were 50 % and undertaken bi-weekly in order to provide sufficient nutrients, retain exocytosed growth factors, and maintain surface wetness of the substrates. HBMCs were seeded at 2.5×10^5 per substrate (chapter 2.2.5).

The cells were fixed after 28 days. The cellular stains alizarin red (for 1 h) and Coomassie blue (for 1 s) (chapter 2.2.6) were used and images were taken using light microscopy. Substrates from each combination were immunostained for

actin, DNA and OPN or OCN (chapter 2.2.6). The surfaces were examined in their entirety and qualitative comparisons made for cell spread and stain intensity. The settings used for the capture of immunofluorescence images were kept constant.

3.2.3 Horizontal single sided culture for qPCR

Cell culture

The HBMCs used were obtained from locally sourced bone marrow and culture expanded (chapter 2.2.4-2.2.5). HBMCs were cultured on planar and NSQ50 PCL in DMEM for 7 days. Media changes were 50 % and undertaken bi-weekly. HBMCs were seeded at 2.5×10^5 per substrate (chapter 2.2.5) and 3 substrates used to harvest each sample.

RNA extraction

RNA was extracted using Stratagene RNA Miniprep (Agilent technologies) according to the manufacturer's protocol. The elution buffer was warmed to 60°C, in a water bath. 70 % ethanol was made using 30 ml 98 % ethanol and 70 ml RNase free water. Cell lysis was undertaken directly using 300 µl of lysis buffer/βME mix per well (in 6-well plates). Cell scrapers ensured maximal cell disruption. RNA collection was maximized by flushing the wells with a further 50 µl lysis buffer/βME. The lysate samples were passed 3 times through an 18 gauge needle prior to vortexing for 30 s.

DNase digestion buffer was added to RNA free DNase and gently mixed prior to pipetting 55 µl onto the matrix of each spin cup. The spin cups were placed in 1.5 ml centrifuge tubes and 30 µl of warmed elution buffer added to the matrix. A further 20 µl of warmed elution buffer was added, incubated at room temperature for 2 min and microcentrifuged for a further minute. The spin cups were discarded and the RNA analysed using the nanodrop 1000 prior to storage at -80°C.

RT

The 3 samples with the highest purity (230/280 ratio) and or concentration were used for RT and qPCR. Warming of the gDNA wipeout to 37°C until fully dissolved preceded vortexing. Flicking of the tubes mixed the reagents and centrifugation gathered the liquid at the base of each tube. The reagents were stored and the RNA thawed on ice. Appropriate volumes of RNA suspension and RNAase free water combined in 0.2 ml reaction tubes produced a suspension of 9.12 ng of RNA in 12 µl. gDNA wipeout (7x) (2 µl) was added to each suspension. Incubation was undertaken in the thermocycler at 42°C for 2 min.

Combination of 13.2 µl Ominiscript reverse transcriptase (QRTase), 52.8 µl Omniscript RT (ORT) buffer (5x) and 13.2 µl RT primer mix preceded placing on ice. 6 µl of this transcription mix was added to each reaction tube and mixed with the RNA suspension. The reaction tubes were replaced into the thermocycler at 42°C for 15 min followed by 95°C for 3 min. The DNA suspension was frozen at 20°C prior to use in qPCR.

QPCR

QPCR was performed using Taqman gene expression primers for BMP2, osteonectin and OPN. The Taqman gene expression assay protocol was followed for standard rate qPCR (chapter 2.2.9) and a 7500 Fast Real-Time PCR system (Applied Biosystems) used. Gene specific reaction mixes were made, vortexed for 30 s and centrifuged for 30 s. RT product (6.6 µl of cDNA suspension) was added to 59.4 µl gene specific reaction mix, mixed by pipetting and the tubes centrifuged for 15 s. 20 µl of the resultant suspension (per well) was pipetted into each of three wells in the reaction plate yielding 3 technical replicates for the 3 biological replicates. QPCR was undertaken in order to compare NSQ50 with the planar control. Target gene expression was normalised against GAPDH and comparisons undertaken using the T-test in Excel.

3.2.4 Vertical dual sided culture for microscopy

HBMCs were obtained from a single source patient and culture expanded (chapter 2.2.4-2.2.5). Cells were seeded (2.5×10^4 per substrate) using the standard seeding protocol for vertical dual sided culture (chapter 2.2.5). NSQ50 HAPCL with DMEM was added to the aforementioned five combinations of substrate and media, namely planar PCL, NSQ50 PCL, planar PCL in osteogenic media, planar PCL with BMP2 exposed HBMCs, and planar HAPCL (chapter 3.2.3).

Seeding of the second side was undertaken at 24 h and substrates were transferred to vertical culture in a 48 well plate after a further 24 h. Media changes were 50 % and bi-weekly. On day 14 the substrates were aseptically turned 180° across their horizontal axis. Cells were fixed *in situ* at 28 days (chapter 2.2.6). Substrates were stained using alizarin red (for 1 h) with Coomassie blue (for 1 s) (chapter 2.2.6). Immunostaining for actin, DNA and OPN or OCN and microscopy were undertaken (chapter 2.2.6).

3.2.6 Vertical culture for immunofluorescence analysis of phenotype

Four substrate media combinations (planar PCL, NSQ50, NSQ50 HAPCL, and planar PCL cultured in osteogenic media) were used and 2.5×10^4 cells seeded per substrate (chapter 2.2.5). FITC was used to stain for all markers of phenotype, in combination with specific antibodies for COL2a, MYOD, TUBB3, OCN, and PPARG. The settings for image capture were consistent for all images.

3.2.7 Vertical culture for qPCR

Cell culture

3.6×10^4 cells were used per substrate (1.8×10^4 cells per side) using the standard protocol (chapters 2.2.5 and 3.2.5). Four substrate media combinations were used (planar PCL in DMEM, NSQ50 in DMEM, NSQ50 HAPCL in DMEM, and planar PCL in osteogenic media). Sixteen replicates of each substrate were cultured. Cells were cultured for 11 and 28 days. On day 14 the 28-day substrates were aseptically turned 180° across their horizontal axis. Four substrates were used to harvest each RNA sample.

RNA extraction, RT and QPCR

The RNA extraction, RT and qPCR protocols were as described for the horizontal cell culture (chapter 3.2.4). QPCR was performed using Taqman gene expression assays for RUNX2, OCN (BGLAP), SOX9, MYOD, PPARG, GAPDH, and 18S. Three technical replicates for each of the 3 biological replicates were used. Target gene expression was normalised against GAPDH and 18S. Statistical significance was assessed using ANOVA.

3.3 Results

3.3.1 Single sided HBMC culture

HAPCL was the optimal substrate for both localised confluence and OPN/OCN production (figure 3.1). OPN immunofluorescence was also present on NSQ50 and following the use of BMP2 exposed HBMCs in combination with planar PCL. Planar PCL cultured in modified DMEM and in osteogenic media was associated with least OPN expression (figure 3.1). Similarly OCN was maximally visualized on the planar HAPCL substrates. OCN was expressed on NSQ50 and planar substrates seeded with standard HBMCs and BMP2 exposed HBMCs.

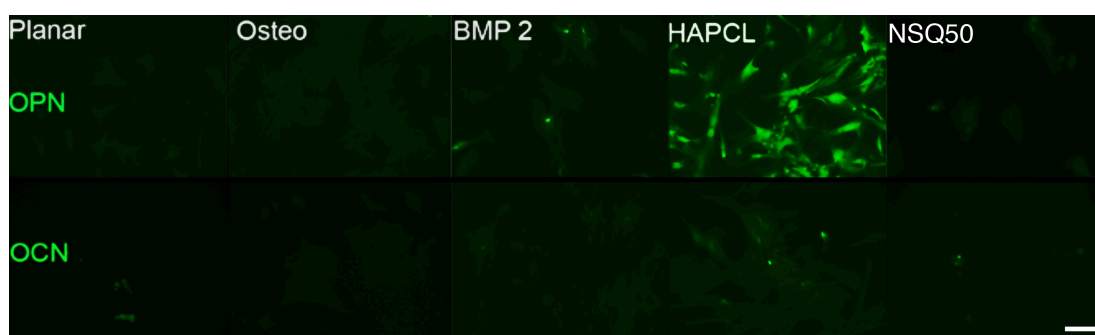


Figure 3.1 Immunofluorescence analysis of OPN and OCN expression. Positive staining for OPN and OCN was seen on all substrates. The relative abundance of OPN and OCN is indicated by colour intensity. OPN and OCN staining were maximal on HAPCL, on NSQ50 PCL and following BMP2 exposure on planar PCL at this 28-day time point. Scale bar 50 μ m.

After 28 days calcium staining was apparent on all substrates (figure 3.2). Osteogenic media and planar HAPCL (and to a lesser extent BMP2 stimulated HBMCs, and NSQ50) were associated with protein aggregates.

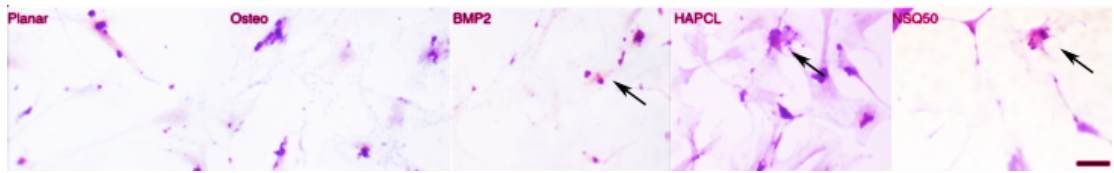


Figure 3.2 Coomassie blue cell staining and Alizarin red staining of HBMCs.

At 28 days staining of the NSQ50 substrates and planar controls using HBMCs from a locally sourced bone marrow sample revealed the presence of calcium on all substrates. Intracellular alizarin red staining (black arrows) was visualized the most on the planar PCL substrates. Aggregates of Coomassie blue staining are noted on the HAPCL and NSQ50 substrates. Scale bar 50 μ m. Blue = protein, Red = calcium.

3.3.2 Single sided culture for qPCR analysis of gene expression

At 7 days NSQ50 expressed significantly greater quantities of BMPR2, osteonectin and OPN. OCN was not expressed by HBMCs on either substrate (figure 3.3).

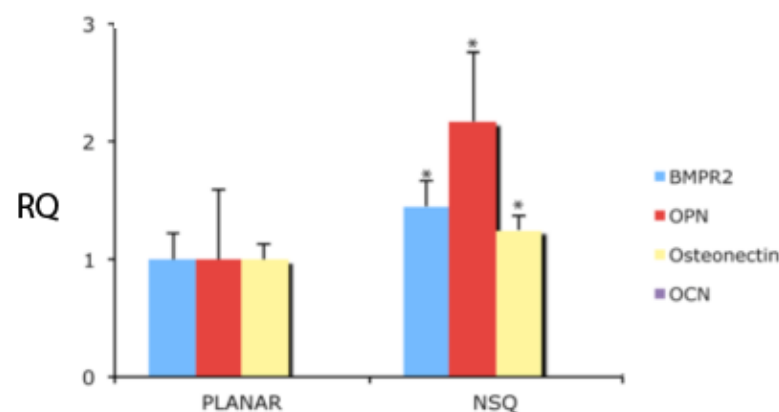


Figure 3.3 Relative gene expression at day 7. NSQ50 was associated with increased BMPR2, OPN and osteonectin expression after 7 days single sided horizontal culture of HBMCs. No OCN was detected. Statistical significance (t-test $p \leq 0.05$) is indicated by “*” when compared against the planar control surface and normalized against GAPDH. Standard error bars are shown (n=3). RQ: relative quantification.

The most immunofluorescently osteogenic material was HAPCL (Figure 3.1) and NSQ50 expressed significantly greater amounts of BMP2, OPN and osteonectin all of which are involved in osteogenic differentiation and expression (figure 3.3.). I chose to combine HAPCL with NSQ50 in the latter experiments in order to assess any enhancement of osteogenicity. The duration of Coomassie blue counter staining was reduced in order to reveal the location of calcium with respect to the cells, but without risking masking its presence with the intense areas of blue stain.

3.3.3 Dual sided culture and OPN, OCN and Alizarin red staining

Images of confluent regions revealed greatest OPN expression on NSQ50 HAPCL and NSQ50 PCL (figure 3.4B, F). OPN was clearly visible on the planar PCL cultured in osteogenic media (figure 3.4C) and from HBMCs exposed to BMP2. OPN immunofluorescence was least on planar PCL cultured in DMEM (figure 3.4A) and planar HAPCL. OPN expression was more widespread and at a lesser intensity across the planar HAPCL surface (figure 3.4E) than the NSQ50 HAPCL (figure 3.4F). OPN staining was both cytoplasmic and intra-nuclear in all samples (figure 3.4A-F). Aggregates of intense staining were seen with an increasing OPN expression.

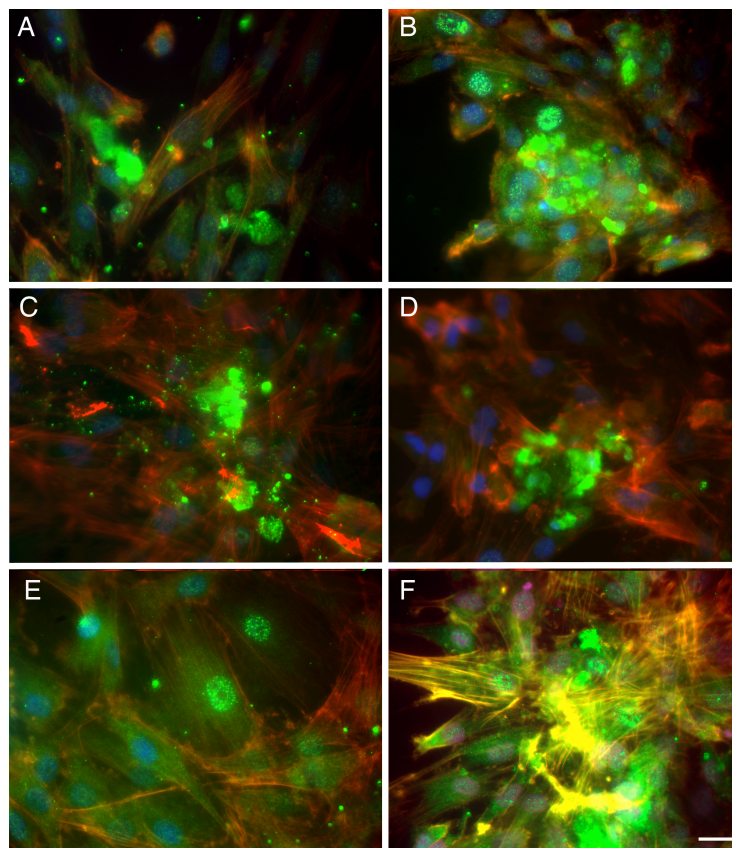


Figure 3.4 Immunofluorescence analysis of OPN expression. At 28 days the greatest OPN expressed was seen on NSQ50 HAPCL (Image F). Images A (planar PCL), B (NSQ50 PCL), C (planar PCL in osteogenic media), D (planar PCL with BMP2 exposed HBMCs), E (planar HAPCL) and F (NSQ50 HAPCL) reveal OPN expression on all substrates to a varying degree and in varying locations within the cells. Scale bar 50 μ m. Red = actin, Green = OPN, Blue=nuclei.

Imaging confluent regions of cells revealed that OCN expression was greatest on NSQ50 HAPCL (figure 3.5F), then NSQ50 PCL and planar HAPCL (figure 3.5B and E). OCN was seen to a lesser extent on the planar PCL surfaces with HBMCs exposed to BMP2 showing most OCN (figure 3.5D), then planar PCL cultured in osteogenic media (figure 3.5C) and in DMEM (figure 3.5A).

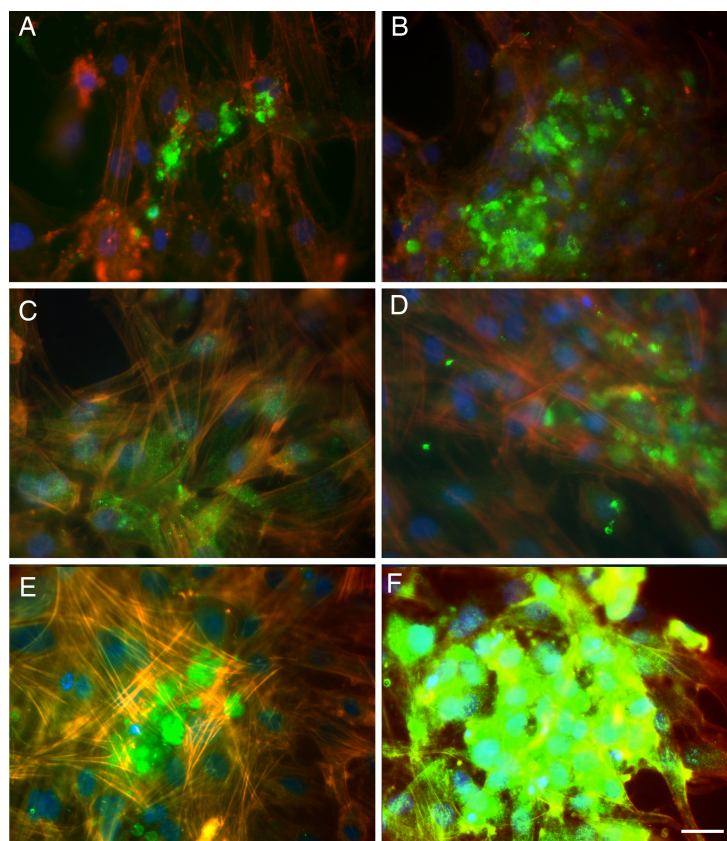


Figure 3.5 Immunofluorescence analysis of OCN expression. At 28 days the greatest OCN expressed was seen on NSQ50 HAPCL (Image F). Images A (planar PCL), B (NSQ50 PCL), C (planar PCL in osteogenic media), D (planar PCL with BMP2 exposed HBMCs), E (planar HAPCL) and F (NSQ50 HAPCL) reveal OCN expression on all substrates in varying locations within the cells. Scale bar 50 μm . Red = actin, Green = OCN, Blue=Nuclei.

OCN was cytoplasmic and nuclear following culture in osteogenic media (figure 3.5C) but nodular with less cytoplasmic staining after using DMEM only (figure 3.5A). OCN was widespread across the planar HAPCL surface (figure 3.5E) and at a lesser intensity to the NSQ50 equivalent (figure 3.5F).

At 28 days the Alizarin red staining of cells on the two NSQ50 nanoembossed substrates was greatest and was greatest on the HAPCL (figure 3.6). Staining of cells on NSQ50 was greater than that on planar PCL cultured in basal and osteogenic media. The staining on NSQ50 HAPCL and NSQ50 PCL, and using BMP2 exposed cells was more aggregated appearance than the less intensely stained alternatives (figure 3.6).

Microscopy of HBMCs cultured using the dual sided vertical technique described (chapter 3.2.5) revealed osteogenic expression by the HBMCs on both sides of the substrates (figures 3.4 - 3.6). Immunostaining using OPN, OCN and cell staining using alizarin red (chapter 3.2.6) has revealed that NSQ50 HAPCL was consistently associated with the greatest expression of the osteoblastic phenotype (OPN, OCN and Alizarin red) (figures 3.4, 3.5 and 3.6).

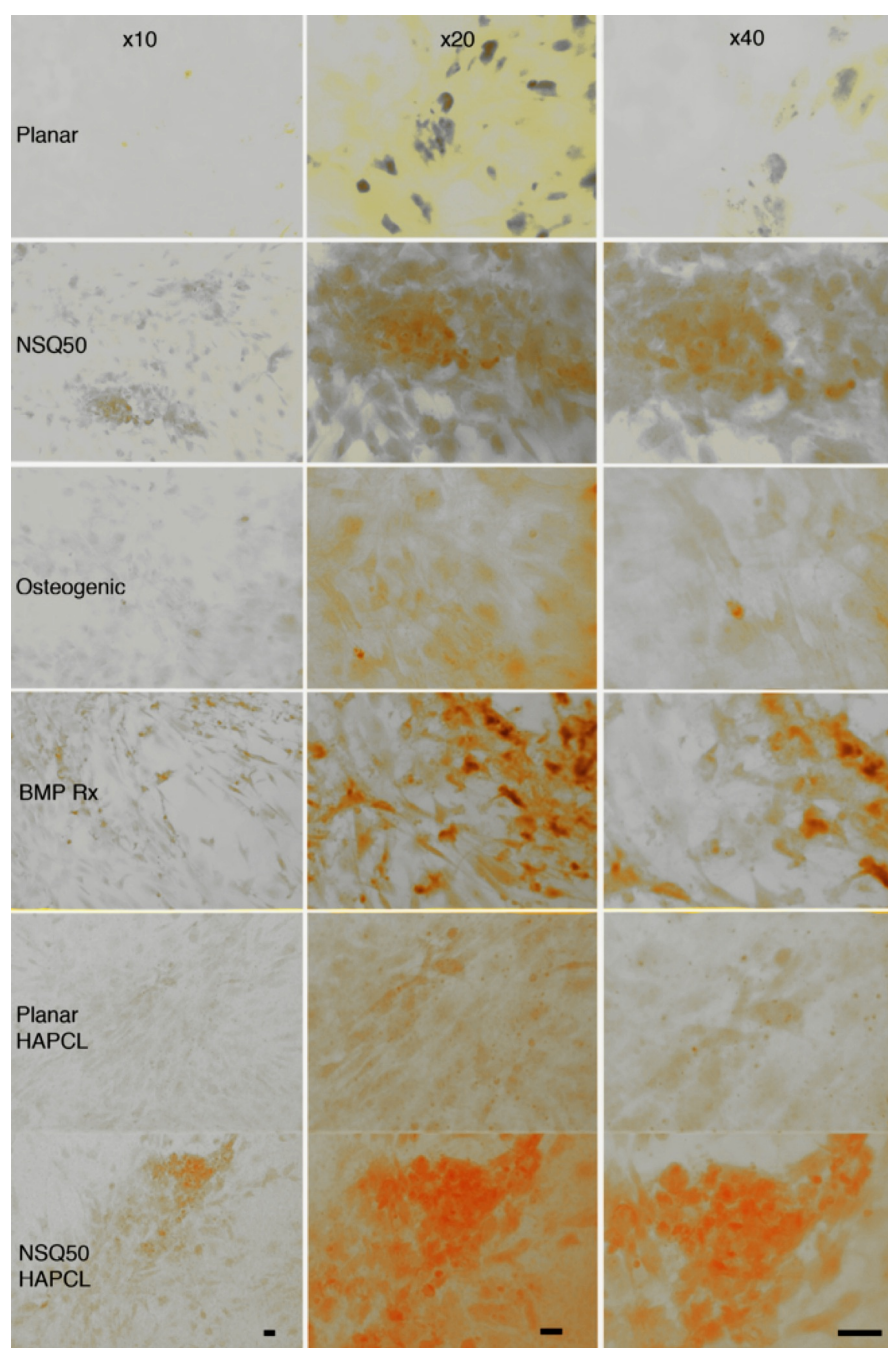


Figure 3.6 Analysis of calcium deposition at 28 days, following vertical culture of HBMCs. The greatest calcium deposition was associated with HBMC culture on: NSQ50 HAPCL, planar HAPCL, NSQ50 PCL and planar PCL with BMP2 exposure of HBMCs (BMP treatment (BMP Rx)). Scale bar 50 μ m. Red = Calcium.

3.3.4 Preliminary analysis of phenotype

In the assessment of phenotype, given the number of genes I plan to examine (both for screening markers of the predominant mesenchymal phenotypes and also for more detailed analysis of the osteogenic phenotype) I decided to limit the number of test substrates to four in order to make the experiments more manageable. The planar PCL control and the *in vitro* comparator osteogenic media were obvious choices. BMP2 exposure did not appear more osteogenic than NSQ50 on horizontal single or vertical dual sided culture I therefore discontinued its use. Planar HAPCL was less osteogenic than NSQ50 HAPCL and I made the decision to use NSQ50 HAPCL in the latter experiments. The four substrates chosen for the immunofluorescence analysis of phenotype were planar PCL, NSQ50 PCL, NSQ50 HAPCL, and planar PCL with osteogenic media.

Immunofluorescent analysis of phenotype at 21 days

Culture of HBMCs on all substrates was associated with expression of the bone marker OCN at 21 days (figure 3.7). Staining for the alternative phenotype markers was minimal; some PPARG staining was seen on the planar PCL and to a lesser extent the NSQ50. Pselectin, a marker of activated endothelial cells and platelets, was expressed solely on the NSQ50 HAPCL. The chondrogenic, myogenic and neurogenic markers COL2a, MYOD and TUB β_3 were universally absent. The images showing minimal or an absence of staining were not included (figure 3.7).

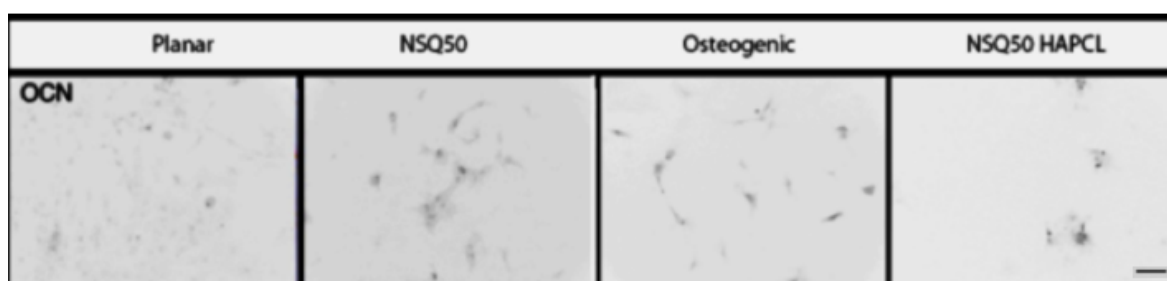


Figure 3.7 Immunofluorescence analysis of phenotype. OCN (black) is relatively scarce at this 21-day time point but is seen on all four substrates. Scale bar 50 μ m.

3.3.5 QPCR analysis of phenotype

At 11 days OPN expression was significantly increased by NSQ50 PCL and NSQ50 HAPCL relative to control (planar PCL) (ANOVA $p \leq 0.05$) (figure 3.8). The presence of HA in the PCL in association with the NSQ50 topography resulted in a further statistically significant increase in OPN expression compared to NSQ50 PCL without HA (figure 3.8). A lower OPN expression was noted on the planar PCL in the presence of osteogenic media (figure 3.8). The relative increase in OCN expression under all test conditions (compared to planar control) was significant (ANOVA $p \leq 0.05$) (figure 3.8). The rna yield and integrity is detailed in appendix 7 (table A1).

No statistically significant difference was seen in RUNX2 or TUB β_3 (neurogenic) expression between substrates. The reduction in SOX9 expression (compared to planar control) was statistically significant ANOVA $p \leq 0.05$) (figure 3.8). MYOD (myogenic) expression was universally absent (figure 3.8).

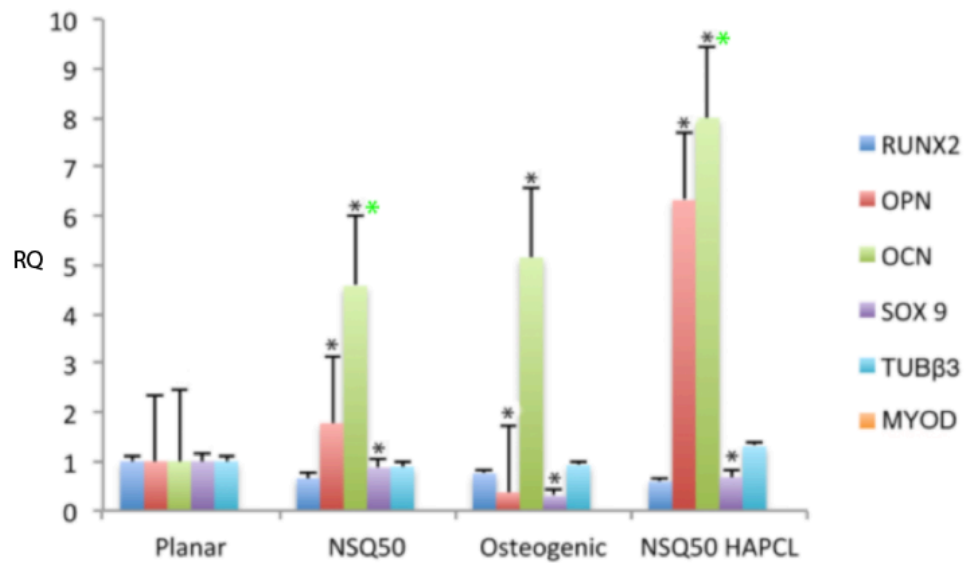


Figure 3.8 Relative gene expression at day 11. OPN expression was significantly increased by the NSQ50 topography using PCL and HAPCL. OCN expression was also increased by the use of osteogenic media. The relative gene expression after this dual sided vertical culture of HBMC was normalized against GAPDH. Statistically significant differences were identified between substrate types is indicated by “*” (ANOVA $p \leq 0.05$). A statistically significant difference was noted between NSQ50 and NSQ50 HAPCL with respect to OPN expression indicated by “**” (ANOVA $p \leq 0.05$). Standard error bars are shown (n=3). RQ: relative quantification.

The differences in gene expression seen in OCN and SOX9 expression at 28 days were statistically significant, however all of the differences measured were small and may not be clinically significant. The osteogenic marker OCN was reduced in association with the test conditions, indicating the transient nature of the comparatively elevated OCN at day 11, with respect to the planar control. The apparent increase in RUNX2 and reduced OPN expression on the NSQ50 topographies were not statistically significant (figure 3.9). The rna yield and integrity is detailed in appendix 7 (table A2).

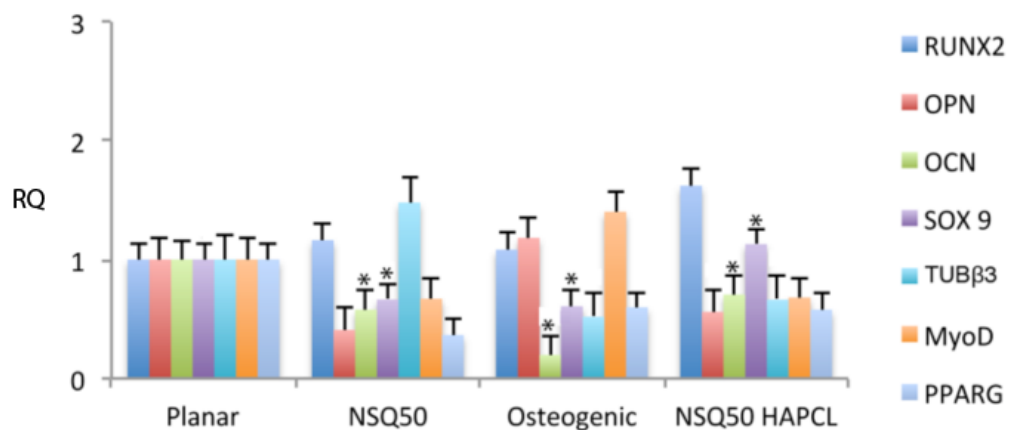


Figure 3.9 Relative gene expression at day 28. OCN expression was significantly lower on NSQ50 PCL and HAPCL, and after culture in osteogenic media in comparison to the planar control. The relative gene expression after this dual sided vertical culture of HBMC was normalized against GAPDH. Statistical significance (ANOVA $p \leq 0.05$) is indicated by “*”. Standard error bars are shown (n=3). RQ: relative quantification.

3.4 Discussion

The results outlined above are indicative of the success of the bone marrow aspiration, cell separation by Ficoll gradient and adherence to plastic techniques. The HBMCs used in all of these results were produced according to the protocol I developed and detailed in chapter 2.2.4. HBMC seeding and culture protocols for both single-sided horizontal and dual sided vertical culture have yielded positive results. The osteogenic phenotype has predominated both microscopically and on PCR analysis.

The vertical culture technique I have developed has simply and cheaply rendered dual sided culture possible for periods of up to and including 28 days (chapter 2.2.5). Immunofluorescence and alizarin red staining have revealed the presence of the osteogenic phenotype on both sides of all substrates at 11 and 28 days (figures 3.4, 3.5 and 3.6). The early difficulties encountered with respect to the effect of cell accumulation in gravity dependent regions I have overcome by turning substrates at 14 days (chapter 2).

NSQ50 nanotopography has consistently expressed the greatest osteogenicity on both PCL and HAPCL. Semi-quantitative analysis of the horizontal culture results (table 3.1) following culture of HBMCs for 28 days revealed that HAPCL was associated with maximal osteogenicity based upon immunofluorescent results (figure 3.4). The use of the NSQ50 nanotopography was at least comparable to the exposure of HBMCs to BMP2 (table 3.1). The early qPCR and immunofluorescence results were consistent. A pilot 7-day qPCR experiment revealed an increased expression of BMP2, OPN and osteonectin on NSQ50 in comparison to planar PCL (figure 3.3). All of these proteins are involved in early osteogenic differentiation (chapter 2.1.5). OCN a marker for mature osteoblasts was absent.

	Planar	Osteogenic	BMP2	HAPCL	NSQ50
OPN	+	+	++	+++	++
OCN	+	-	+	++	+
Alizarin red	++	++	++	+	+

Table 3.1 Summary of horizontal single sided culture results at 28 days, from chapter 3.3.1 (figures 3.1 and 3.2). Planar HAPCL appeared most osteogenic on immunofluorescent staining (figure 3.1 and 3.2). Differences in Alizarin red staining were not as marked, although greatest calcium appeared to be present on the less osteogenic substrates by immunofluorescent analysis.

Combined alizarin red and Coomassie blue images (figure 3.2) may have resulted in a masking of calcium deposits, for example by blue coloured staining of proteins involved in the endocytic process. All five substrates were used for further investigation during the work upon the dual sided culture techniques.

The semi-quantitative microscopy results obtained at 28 days and shown in table 3.2 reveal that combining the NSQ50 nanotopography with HA in the PCL had an additive effect on the osteogenicity of the substrates. Compared to the two planar controls, OPN and OCN expression, maximal on NSQ50 HAPCL, was expressed to a markedly greater degree on NSQ50 PCL than on the planar control (figures 3.4 and 3.5). Differences between planar PCL, with and without osteogenic media and following the use of BMP were less apparent (table 3.2).

Imaging of confluent regions of HBMCs at 28 days has revealed that NSQ50 is associated with increased bone marker (OPN and OCN) expression compared with the planar alternatives including those using osteogenic media and HBMCs exposed to BMP2 (figures 3.4, and 3.5). Immunofluorescence and alizarin red staining of planar PCL revealed the least expression of osteogenic markers and calcium deposition (figures 3.4, 3.5 and 3.6, table 3.2). Differences have been noted in the cellular location (cytoplasmic and nuclear) of OPN and OCN in addition to the degree of OPN and OCN aggregation.

	Planar	NSQ50	Osteogenic	BMP2 exposure	Planar HAPCL	NSQ50 HAPCL
OPN	++	+++	++	++	++	++++
OCN	++	+++	+	++	+++	++++
Alizarin red	+	+++	++	+++	++	++++

Table 3.2 Summary of vertical dual-sided culture results at 28 days, from chapter 3.3.3 (figures 3.4 - 3.6). The NSQ50 topography was associated with enhanced osteogenicity, in comparison to planar equivalents. On microscopy NSQ50 HAPCL was consistently the most osteogenic.

Alizarin red staining of calcium deposits on vertically cultured substrates (figure 3.6) was much clearer than following the horizontal culture (figure 3.2), due to the shorter duration of Coomassie blue counter-staining performed. The alizarin red images support the immunofluorescence findings in determining the osteogenicity of the substrates. The microscopy results suggested that all substrates supported differentiation into mature osteoblasts and that NSQ50 HAPCL and NSQ50 PCL were optimal. Slight variations between the results given by OPN, OCN and alizarin are noted with respect to differentiating between planar HAPCL, BMP2 and to a lesser extent osteogenic media, although they were all more osteogenic than planar PCL. I took the decision to use RT and qPCR to further analyse the osteogenic effects of NSQ50, NSQ50 HAPCL and the use of osteogenic media in comparison to planar PCL. In addition I decided to ensure that the enhancement of the osteogenic phenotype was specific and that other mesenchymal phenotypes were not similarly affected.

A time lag is inherent in comparisons between mRNA analysis and protein identification. Fluorescence on microscopy identifies the presence of proteins such as OPN and OCN whereas the evidence of gene expression obtained on qPCR relates to the presence of mRNA secondary to gene transcription. The time dependent expression of osteogenic markers has been well documented (Stein and Lian, 1993). OCN and calcium deposition are markers of differentiated osteoblasts whereas BMP2, RUNX2, and osteonectin are transcribed relatively early in the differentiation pathway. OPN is expressed in between these two extremes and you would expect the mRNA to be detectable before the protein itself.

RUNX2 expression was at or below control levels at day 11 (figure 3.8) and with the exception of NSQ50 HAPCL was at control levels on day 28 (figure 3.9). RUNX2 was marginally but significantly elevated on NSQ50 HAPCL (ANOVA $p \leq 0.05$) (figure 3.9).

OPN expression, relative to control (planar PCL in combination with DMEM), was significantly increased by the NSQ50 topography in association with both PCL and HAPCL at 11 days. OPN appeared reduced by these topographies at 28 days however, this was not statistically significant ($p \leq 0.05$) (figures 3.8 and 3.9, tables 3.3 and 3.4). At day 11 OCN expression was significantly increased by the presence of the NSQ50 topography (PCL and HAPCL) and osteogenic media (figure 3.8) whilst by day 28 it was significantly reduced especially with reference to HBMCs cultured using osteogenic media and on the NSQ50 topography (figure 3.9, tables 3.3 and 3.4).

The qPCR results and immunofluorescence results support each other in terms of the identification of the optimal substrate, NSQ50 HAPCL. It is likely that the apparent reduction of OPN and OCN expression shown by the qPCR results at the 28-day time point (in comparison to the day 11 qPCR and to the immunofluorescence) relates to progression from the transcriptional level to the protein level by the later time point (tables 3.3 and 3.4). Nonetheless it should be noted that NSQ50 PCL was more osteogenic than planar PCL alone or in combination with osteogenic media. The inclusion of HA into the PCL is therefore preferable, however, should this prove disadvantageous during pre-clinical or clinical trials NSQ50 PCL would also produce the desired effects.

	NSQ50	Osteogenic	NSQ50 HAPCL
RUNX2	-	-	-
OPN	++*	- *	+++ *
OCN	++*	++*	+++*
SOX9	-*	-*	-*
TUB β_3	-	-	+
MYOD	Absent	Absent	Absent

Table 3.3 Phenotype analysis at day 11. The osteogenic phenotype predominates in relative expression under test conditions (NSQ50, osteogenic media and NSQ50 HAPCL. Statistical significance (ANOVA $p \leq 0.05$) indicated by “*” (n=3).

A reduction in relative gene expression has been noted at day 28. It appears that expression of the osteogenic phenotype (OPN and OCN) has reduced at 28 days with mRNA detected at lower than control levels. The reduction in OCN was statistically significant on all test substrates (table 3.4, figure 3.9).

	NSQ50	Osteogenic	NSQ50 HAPCL
RUNX2	+	+	+
OPN	-	+	-
OCN	-*	--*	-*
SOX9	-*	-*	+*
TUB β_3	+	-	-
MYOD	-	+	-
PPARG	-	-	-

Table 3.4 Phenotype analysis at day 28. The expression of the osteogenic phenotype was greatest on the planar topography at day 28. Statistical significance (ANOVA $p \leq 0.05$) indicated by “*” (n=3).

The osteogenic phenotype expressed on NSQ50 to a comparatively greater extent on NSQ50 at 7 days than on planar PCL (figure 3.3) was also present on substrates at 21 days (figure 3.7). OCN was also shown by immunofluorescence at 28 days (figure 3.5). The minimal expression of the adipogenic phenotype noted on the planar and NSQ50 PCL (chapter 3.3.4) was comparable to planar control levels at day 28 (figures 3.9). Expression of the chondrogenic marker SOX9 was reduced in association with NSQ50 and osteogenic media (figure 3.9) although statistically significant the less than 2 fold differences are not thought to be clinically significant. The myogenic lineage (MYOD) most notable in its absence at days 11 to 21 (chapter 3.3.4, immunofluorescence figure 3.7 and qPCR figure 3.8) was present on all substrates at day 28 (figure 3.9). The adipogenic lineage (PPARG) also relatively poorly represented on immunofluorescence was present at levels comparable to the planar control at day 28 (figure 3.9).

Sources of error, limitations and future plans

On considering the results described in chapter 3.3 and discussed in chapter 3.4 it is important to realize the potential limitations of the experiments undertaken. The microscopy images reveal a small area of the entire substrates. Whilst images were taken using the same resolution and camera settings they rely upon the stain uptake being proportional to the quantity of the test substance (OPN, OCN, and calcium). Representative images were taken and the entire surface considered when drawing conclusions; nonetheless these are qualitative data.

In chapter 2 the difficulties of stains showing through the substrates in microscopy of dual sided substrates were described. As a result there was a need to reduce stain intensity, this rendered microscopic analysis without excessive show through possible. Some difficulty in obtaining clear images was still encountered and affected the choice of representative images. Regions overlying intense staining on the contralateral side did not produce the contrasts necessary for clear images. The background of the HAPCL substrates stained to a degree with Coomassie blue (figure 3.2), alizarin red (figure 3.2, 3.6) and also had a tendency to autofluoresce (figure 3.1, 3.4, 3.5). I adjusted the contrast and brightness of these images as necessary to eliminate the influence of this problem on the results. The selection of the regions imaged and the adjustment of the HAPCL images to produce images with the same background staining is a potential source of error. The microscopy results have been looked at in combination with the quantitative qPCR results and found to be consistent. It is for this reason I am confident that the qualitative differences noted on microscopy are real.

The HBMCs used within each experiment were from a single source patient. However, the research in its entirety was undertaken using HBMCs from a number of source patients. The 1 or 2 bone marrow samples that did not yield 300×10^4 HBMCs, sufficient to experiment with, were discarded. This in itself, whilst necessary by the experimental protocol, yields a potential source of bias in terms of HBMC quality.

In combination, the results of the microscopy and qPCR provide proof of principal based upon a large number of patient samples. However, individually, each experiment has not been repeated with multiple source patients. Differences in the 21 and 28 day results for OCN may be time dependent with OCN being a later marker of osteogenicity or may represent differences between source patients.

RNA levels depend upon both growth and differentiation of cells. Early differentiation is associated with an earlier cessation of proliferation. The difference in RNA acquisition may relate to the number of cells present in addition to the stage of differentiation. At first glance cells may appear less active whereas it may be that the cells are further ahead in terms of their differentiation than the transcriptionally active cells. In post-transcriptional cells the activity is concentrated at the protein level. The combination of immunofluorescence, alizarin red and qPCR assays assists in the differentiation between pre and post and transcriptional cells.

Visible differences in expression were apparent in the qPCR results in the absence of statistical significance. Ideally repeats using greater substrate numbers would be undertaken to reduce variance and confirm or refute the significance of these differences. Such experiments would necessitate either a greater cell number to be culture expanded prior to seeding or a reduction in the number of primer-probes chosen.

A time course experiment could be undertaken looking at the expression of the different osteogenic mediators over a period of weeks, ideally this would be undertaken using the same source patient for all time points and repeated 2 or 3 times with different patients. The number of cells required precluded this from being undertaken during this research. In other research within the department work is being undertaken to facilitate the culture expansion of stem cells and

HBMC to enable greater volumes of cells to be produced without any differentiation occurring (McMurray et al., 2011).

NSQ50 HAPCL has been shown to be optimal in the culture of HBMC showing osteogenic properties and aiding differentiation with the production of mineral deposits. A cheaper alternative topography with the same osteogenic properties would enable these findings to become more commercially interesting.

Chapter 4 Analysis of nanoisland embossed PCL

4.1 Introduction

Block co-polymer phase separation can be used to fabricate a nanotopography, which exhibits a controlled level of disorder, both reproducibly and cost-effectively. This is interesting as nanoscale techniques borrowed from the electronics sector (such as EBL) are expensive, time consuming and are limited to small areas. The focus of this chapter is the hypothesis that HOBs interact with a non-random but disordered array of nanoislands in an osteogenic manner in comparison to planar controls. The topographies created through the use of the block co-polymer separation of two different molecular weights of poly(styrene-*block*-poly-2-vinylpyridine) (PS-*b*-P2VP) provide a rapid and cheap alternative to surfaces fabricated by EBL.

The osteogenic potential of the nanoisland topographies has been assessed through analysis of calcium deposition, OPN and OCN expression, over a 28-day period. Relative RUNX2 expression was assessed after 25 days in culture. Osteogenic nanotopographies could have massive clinical impact through facilitating the osseointegration of implants and/or the *in vitro* expansion of HOBs for replantation. The relatively cheap and reproducible method of block co-polymer phase separation in the manufacture of osteogenic nanotopographies would render the potential clinical applications somewhat more feasible than that detailed previously.

4.2 Materials and methods

Two nanoisland topographies, produced through the use of block co-polymer phase separation, were embossed onto the PCL. Analysis of the topography itself was undertaken with AFM, and the topography's effect on HOBs studied through the use of immunocytochemistry, fluorescence microscopy, and qPCR. I performed the experiments on the nanoislands before I undertook the work on HBMC extraction and on NSQ50. HOBs obtained from Promocell were used in all experiments excepting the assessment of RUNX2 using qPCR. This experiment was performed after HBMC acquisition had been optimized and was performed using my own locally sourced HBMCs. The media used in 90% of the experiments

was α -MEM. Modified DMEM was used for the qPCR because of changes in protocol after it was noted that this change would represent a marked financial saving without detrimental effects on HBMC culture.

4.2.1 Shim production, substrate manufacture, and acellular substrate analysis

The three-step process of substrate manufacture (using shims produced using block co-polymer phase separation detailed below) was used in combination with hot-embossing (chapter 2.2.2). Two master shims with different topographical characteristics were produced: shims 'A' and 'B'.

In the preparation of masters for the nanoisland topography PS-*b*-P2VP inverse micelles were prepared in *o*-xylene with a solution concentration of 0.5 % by weight. The two molecular weight forms of PS-*b*-P2VP used to create the two masters were 190 500-*b*-190 000 grams/molecule and 91 500-*b*-105 000 grams/molecule respectively (Krishnamoorthy S, 2006). A thin film of PS-*b*-P2VP micelles was spin coated onto clean silicon wafers at 5000 r.p.m. in a relative humidity of 20-35 %.

Ni-V was sputter coated onto the masters, which were subsequently electroplated to a nickel shim thickness of approximately 300 μm (Dalby et al., 2006a). In this phase of the research the PCL beads (Sigma, UK) were heated to 80°C for 1.5 h in order to create the PCL sheets. 2.5 cm² squares of PCL were thumb embossed to create the planar and single-side nanoembossed substrates (planar, 14 nm and 18 nm nanoisland topographies) (chapter 2.2.2).

The topographical characteristics of the planar and nanoembossed surfaces were delineated using AFM, including surface roughness and section analysis. 15 islands on each nanopatterned surface were section analysed to ascertain typical height values. A 2 nm radius tip was used in combination with a scan speed 0.4 Hertz (Hz) and a scan size of 5 x 5 μm .

4.2.2 Cellular substrate analysis using light and immunofluorescence microscopy

Primary HOBs were seeded at 3×10^4 cells per substrate, one substrate per well, in twelve well plates. Cells were cultured in 3 ml modified α -MEM initially and modified DMEM latterly for 7, 14, 21, and 28 days and media changes were bi-weekly. HOBs were fixed at each time point using the protocol previously described (chapter 2.2.6). The alizarin red, immunostaining, and microscopy protocols outlined (chapter 2.2.6) were combined with the following durations of stain exposure. Staining with alizarin red 2 % in H₂O for 5 min facilitated viewing using the Zeiss Axiovert 25 microscope (chapter 2.2.6). Immunostaining was performed by incubating substrates for 1 h with a 1:50 concentration of rhodamine phalloidin and primary antibody (OPN or OCN), biotinylated monoclonal horse anti-mouse at 1:50 for 1 h (37°C), and finally FITC conjugated streptavidin at 1:50 at 4°C for 30 min.

4.2.3 RUNX2 analysis using qPCR

Three 2.5 cm² substrates of each type (planar, 14 nm and 18 nm nanoisland topographies) were prepared. The substrates were seeded with 2.1×10^4 cells, and cultured in modified DMEM for 25 days (chapter 4.2.2). The RNA harvest, RT and qPCR protocols previously described (chapter 2.2.7-2.2.9) were used in combination with the following reagents and quantities. RNA was extracted using Stratagene RNA Miniprep. Cell lysis was undertaken directly, using 600 μ l of lysis buffer per substrate. Cell scrapers ensured maximal cell disruption. RT was undertaken using the Quantitect RT kit. QPCR was performed using Taqman gene expression primers for RUNX2 and GAPDH. RUNX2 expression was normalised against GAPDH and compared against the planar control surface. Statistical analysis was undertaken using the T-test.

4.3 Results

4.3.1 Acellular analysis of planar and nanoisland embossed surfaces

Thumb embossing between 2 glass slides satisfactorily creates planar controls. AFM analysis of the planar controls revealed a Ra of 0.93 nm (figure 4.1A). The height of the topographies used to make shims A and B were 20 nm (figure 4. 1B)

and 30 nm (figure 4.1C) respectively. The RMS roughness of the scan area was 4.75 nm for substrate A, and 4.98 nm for substrate B. Figures 4.1D and E show the successful embossing of the disordered pattern into the PCL polymer. The pattern spatial arrangement was transferred with high fidelity, but a slight loss of height was observed (figure 4.1D and E).

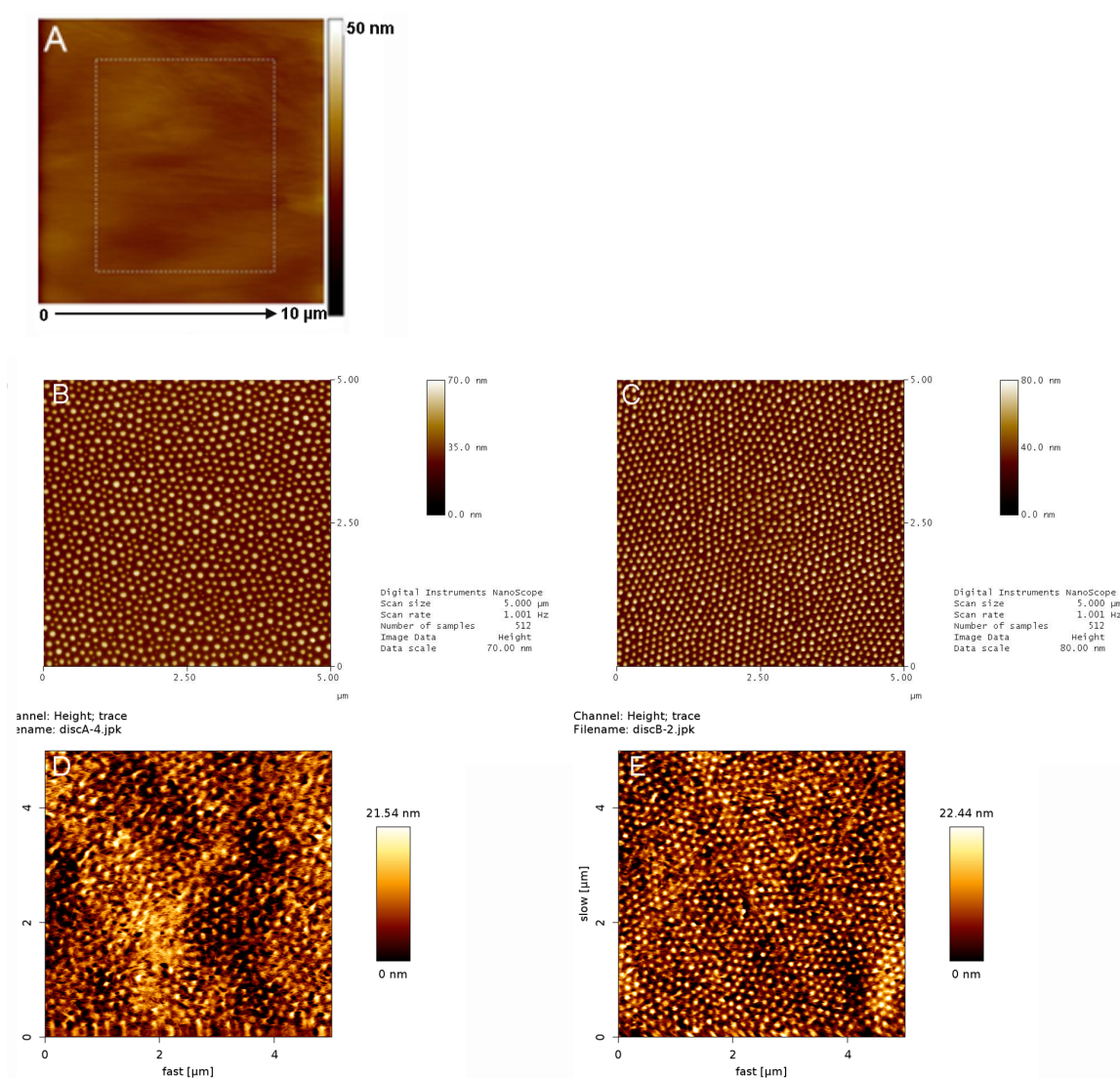


Figure 4.1 AFM micrographs of control and test samples. (A) Planar control. (B) Image of the master of 'A' showing 20 nm high islands and the disorganized, but not random, arrangement and (D) the embossed pattern from shim 'A' in PCL showing retained spatial fidelity but loss of nanoisland height. (C) Image of the master 'B' showing 30 nm high islands and their disorganized, but not random, arrangement and (E) the embossed pattern in PCL showing retained spatial fidelity but, again, loss of height (Maclaine et al., 2012).

Section analysis of fifteen regions of representative PCL substrates for topography 'A' and 'B' revealed an average nanoisland height of 14 nm and 18 nm respectively. Illustrative views are shown in Figure 4.2A and 4.2B. The centre-centre periodicity is constant at 150 nm for both A and B before and after embossing (MacLaine et al., 2012).

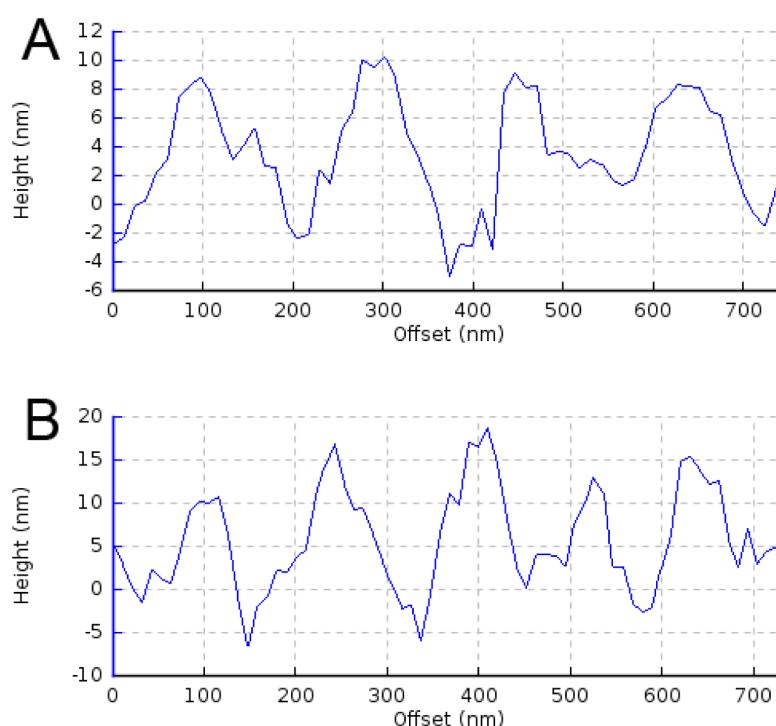


Figure 4.2 Section analysis of substrates A and B. A loss of height reproduction is noted on section analysis of the PCL substrates produced using shims A and B.

4.3.2 Cellular analysis of substrates using microscopy

OPN and OCN were measured after 7, 14, 21 and 28 days of culture for all time points and materials. OPN was first noted in the nucleus, subsequently in the cytoplasm, and finally in the extracellular environment. The cell number (cell growth) was seen to increase with time on control and test materials, but OPN was expressed earlier (day 14) on the test topographies (14 nm and 18 nm) and in far higher levels by days 21-28 on the topographies compared to planar controls (figure 4.3).

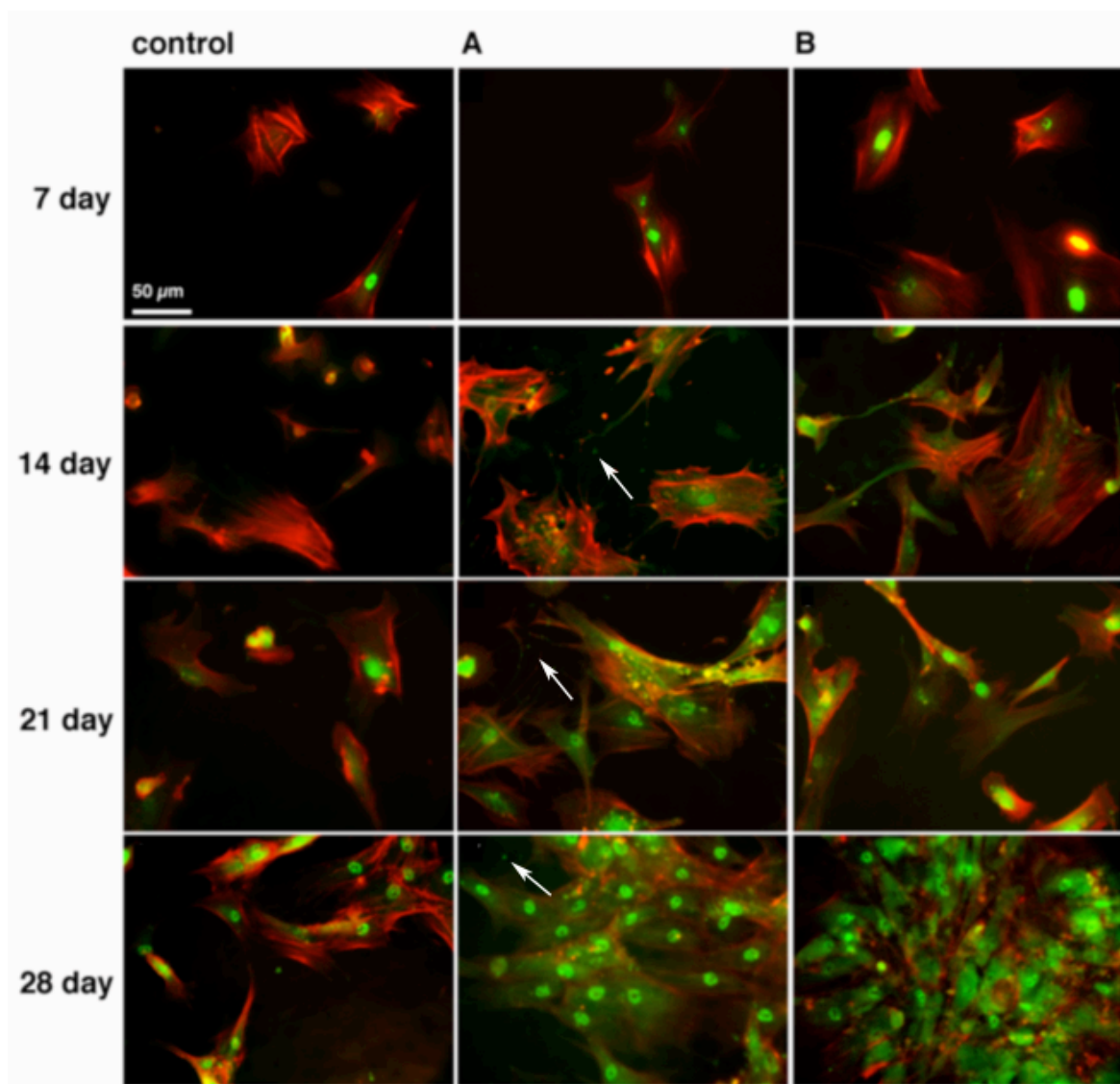


Figure 4.3 Temporal immunofluorescence analysis of OPN expression. Good cell growth was observed on all materials. By day 14, OPN expression was only noted on the 14 nm (A) and 18 nm (B) topographies, not planar control. After 21 days some cells on the flat material were expressing the marker around the nucleus, but by this time OPN expression was clearly observed within the cytoplasm of HOBs on the 14 nm and 18 nm topographies. By 28 days, whilst OPN expression was still peri-nuclear on the control, extracellular OPN was seen on the 14 nm topographies (white arrow). Red = actin, Green = OPN. Scale bar 50 μm .

OCN (a definitive marker of the osteoblast phenotype) was only noted at above background levels in HOBs on the 14 nm islands at 21 and 28 days of culture. Very few cells expressed OCN on the planar material and expression on the 18 nm islands was at a level between the controls and 14 nm islands (figure 4.4).

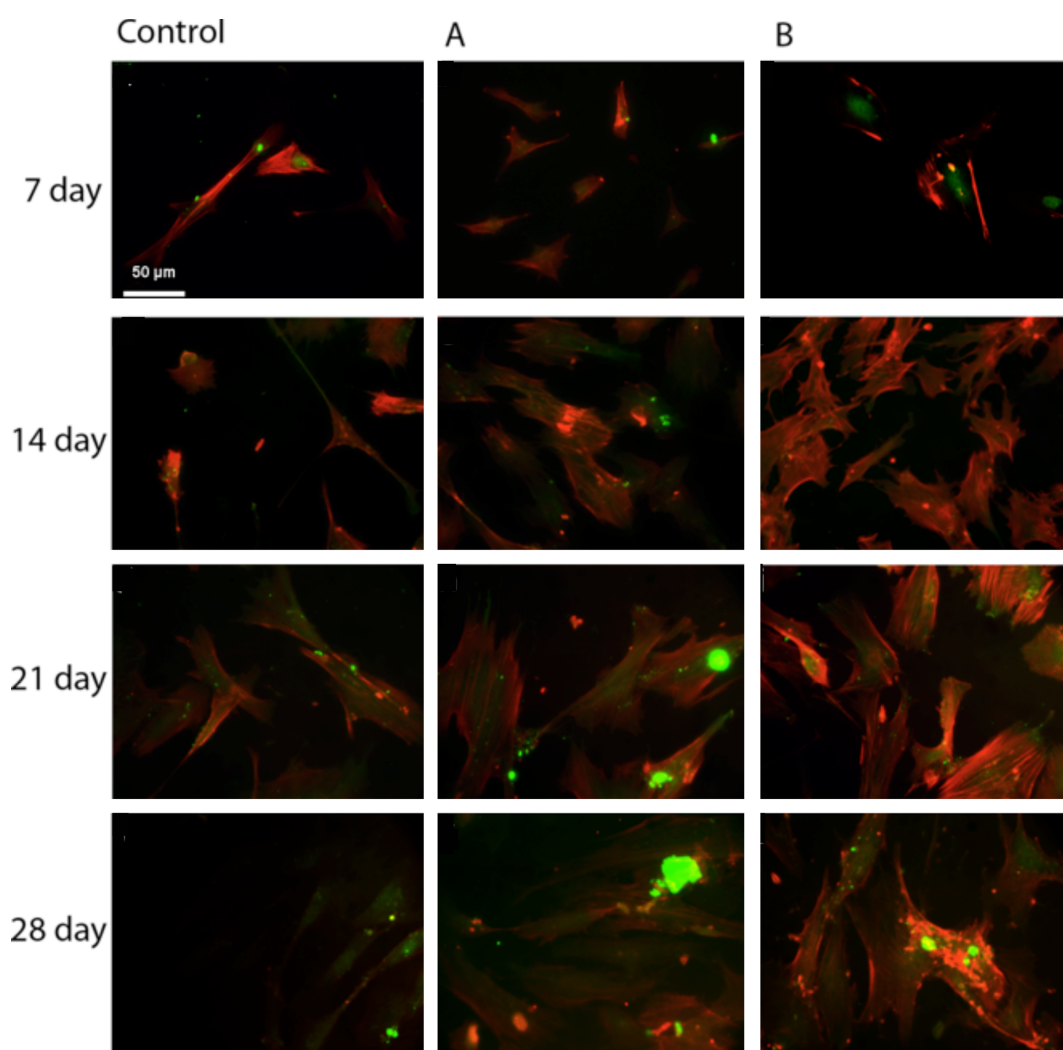


Figure 4.4 Temporal immunofluorescence analysis of OCN expression. Very few cells on the planar control and on the 18 nm nanoislands (B) expressed OCN. Dense foci of green immunofluorescence were noted on the 14 nm substrates (A) after 21 and 28 days of culture. Red = actin, Green = OCN. Scale bar 50 μm .

4.3.3 Cellular analysis of substrates using qPCR

The 14 nm topography expressed more RUNX2 (ct value 1.92, s.d. 0.68) at 25 days than the planar control (ct value 1.049, s.d. 0.42) and 18 nm topography (ct value 1.04, s.d. 0.61) (figure 4.5). Statistical analysis using T-test revealed a significant difference ($p < 0.05$) between the RUNX2 expression on 14 nm nanoislands in comparison with the planar and 18 nm substrates. The rna yield and integrity is detailed in appendix 7 (table A3).

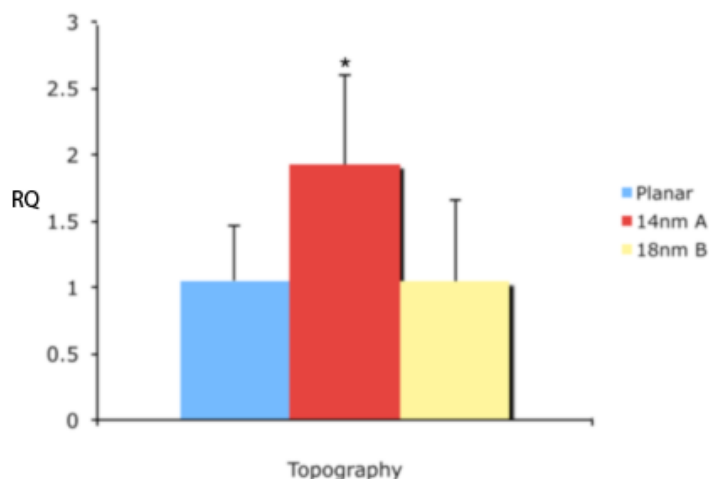


Figure 4.5 RUNX2 expression at 25 days. RUNX2 expression is greatest on the smallest nanotopography (14 nm). The difference between the level of expression on the 14 nm islands and both the planar material and the 18 nm islands is statistically significant (* $p < 0.05$ T-Test). Results = mean \pm standard deviation, $n=3$. RQ: relative quantification.

4.4 Discussion

The technique in this chapter facilitates rapid and cost effective fabrication of large areas (in this case 2 cm², but could easily be larger) of disordered, but not random, nanoscale topography. The AFM images show that the islands had a fixed and controlled periodicity of 150 nm, and islands packed largely as honeycomb-hexagonal arrays.

Reports have also focused on the importance of nanoscale height in the elicitation of a cell response. In 2004 it was proposed that sub-20 nm was important for stimulation of cell activities (Dalby et al., 2004b; Sjostrom et al., 2009a). AFM results revealed a loss of nanoisland height, from the 20 nm and 30 nm dimensions used to produce the shims, to the 14nm and 18nm dimensions obtained from AFM analysis of the substrates. The disordered features presented to the cells were sub-20 nm in height, 14 nm and 18 nm. It is postulated that the height loss may be due to polymer coating the shim coupled with the small sizes of the features involved. Measurement limitations were also present due to the size of the nanoprobe.

The differentiation time course used in this report is based on a seminal paper by Stein *et al* regarding the molecular mechanisms through which cells of the osteoblast phenotype undergo proliferation and differentiation, and the inter-relationships between the two (Stein and Lian, 1993). In their work, the proteins secreted by osteoblasts were identified and characterized, and the proteins and growth factors relating to bone ECM and the mRNA transcripts analysed (Stein and Lian, 1993).

My work has revealed cell proliferation and expression of the osteogenic phenotype, with OPN expression seen cytoplasmically at 14 days on the smaller topography. The more specific and latterly expressed bone marker protein OCN was maximal on the smaller topography, with increased levels seen at days 21 and 28. The increased production of RUNX2 at 25 days on the 14 nm high topography was supported by the immunofluorescence. In this report topography 'A' with the 14 nm high nanoislands produced the highest levels of osteoinduction in a notable absence of osteogenic media. As expected, the osteoblastic phenotype was minimally expressed on the planar control.

The results presented within are in agreement with observations that disorder and sub-20 nm height are important factors for cell response (in this case bone formation). The 14 nm islands are more bioactive than their 18 nm islands counterparts suggesting that cells are highly responsive to very small features. The smallest they have been seen to respond to previously were 10 nm, at which height filopodial interaction was observed (Dalby et al., 2004c; Sjostrom et al., 2009a).

The nanoislands created by block co-polymer phase separation have been embossed onto the surface of PCL. The loss of nanoisland height associated with thumb embossing proved beneficial whilst the spatial orientation of the pattern was retained. The loss of height is likely attributable to the moulding of

nanoscale features into a concave shim - i.e. some polymer may stick to the bottom of the pits in the shim resulting in smaller features in the embossed replica.

4.5 Conclusion

Highly osteogenic, disordered nanotopographies can be manufactured into thermoplastics in a rapid and cost-effective way through the use of block copolymer phase separation. Osteogenic topographies reproducibly and cost-effectively produced have a potentially useful application in the fields of implant technology and regenerative orthopaedics.

5 Discussion

5.1 Background

The invention of the microscope in the 1800s facilitated both an increase in the understanding of human cells, and lead to the discovery in the early 1900s that red blood cells, white blood cells and platelets originated from a single “stem”. Since the discovery of stem cells, research has increased exponentially. Transplantation of human stem cells began in the 1950s as a management for depleted functional bone marrow, caused by haematological and oncological conditions, and in 1963 Ernest McCulloch and James Till quantitatively described the self-renewing properties of murine bone marrow cells (Till and McCulloch, 1963).

Stem cells can differentiate into multiple lineages. For example, MSCs can form the mesenchymal lineages (predominantly osteocytic (bone), adipocytic (fat), chondrocytic (cartilage) and fibroblastic (fibrous)), whilst embryonic stem cells can form all tissue layers found in a developing embryo (endo-, meso- and ectodermal). MSCs are regarded as non-immunogenic (Chamberlain et al., 2007) and are potentially transplantable into allogeneic recipients without the use of immunosuppressants.

MSCs are being harvested from arthroplasty patients at the time of surgery. The proliferative capacity, cellular spectrum and usefulness of stem cells harvested from bone marrow is independent of age and OA aetiology (Webster et al., 2009). The HBMCs harvested come from the very patients who require orthopaedic implants and display much of the phenotypic character of the cell population encountered when devices are implanted. This facilitates research into the fundamental properties of the cells and their interactions with biomaterials. The harvest of stem cells and human bone marrow has become more widespread but despite nearly four decades of research a specific cell-surface marker, which could uniquely identify and select for the MSC/SSC phenotypes, remains elusive (Tare RS, 2009). A new generation of cell markers and antibodies are anticipated and it may become commonplace to isolate progenitors or stem cells using a “cocktail” of antibodies (Tare RS, 2009).

Concurrently, stem cell research continues to contribute to chemical and topographical advancements in implant design. Composite grafts, formed from combinations of two or more materials, are being used to harness stem cell multipotency (Brady et al., 2010). Two cell types simultaneously cultured within a biphasic gel resulted in demarcated layers of bone and cartilage like cells (Brady et al., 2010). At cellular and sub-cellular levels, morphological and gene expression differences have been noted with changes in the culture environment presented to stem cells (including 2d culture versus 3d scaffolds). Culture of mouse embryonic stem cells (in porous tantalum and on solid substrates) revealed the exclusive expression of several genes following 3d culture, including the gene encoding BMP4 (Liu et al., 2006).

Knee surgeons have set a precedent for the use of MSCs and HBMCs (or SSCs) in the prevention of osteoarthritis by the management of focal cartilage defects. Developed between the late 1950s and the late 1980s, techniques such as prairie drilling (Pridie, 1959), spongialization (Ficat et al., 1979), abrasion (Johnson, 1986) and microfracture (Key, 1931) penetrate the subchondral bone facilitating the release of blood and bone marrow (containing multipotent MSCs) into the area of articular surface damage and the intra-articular space. Their success was limited by the resultant production of fibrocartilage, as opposed to the preferred hyaline cartilage.

Developments in cell biology led to a change in focus away from a disruption of the subchondral plate to direct chondrocyte implantation within the defect. In mosaicplasty the chondrocytes take the form of an autogenous chondral or osteochondral graft, obtained from the peripheral, non-weight bearing regions of the joint (Yamashita et al., 1985). Autologous chondrocyte implantation (ACI) involves the ex vivo expansion of harvested chondrocytes followed by deposition into the primary defect (Brittberg et al., 1994). ACI was first introduced in Sweden in 1987, and was used clinically in the USA in 1995. In some cases chondrocytes are cultured within an implantable collagen matrix, a technique known as matrix-guided ACI (MACI).

Combination of the two principles (subchondral bone disruption and chondrocyte implantation) led to the next progression in the series: bone marrow or BMSC deposition. Fresh non-culture expanded BMSCs are obtained using a cell separator, mixed with a protein matrix and collagen HA scaffold. They are then transplanted into microperforated and abraded osteochondral defects using minimally invasive arthroscopic techniques (where instruments and a small camera (arthroscope) are introduced into the knee joint through small portals (knee arthroscopy) (Assor, 2010).

MSC isolation from autologous bone marrow and culture expansion has also been undertaken for the primary management of osteoarthritis. In an ongoing feasibility and safety study patients suffering from gonarthrosis II-III are being recruited. Twenty-one days after MSCs are isolated, a single intra-articular injection of approximately 40 million MSCs is being undertaken, with clinical questionnaire and MRI follow-up. The theory is that the injected MSCs will have a sufficiently regenerative effect on articular cartilage to be evident on MRI (Coll R, 2010).

Implant osseointegration represents a combination of bone apposition to the implant with functional fixation (Petrie T, 2008) and is a prerequisite for the success of uncemented orthopaedic implants. It requires the adhesion and proliferation of osteoblastic cells, and differentiation of osteoblastic precursors, such as SSCs/BMSCs. Cells are known to be responsive to chemical cues (Curran et al., 2006), stiffness in 2D and 3D culture (Wang et al., 2010) and topographical features (Dalby et al., 2007). Attempts to functionalise orthopaedic implants with topographical cues have generally focused on non-specific roughening, using techniques such as acid etching (Cho and Park, 2003), grit and sand blasting.

Topography (the surface features of a material) offers the potential to present osteogenic stimuli in situ, ideally without the need for soluble mediators (which

may become transported away from the site of implantation with the inherent possibility of undesirable effects at distant regions). Topography, when designed well, has the particular advantage that the features can be retained over time, especially if concave in nature. This is in contrast to osteogenic surface chemistries (such as BMP or HA), which may be gradually degraded or lost as a consequence of the tissue environment (Rokkum et al., 2002).

The control of MSC differentiation by topography at the nanoscale has been demonstrated (Dalby et al., 2007). A surface disordered at the nanoscale level has, in the absence of osteogenic media, been shown to stimulate MSCs to produce bone mineral on a surface comprised of PMMA (Wilkinson et al., 2011). Although a different grade, this is the main constituent of bone cement, a substance not known for its osseointegrative properties. It seems likely that the incorporation of biomimetic elements, such as partially disordered environmental cues (Wilkinson et al., 2011) and features resembling osteoclast resorption pits, into the design of future devices could assist in promoting osseointegration (Wilkinson et al., 2011).

Recently it became possible to generate nanopatterned diamond surfaces using chemical vapour deposition (CVD), a technique that could offer a valuable means of patterning bulk areas of material with nanoscale features. An *in vitro* study of CVD deposited features suggested that the smaller features (in the range of 30-100 nm) were more supportive of osteoblastic functions than larger features approaching 100-600 nm in size, although differences in clustering of the features was also likely to have contributed to this (Webster et al., 2009). Most interestingly, it has been possible to generate defined pillar-like titania nanofeatures using through-mask anodisation, and 15 nm high pillars were particularly effective at promoting the differentiation of MSCs into osteoblasts (McNamara et al., 2011) (Sjostrom et al., 2009a).

MSC differentiation can also be controlled through modification of the maximum distortional strain and interstitial fluid flow. Differential control of the maximum

shear strain and relative fluid/solid velocity can be useful in the formation of different tissue types, possibly with variation within the same implant; to produce bone and articular cartilage for example. High levels of these stimuli favor MSC differentiation into fibroblasts, intermediate levels into chondrocytes, and low levels into osteoblasts (Huiskes et al., 1997). Application of the above principles could lead to the development of 3d scaffolds seeded with stem cells and cultured in the form of an autologous osteochondral graft suitable for use as a biologic arthroplasty. However, it is likely that the development of 3d scaffolds, especially custom made to a patient's own anatomy would be expensive and interstitial flow, whilst controllable *in vitro*, would be less predictable *in vivo*.

Research, combining chemical and topographical work, revealed that the effect of HAPEx on HOBs was enhanced by the addition of micrometric topography. The cells attached more rapidly and in greater numbers to the optimized surface (Dalby et al., 2002a). Nanoparticulate coating with HA on microstructured titania has also been undertaken (Nishimura et al., 2007). In addition, new osteogenic compounds are being developed with optimised topography (Kantawong et al., 2010). An acellular composite of poly-varepsilon-caprolactone and HA, spatially infused with TGF β_3 -adsorbed or TGF β_3 -free collagen hydrogel, was successfully implanted as a distal humeral replacement in rabbits (Lee et al., 2010). The result, a load-bearing composite of avascular regenerated cartilage integrated with regenerated subchondral bone containing well-defined blood vessels, formed using the recruitment of endogenous cells liberated at the time of distal humeral excision (Lee et al., 2010).

5.2 My research choices

My focus has been the production of bone graft material for orthopaedic usage in order to address the limited availability of autogenous bone graft. To this end I desired substrates that would be positively and exclusively osteoinductive. Recent work from our group and others (Biggs et al., 2009; Biggs et al., 2008; Dalby et al., 2006a; Dalby et al., 2006b; Sjöström et al., 2009a) demonstrated the osteogenic potential of nanotopography. HA, a crystalline molecule of

calcium and phosphorus (a synthetic analogue of apatite, the mineral fraction of human bone) has been used in surgery since 1920 (Petit, 1999). HA is osteoconductive and has the potential to draw osteoblasts out from bone. However, more recent work on HA coating silk for ligament scaffolds has suggested that HA may also be osteoinductive (He et al., 2013). Dexamethasone and BMP2 have been used *in vitro* to induce the osteoblast phenotype (Jorgensen et al., 2004). Dexamethasone promotes ALP and OCN secretion *in vitro* (Yang et al., 2003) and recombinant BMP2 has been shown in pre-clinical and clinical studies to induce union in critical sized defects and spinal fusion (both intervertebral and posterolateral) (Chen et al., 2004). BMP2 has also been FDA approved for use in acute open tibial shaft fractures (Woo, 2012a).

I chose a wide variety of test substrates in addition to the planar PCL control and the *in vitro* comparator osteogenic media. I added chemistries that have already found clinical application (namely BMP2 and HA) and topographies, the efficacy of which is beginning to emerge; NSQ50 (Dalby, 2009) and nanopillars (nanoislands) (McNamara et al., 2011) (Sjostrom et al., 2009a). The substrates used have evolved over the period of experimentation. The osteogenicity of HAPCL relative to PCL and the enhancing effect of the NSQ50 topography on PCL resulted in my decision to use NSQ50 HAPCL. To my knowledge the concept of combining HA with a bioabsorbable biomaterial is a new one, although more permanent substrates have previously obtained clinical use in the form of HAPEX (Dalby et al., 2002a) and HA coated implants (chapter 1.5.5). They have also been researched as HA coated structured titania (Nishimura et al., 2007), and HA coated silk (He et al., 2013).

The bioactivity of the entire surface of a clinically viable substrate must be controlled. I successfully developed a dual embossing technique capable of embossing both sides of a substrate in its entirety (chapter 2). As a substrate for implantation, and potentially osteoinduction, seeding of both sides would not have been necessary, however as a proof of concept and as a transport medium for *in vitro* expanded and potentially differentiated HBMCs, dual sided culture was important. HBMC seeding and culture protocols for both single-sided

horizontal and dual sided vertical culture (chapter 2.2.5) have yielded positive results with the osteogenic phenotype predominating both microscopically and on PCR analysis.

AFM and SEM results revealed that the NSQ50 and nanoisland topographies were reproduced with high fidelity into the PCL substrates (figures 2.12-2.15 and 4.1). All of the topographies were shown to incorporate a controlled degree of disorder. In the case of NSQ50 this disorder was produced using e-beam technology and resulted in a controlled displacement of centre-centre spacing (chapter 2.2.1). The nanoisland disorder was produced by the cheaper to manufacture option of block co-polymer separation (chapter 4.2.1). The nanotopographies reproduced in PCL using hot embossing techniques (chapter 2.2.2) were associated with osseointegration to a varying degree. It is speculated that disorder is of fundamental biological importance. Cells have many nanoscale cues in their environment and these may be well ordered (e.g. 66 nm collagen banding pattern), however it is unlikely to be to the degree obtainable at the limits of EBL resolution. Intriguingly collagen type 10 forms a nanodisordered hexagonal lattice (Kwan et al., 1991) of similar scale to the nanofeatures presented by NSQ50 and the 14 nm nanoislands. This non-fibrillar collagen is found in cartilage during endochondral ossification, and at sites of large volume fracture healing (Kwan et al., 1991; Stephens et al., 1992).

The osteogenic differentiation of cultured human mesenchymal cells derived from adult bone marrow has been characterized (Marom et al., 2005). Fetal calf serum (FCS) isolated mesenchymal cells (under the influence of dexamethasone, β -glycerol phosphate, and ascorbate, and in the presence of 10 % v/w) form aggregates or nodules expressing a 4- to 10-fold increase in alkaline phosphatase activity and calcium accumulation at 1 week, and increasing over time (Pittenger et al., 1999). The results outlined in this thesis are indicative of the success of my bone marrow aspiration, cell separation by Ficoll gradient, and adherence to plastic techniques. The HBMCs that I used in the production of these results were produced according to the protocol I developed and detailed in chapter 2 (chapter 2.2.4). I have taught these techniques to researchers

within and out-with the Centre of Cell Engineering and these techniques supply the HBMCs currently used for Msc, MD, PhD and post-doctoral research.

The dual embossing substrates have been shown to be reproducible. The NSQ50 nanotopography alone is capable of inducing osteogenic differentiation over and above that which occurs on planar controls. The 14 nm nanoisland topography has also been shown to support differentiation and support the osteogenic phenotype (chapter 4). The vertical culture technique has simply and cheaply rendered dual sided culture possible for periods of up to and including 28 days (chapters 2 and 3). Following shim production the NSQ50 and 14 nm nanoisland topographies share a manufacturing pathway, i.e. hot embossing (chapter 2.2.2). The nanoisland topography has the advantage of using block-copolymer technology (chapter 4.2.1) inherent in which is a markedly cheaper and more available manufacturing process.

The following discussion considers the results of the transcription analysis (qPCR) and immunofluorescence from the NSQ50 (chapter 3) and nanoisland topographies (chapter 4). These paragraphs are written with the caution that only the latter time-points of 21 and 28 days were used to visualize OCN during the NSQ50 work and only the 28-day time-point used in order to visualise OPN. Whilst bearing this in mind it should also be noted that whilst HOBs were used for the immunofluorescence experiments with regards to the nanoisland topographies (performed first and before the HBMC harvest and culture expansion was undertaken) and HBMCs were used with regards to NSQ50, the planar substrates themselves were consistent throughout. The transcribed proteins RUNX2, OPN and OCN discussed in chapter 1.4.2 are considered in turn here. The section concludes with a discussion of the calcium deposition.

When HBMCs are placed in culture, bone-related genes are down regulated, the cells enter a proliferation phase, and manipulation of the time taken for the three phases of *in vitro* osteoblastic differentiation is possible. For example dexamethasone in media accelerates differentiation and increases expression of

post-proliferative genes and relatively early mineralised nodule formation (Stein and Lian, 1993). RUNX2 is expressed at early stages of the MSC line, prior to bone formation, and has been described as the ‘principal osteogenic master gene for bone formation’ (Lian et al., 2006), it was detected by qPCR at day 7 following culture of HBMCs on planar and NSQ50 PCL (figure 3.3) and at day 25 on the planar and nanoisland topographies (figure 4.5). In addition it was found at days 11 and 28 on all planar and NSQ50 topographies (figures 3.8-3.9, tables 3.4 and 5.3).

OPN and OCN expression increase in parallel with increasing mineralization. OPN expression is active in the proliferative phase and also increases at the onset of mineralization. Under control conditions this would equate to expression on days 10-12 and peaking at days 16-20 (Stein and Lian, 1993). OPN transcription was apparent on all planar and NSQ50 substrates at days 11 and 28 and maximal on the NSQ50 PCL and NSQ50 HAPCL at day 11 (figure 3.8, table 5.3). The OPN protein seen by 7 days on the nanoisland topographies was clearly visualised using immunofluorescence on all planar, NSQ50 (figures 3.1 and 3.4, table 5.1) and nanoisland topographies (figure 4.3, table 5.2) on day 28.

OCN is post-proliferative, and expression correlates with mineralization thus OCN expressing cells are only found within mineralizing nodules (Stein and Lian, 1993). OCN transcription was apparent on planar and NSQ50 topographies at days 11 and 28. The relatively greater expression of OCN on the NSQ50, NSQ% HAPCL and osteogenic media were significant at day 11 (ANOVA $p \leq 0.05$) (figure 3.8). In addition the differences in OCN expression between these substrates were also significant. At day 28 OCN levels on the NSQ50 topographies, and following use of the osteogenic media, were below control levels (planar PCL) (ANOVA $p \leq 0.05$) (figure 3.9, table 5.3). OCN is more bone specific than OPN and was seen at 14 days on the 14 nm topography and days 21 to 28 on the planar and 18 nm nanoisland substrates. OCN was relatively scarce on all four planar and NSQ50 topographies following 21 days vertical culture (figure 3.7) however was visualised clearly using immunofluorescence on all planar, NSQ50 (figure 3.5

, table 5.1) and nanoisland topographies by day 28 (figure 4.4, table 5.2).

In cell culture of BMSCs, up to days 10-18 mainly intracellular mineralization is visible by numerous needle-like crystal structures in the cell cytoplasm and in vacuoles. After 20-30 days, the crystal content of these vacuoles is released, most probably by membrane fusion to the outside of the cells. At days 20-25, crystals accumulate extracellularly in the collagen matrix resulting in large plate-like and noncollagen associated crystallites on the culture disk surface (Zhao et al., 2008). On all six substrates used in chapter 3, calcium staining was noted at day 28. Of these substrates maximal calcium deposition was noted on the NSQ50 PCL and NSQ50 HAPCL.

The osseointuctivity of the NSQ50 nanopit topography was enhanced by incorporation of HA into the PCL (chapter 3). The 14 nm nanoisland topography was the most osseointuctive of the substrates tested in chapter 4. A comparison of the results described in chapters 3 and 4 has been outlined below (tables 5.1-5.3).

		Planar	Osteogenic	BMP2	HAPCL	NSQ50	NSQ50 HAPCL
Horizontal	OPN	+	+	++	+++	++	
	OCN	+	-	+	++	+	
	Alizarin red	++	++	++	+	+	
Vertical	OPN	+	++	+	+++	+++	++++
	OCN	++	+	++	+++	+++	++++
	Alizarin red	+	++	+++	++	+++	++++

Table 5.1 Summary of microscopy results (chapter 3) Horizontal culture revealed osseointuction by HAPCL, BMP2 and NSQ50 at the 28-day time-point analysed (figures 3.1, 3.2). NSQ50 HAPCL was optimally osteointuctive during the vertical culture; HAPCL and NSQ50 were both comparatively inductive of the osteogenic phenotype (figures 3.4, 3.5 and 3.6).

	Planar				14 nm				18nm			
	7	14	21	28	7	14	21	28	7	14	21	28
OPN	+	-	+	-	+	++	+++	+++	++	+++	++++	++++
OCN	+	-	++	+	+	++	+++	+++	+	-	+	++

Table 5.2 Summary of immunofluorescence results (chapter 4). OPN expression was seen by 7 days on the nanoisland topographies. The more specific and latterly expressed bone marker OCN was seen at 14 days on the 14 nm topography and days 21 to 28 on the other substrates.

		NSQ50	Osteogenic	NSQ50 HAPCL
Day 11	RUNX2	-	-	-
	OPN	+ + *	- *	+++ *
	OCN	++*	++*	+++*
Day 28	RUNX2	+	~	+
	OPN	-	+	-
	OCN	-*	--**	-*

Table 5.3 Summary of qPCR results comparing planar PCL and the NSQ50 nanotopography (chapter 3, figures 3.8 and 3.9). Osteogenic markers were identified on qPCR at days 11 and 28 in all cases. OPN expression was greater at day 11 on the optimally osteogenic NSQ50 topographies reducing comparative to the planar control by day 28.

A decrease in cell proliferation is associated with increasing osteoblast differentiation, thus OCN expression is post-proliferative (Stein and Lian, 1993). It is therefore unsurprising that the cells which expressed OCN first were also the ones associated with least confluence and the least RNA extracted, and vice versa (chapter 2.3.6, table 2.3). Dexamethasone in media accelerates differentiation, increases expression of post-proliferative genes, leads to relatively early mineralised nodule formation, and may deplete the pool of proliferating undifferentiated cells (by pushing cells to a terminal degree of

differentiation beyond their natural rate) (Stein and Lian, 1993). In my research PCL in association with osteogenic media yielded less RNA than planar PCL.

The location of the OPN immunofluorescence and alizarin red staining of calcification in the cells was temporally consistent between the topographies (NSQ50 and nanoisland) as well as their planar controls. OPN is an acidic protein encoded by a single gene that is responsive to a number of different transcription factors. It may be soluble, working as a cytokine, or immobilised, as an ECM protein (Standal et al., 2004). OPN has electronegative glutamic acid and aspartic acid residues as well as a Ca^{2+} motif making it bind tightly to HA, inhibiting the growth of HA crystals. The secretory pathways and their mediators in osteoblasts remain largely unknown (Zhao et al., 2008). Exocytosis is a fundamental process through which eukaryotic cells release hydrophilic secretory products into the extracellular space, or translocate specific functional proteins to the plasma membrane (Chieriegatti and Meldolesi, 2005; Verhage and Toonen, 2007), and it is a prerequisite for osteoclast and osteoblast function (Zhao et al., 2008). At least two types of secretory activities mediate bone formation by osteoblasts, the first is deposition of bone matrix proteins and the second is delivery of matrix vesicles into the extracellular space to facilitate mineralization. During osteoblast maturation, vesicles containing OPN and OCN change from peri-nuclear to nodular (Zhao et al., 2008). This change in location is consistent with the staining seen in figures 3.5, 3.6 and 4.3.

One model of mineralization by osteoblasts involves amorphous calcium phosphate material which is secreted via an exocytotic process directly from vacuoles of osteoblasts. It is deposited extracellularly, propagates into the collagen fibril matrix, and matures into HA (Zhao et al., 2008). This model is supported by the presence of intracellular needle-like crystalline bone apatite in vacuoles *in vivo* in the osteoblastic cells of the periosteum of tibiae (Zhao et al., 2008). I postulate that the appearances of the co-stained Coomassie blue and alizarin red images (figure 3.2), in which the topographies associated with greatest osteoinductivity appeared to have least calcified deposits, can be

explained by masking of the calcification by Coomassie blue staining of the protein vesicles surrounding them.

Previous studies have shown induction of the osteogenic phenotype using chemistry, nanotopography and a combination of the two (Dalby et al., 2002a; Dalby et al., 2007; Dalby et al., 2006a; Hamilton and Brunette, 2007; He et al., 2013). The phenotype analysis performed in this research was new and confirmed that the HBMC differentiation was targeted towards osteogenesis and that the induction of differentiation was not random in nature. I have used immunofluorescence and qPCR to ascertain that the NSQ50 topography in association with PCL and HAPCL was specifically osteoinductive. The differentiation of the HBMCs was ‘targeted’ towards osteogenesis, to the virtual exclusion of all other mesenchymal tissue types (chapter 3.3.4-3.3.6, figures 3.7-3.9, tables 3.3, 3.4 and 5.3). Whilst I have not undertaken the same test of targeting for the 14 nm nanoislands, the osteoinductivity was marked.

Work within our group has been undertaken to use nanotopography to culture expand undifferentiated HBMCs (McMurray et al., 2011), work is on-going to determine whether this may also be possible by using hydrogels. The potential to combine the rapidly dividing potential of HBMCs in the undifferentiated state (MSCs) with the substrates for subsequent cell differentiation and implantation is exciting and may well form the basis for the bone graft of the future. Dual embossed substrates of either of the nanotopographies studied could have a number of uses, with and without the inclusion of HA in the PCL. They could be applied purely as an osteoinductive agent and implanted cell free, used as a transport medium for *in vitro* culture expanded cells, or potentially used for a combination of both, in which dual embossing is undertaken but cell seeding is single-sided. This latter technique would depend upon locally available HBMCs and MSCs (available in the patients’ blood) colonising the un-seeded surface. Care would need to be taken to protect the cell-free embossed surface during cell culture and substrate handling.

Problems to be overcome.

Concerns regarding the possible induction of neoplasia (cancer) by inoculation of stem cells have thus far been unfounded. MRI at 2 years following the inoculation of patient's inter-vertebral discs and osteoarthritic joints was negative for neoplasia in all but one of the two hundred and twenty-six patients; in that case neoplasia was thought to be independent of the treatment. This analysis of feasibility and safety did not determine the efficacy of culture-expanded MSC inoculation (Centeno et al., 2010). It is my opinion, however, that patients would be much happier receiving their own cells back than taking the perceived risk of receiving someone else's.

Some concerns regarding the use of animal-derived media supplements for culture purposes have been expressed. Association of FCS proteins with cells expressing major histocompatibility complex class I molecules can result from long-term expansion of skeletal stem cells in FCS. This can lead to a potentially damaging mixed lymphocyte reaction through an induction of T-cell proliferation (MacDermott and Bragdon, 1983). Alternative media supplements such as autologous human platelet lysate are being popularized (Centeno et al., 2010). This could be used for cell culture in place of FBS, in order to reduce usage of animal derived products and alleviate any concerns expressed with respect to the safety of cell culture for re-implantation using FBS.

BMP usage has been losing favour *in vivo* in spinal patients in whom stimulation of osteoclasts appears to be responsible for failures in fixation. In addition, hypersensitivity seems to follow BMPs first use preventing multiple applications to the same patient (by personal communication with Meek). Recombinant BMP2 usage was involved in 62 adverse events outwith the spinal surgery and 834 in association with spinal procedures (to December 2011). 44-48 % of these patients required secondary procedures. Adverse events included osteolysis, heterotopic bone formation and pseudarthrosis (Woo, 2012a, b).

In terms of orthopaedic application it could be envisaged that patterns embossed onto polymers could be used in fracture healing as biodegradable templates for growth of living, bone-marrow-derived, *in vitro* expanded autologous osteoblasts. Application to the development of metal implant surfaces would also be interesting. The phase separated master materials could be used to template for directed anodisation of e.g. Ti (Chu et al., 2005; Sjostrom et al., 2009a; Sjostrom et al., 2009b). Transfer of the patterns into a titania oxide layer may facilitate its use in the osseointegration of load bearing metal implants.

Future ideas

It would be of academic interest to confirm the timeline of transcription factors versus protein expression on immunofluorescence however this would require a significant amount of work and large cell numbers. It would be challenging to culture enough cells to analyse RUNX2, OPN and OCN by qPCR and immunofluorescence at the multiple time-points using the same cell-line without first culture expanding the cells within the MSC state first.

Additional research would be required to determine whether chemical and topographical cues act in a genuinely synergistic manner, independently, or potentially even antagonistically by stimulating different pathways and resulting in unwanted cross talk. In view of the increase in osseointegration shown by NSQ50 HAPCL and NSQ50 PCL I believe the latter is unlikely. The intra-cellular level of the topographical and chemical influences is yet to be fully understood.

The results of these ideas would be of personal interest and may determine future regions for genetic manipulation. The osteoinductivity of NSQ50, NSQ50 HAPCL and 14 nm nanoislands has already been identified, however, and therefore with the aim of a clinically useable substrate in mind I believe that a direct comparison of NSQ50 with 14 nm nanoislands. This work would be facilitated by the use of local supplies of bone marrow and the HBMC isolation protocols described and would be in my opinion a more urgent area of study.

As a transport medium I would expect the two-sided substrates (such as those described in chapters 2-3) in combination with either the NSQ50 or 14nm nanoisland topographies to function well. I have considered potential 3d options for protecting the topographies, including options of stacking substrates on top of each other or rolling the PCL into spirals after seeding. Pilot investigation with spirals has shown that PCL can be curled around 360 to 540° and held with 18 gauge needles without the surfaces touching. These spirals can also be stood on their ends in 12-well plates and turned according to the vertical culture protocol outlined in chapter 2.

5.3 Conclusion

Highly osteogenic, disordered nanotopographies can be manufactured into thermoplastics in a rapid and cost-effective way through the use of block copolymer phase separation. These osteogenic topographies will have a potentially massive impact on the fields of implant technology and regenerative orthopaedics. The field of cartilage repair has seen HBMC usage progress from lab research to clinical usage. This suggests that the *ex vivo* culture expansion of cells extracted from human bone marrow and their re-implantation as autogenous bone graft (as explored in this thesis) has great potential to become a viable clinical entity.

References

- Affrossman, S., Jerome, R., O'Neill, S.A., Schmitt, T., and Stamm, M. (2000). Surface structure of thin film blends of polystyrene and poly(n-butyl methacrylate). *Colloid Polym Sci* 278, 993-999.
- Affrossman, S., and Stamm, M. (2000). The effect of molecular weight on the topography of thin films of blends of poly(4-bromostyrene) and polystyrene. *Colloid Polym Sci* 278, 888-893.
- Amrich, M., and Burghouwt, A. (2010). Barely scratching the surface. *Orthotec, orthopaedic trends, technology and manufacturing 1*, 1-4.
- Andrianarivo, A.G., Robinson, J.A., Mann, K.G., and Tracy, R.P. (1992). Growth on type I collagen promotes expression of the osteoblastic phenotype in human osteosarcoma MG-63 cells. *J Cell Physiol* 153, 256-265.
- Anselme, K., Linez, P., Bigerelle, M., Le Maguer, D., Le Maguer, A., Hardouin, P., Hildebrand, H.F., Iost, A., and Leroy, J.M. (2000). The relative influence of the topography and chemistry of TiAl6V4 surfaces on osteoblastic cell behaviour. *Biomaterials* 21, 1567-1577.
- Antoniac, I., Laptoiu, D., Miculescu, M., Bunea, V., and Miculescu, F. (2003). Retrieval analysis of some cementless HA-coated smooth surface acetabular implants. *European cells and materials* 5, 51-52.
- Assor, M.S., S (2010). Pilot Study of A One-Step Procedure for the Use of Autologous Bone Marrow Mesenchymal Stem Cells Stimulated by Proteins Scaffold to Heal Under Arthroscopy Full-Thickness Defects Articular Cartilage and Osteoarthritis of the Knee. *ClinicalTrials.gov identifier: NCT01159899*.
- Bain, B.J., and Clark, D.M. (2001). *Bone marrow pathology*, 3rd edn (Blackwell science limited).
- Berry, D.J., Harmsen, W.S., Cabanela, M.E., and Morrey, B.F. (2002). Twenty-five-year survivorship of two thousand consecutive primary Charnley total hip replacements: factors affecting survivorship of acetabular and femoral components. *J Bone Joint Surg Am* 84-A, 171-177.
- Biggs, M.J., Richards, R.G., and Dalby, M.J. (2010). Nanotopographical modification: a regulator of cellular function through focal adhesions. *Nanomedicine*.
- Biggs, M.J., Richards, R.G., Gadegaard, N., Wilkinson, C.D., Oreffo, R.O., and Dalby, M.J. (2009). The use of nanoscale topography to modulate the dynamics of adhesion formation in primary osteoblasts and ERK/MAPK signalling in STRO-1+ enriched skeletal stem cells. *Biomaterials* 30, 5094-5103.
- Biggs, M.J., Richards, R.G., McFarlane, S., Wilkinson, C.D., Oreffo, R.O., and Dalby, M.J. (2008). Adhesion formation of primary human osteoblasts and the functional response of mesenchymal stem cells to 330nm deep microgrooves. *J R Soc Interface* 5, 1231-1242.
- Birmingham, E., Niebur, G.L., McHugh, P.E., Shaw, G., Barry, F.P., and McNamara, L.M. (2012). Osteogenic differentiation of mesenchymal stem cells is regulated by osteocyte and osteoblast cells in a simplified bone niche. *European cells & materials* 23, 13-27.
- Bloebaum, R.D., Mihalopoulos, N.L., Jensen, J.W., and Dorr, L.D. (1997). Postmortem analysis of bone growth into porous-coated acetabular components. *J Bone Joint Surg Am* 79, 1013-1022.
- Bloebaum, R.D., Rhodes, D.M., Rubman, M.H., and Hofmann, A.A. (1991). Bilateral tibial components of different cementless designs and materials. Microradiographic, backscattered imaging, and histologic analysis. *Clin Orthop Relat Res*, 179-187.
- Blumenthal N, R.J., Alexander H (1989). The effects of implant surfaces on bone mineral formation in vitro. . *Trans Annu Meet Soc Biomater* 1989 12.
- Bonfield, T.L., and Caplan, A.I. (2010). Adult mesenchymal stem cells: an innovative therapeutic for lung diseases. *Discovery medicine* 047.

- Bonfield, W., and Tanner, E. (2002). Hydroxyapatite composite biomaterials- evolution and applications (AZOM.com).
- Boyce, T., Edwards, J., and Scarborough, N. (1999). Allograft bone. The influence of processing on safety and performance. *Orthop Clin North Am* 30, 571-581.
- Brady, M.A., Sivananthan, S., Mudera, V., Liu, Q., Wiltfang, J., and Warnke, P.H. (2010). The primordium of a biological joint replacement: Coupling of two stem cell pathways in biphasic ultrarapid compressed gel niches. *J Craniomaxillofac Surg*.
- Brittberg, M., Lindahl, A., Nilsson, A., Ohlsson, C., Isaksson, O., and Peterson, L. (1994). Treatment of deep cartilage defects in the knee with autologous chondrocyte transplantation. *N Engl J Med* 331, 889-895.
- Caterson, E.J., Nesti, L.J., Danielson, K.G., and Tuan, R.S. (2002). Human marrow-derived mesenchymal progenitor cells. *molecular biotechnology* 20, 245-256.
- Centeno, C.J., Schultz, J.R., Cheever, M., Robinson, B., Freeman, M., and Marasco, W. (2010). Safety and complications reporting on the re-implantation of culture-expanded mesenchymal stem cells using autologous platelet lysate technique. *Curr Stem Cell Res Ther* 5, 81-93.
- Chamberlain, G., Fox, J., Ashton, B., and Middleton, J. (2007). Concise review: mesenchymal stem cells: their phenotype, differentiation capacity, immunological features, and potential for homing. *Stem Cells* 25, 2739-2749.
- Charnley, J. (1970). Total hip replacement by low-friction arthroplasty. *Clin Orthop Relat Res* 72, 7-21.
- Chen, D., Zhao, M., and Mundy, G.R. (2004). Bone morphogenetic proteins. *Growth Factors* 22, 233-241.
- Chen, W.J., Tsai, T.T., Chen, L.H., Niu, C.C., Lai, P.L., Fu, T.S., and McCarthy, K. (2005). The fusion rate of calcium sulfate with local autograft bone compared with autologous iliac bone graft for instrumented short-segment spinal fusion. *Spine (Phila Pa 1976)* 30, 2293-2297.
- Cheng JY, R.C., Thomas EL, Smith HI, Vancso GJ (2002). Fabrication of nanostructures with long-range order using block copolymer lithography. *Applied Physics Letters* 81, 3657-3659.
- Cheng, L. (2007). E-beam lithography.
- Chieriegatti, E., and Meldolesi, J. (2005). Regulated exocytosis: new organelles for non-secretory purposes. *Nature reviews Molecular cell biology* 6, 181-187.
- Cho, S.A., and Park, K.T. (2003). The removal torque of titanium screw inserted in rabbit tibia treated by dual acid etching. *Biomaterials* 24, 3611-3617.
- Chu, S.Z., Inoue, S., Wada, K., Hishita, S., and Kurashima, K. (2005). Self-organized nanoporous anodic titania films and ordered titania nanodots/nanorods on glass. *Advanced Functional Materials* 15, 1343-1349.
- Coll R, G.J. (2010). Adult Stem Cell Therapy for Repairing Articular Cartilage in Gonarthrosis.
- Corporate, L. (2013). Trabecular Titanium Naturae Imitatio.
- Croft, W.J. (2006). under the microscope, a breif history of microscopy (World Scientific Publishing Co Pte Ltd).
- Curran, J.M., Chen, R., and Hunt, J.A. (2006). The guidance of human mesenchymal stem cell differentiation in vitro by controlled modifications to the cell substrate. *Biomaterials* 27, 4783-4793.
- Curtis, A., and Wilkinson, C. (1999). New depths in cell behaviour: reactions of cells to nanotopography. *Biochem Soc Symp* 65, 15-26.
- Curtis, A.S., and Varde, M. (1964). Control of Cell Behavior: Topological Factors. *Journal of the National Cancer Institute* 33, 15-26.
- Curtis, A.S.G., and Wilkinson, C.D.W. (2001). Nanotechniques and approaches in biotechnology. *Trends Biotechnol* 19, 97-101.

- Dalby, M.J. (2009). Nanostructured surfaces: cell engineering and cell biology. *Nanomedicine (Lond)* 4, 247-248.
- Dalby, M.J., Di Silvio, L., Davies, G.W., and Bonfield, W. (2000). Surface topography and HA filler volume effect on primary human osteoblasts in vitro. *J Mater Sci Mater Med* 11, 805-810.
- Dalby, M.J., Di Silvio, L., Gurav, N., Annaz, B., Kayser, M.V., and Bonfield, W. (2002a). Optimizing HAPEX topography influences osteoblast response. *Tissue Eng* 8, 453-467.
- Dalby, M.J., Gadegaard, N., Riehle, M.O., Wilkinson, C.D., and Curtis, A.S. (2004a). Investigating filopodia sensing using arrays of defined nano-pits down to 35 nm diameter in size. *Int J Biochem Cell Biol* 36, 2005-2015.
- Dalby, M.J., Gadegaard, N., Tare, R., Andar, A., Riehle, M.O., Herzyk, P., Wilkinson, C.D., and Oreffo, R.O. (2007). The control of human mesenchymal cell differentiation using nanoscale symmetry and disorder. *Nat Mater* 6, 997-1003.
- Dalby, M.J., Giannaras, D., Riehle, M.O., Gadegaard, N., Affrossman, S., and Curtis, A.S. (2004b). Rapid fibroblast adhesion to 27nm high polymer demixed nano-topography. *Biomaterials* 25, 77-83.
- Dalby, M.J., McCloy, D., Robertson, M., Agheli, H., Sutherland, D., Affrossman, S., and Oreffo, R.O. (2006a). Osteoprogenitor response to semi-ordered and random nanotopographies. *Biomaterials* 27, 2980-2987.
- Dalby, M.J., McCloy, D., Robertson, M., Wilkinson, C.D., and Oreffo, R.O. (2006b). Osteoprogenitor response to defined topographies with nanoscale depths. *Biomaterials* 27, 1306-1315.
- Dalby, M.J., Riehle, M.O., Johnstone, H., Affrossman, S., and Curtis, A.S. (2002b). In vitro reaction of endothelial cells to polymer demixed nanotopography. *Biomaterials* 23, 2945-2954.
- Dalby, M.J., Riehle, M.O., Johnstone, H., Affrossman, S., and Curtis, A.S. (2004c). Investigating the limits of filopodial sensing: a brief report using SEM to image the interaction between 10 nm high nano-topography and fibroblast filopodia. *Cell Biol Int* 28, 229-236.
- Dalby, M.J., Riehle, M.O., Yarwood, S.J., Wilkinson, C.D., and Curtis, A.S. (2003). Nucleus alignment and cell signaling in fibroblasts: response to a micro-grooved topography. *Exp Cell Res* 284, 274-282.
- Dean, D.D., Schwartz, Z., Liu, Y., Blanchard, C.R., Agrawal, C.M., Mabrey, J.D., Sylvia, V.L., Lohmann, C.H., and Boyan, B.D. (1999). The effect of ultra-high molecular weight polyethylene wear debris on MG63 osteosarcoma cells in vitro. *J Bone Joint Surg Am* 81, 452-461.
- Delloye, C., Cornu, O., Druez, V., and Barbier, O. (2007). Bone allografts: What they can offer and what they cannot. *J Bone Joint Surg Br* 89, 574-579.
- DePuy, a.J.a.J.c. (2013a). Corail hip system surgical technique.
- DePuy, a.J.a.J.c. (2013b). Gription product brochure.
- Dick, H.M., and Strauch, R.J. (1994). Infection of massive bone allografts. *Clin Orthop Relat Res*, 46-53.
- Dickson, G., Buchanan, F., Marsh, D., Harkin-Jones, E., Little, U., and McCaigue, M. (2007). Orthopaedic tissue engineering and bone regeneration. *Technol Health Care* 15, 57-67.
- Du, C., Cui, F.Z., Zhu, X.D., and de Groot, K. (1999). Three-dimensional nano-HAp/collagen matrix loading with osteogenic cells in organ culture. *J Biomed Mater Res B Appl Biomater* 44 407-415.
- Ducy, P., and Karsenty, G. (2000). The family of bone morphogenetic proteins. *Kidney international* 57, 2207-2214.
- Eaton, P., and West, P. (2010). *Atomic Force Microscopy* (Oxford University Press).

- Emms, N.W., Buckley, S.C., Stockley, I., Hamer, A.J., and Kerry, R.M. (2009). Mid- to long-term results of irradiated allograft in acetabular reconstruction: a follow-up report. *J Bone Joint Surg Br* 91, 1419-1423.
- Engl, C.A. (2013). AML hip system design rationale.
- Engl, C.A., and Bobyn, J.D. (1988). The influence of stem size and extent of porous coating on femoral bone resorption after primary cementless hip arthroplasty. *Clin Orthop Relat Res*, 7-28.
- Engler, A.J., Sen, S., Sweeney, H.L., and Discher, D.E. (2006). Matrix elasticity directs stem cell lineage specification. *Cell* 126, 677-689.
- Ficat, R.P., Ficat, C., Gedeon, P., and Toussaint, J.B. (1979). Spongialization: a new treatment for diseased patellae. *Clin Orthop Relat Res*, 74-83.
- Fujibayashi, S., Shikata, J., Tanaka, C., Matsushita, M., and Nakamura, T. (2001). Lumbar posterolateral fusion with biphasic calcium phosphate ceramic. *J Spinal Disord* 14, 214-221.
- Furlong, R.J., and Osborn, J.F. (1991). Fixation of hip prostheses by hydroxyapatite ceramic coatings. *J Bone Joint Surg Br* 73, 741-745.
- Gadegaard, N., Thoms, S., Macintyre, D.S., McGhee, K., and Gallagher, J. (2003). Arrays of nano-dots for cellular engineering. *Microelectron Eng* 67-68, 162-168.
- Gallagher, J.O., McGhee, K.F., Wilkinson, C.D., and Riehle, M.O. (2002). Interaction of animal cells with ordered nanotopography. *IEEE Trans Nanobioscience* 1, 24-28.
- Gaston, M.S., and Simpson, A.H. (2007). Inhibition of fracture healing. *J Bone Joint Surg Br* 89, 1553-1560.
- Giannoudis, P.V., Einhorn, T.A., and Marsh, D. (2007). Fracture healing: the diamond concept. *Injury* 38 Suppl 4, S3-6.
- Glass R, A.M., Cavalcanti-Adam E, Blümmel J, Haferkemper C, Dodd C, Spatz J (2004). Block copolymer micelle nanolithography on non-conductive substrates. *New England Journal of Physics* 6, 1367-2630.
- Gloria, A., De Santis, R., Ambrosio, L., Causa, F., and Tanner, K.E. (2011). A multi-component fiber-reinforced PHEMA-based hydrogel/HAPEX device for customized intervertebral disc prosthesis. *Journal of biomaterials applications* 25, 795-810.
- Gronthos, S., Graves, S.E., Ohta, S., and Simmons, P.J. (1994). The STRO-1+ fraction of adult human bone marrow contains the osteogenic precursors. *Blood* 84, 4164-4173.
- Guo, J., Padilla, R.J., Ambrose, W., De Kok, I.J., and Cooper, L.F. (2007). The effect of hydrofluoric acid treatment of TiO₂ grit blasted titanium implants on adherent osteoblast gene expression in vitro and in vivo. *Biomaterials* 28, 5418-5425.
- Hamilton, D.W., and Brunette, D.M. (2007). The effect of substratum topography on osteoblast adhesion mediated signal transduction and phosphorylation. *Biomaterials* 28, 1806-1819.
- Harrison, R.G. (1911). On the Stereotropism of Embryonic Cells. *Science* 34, 279-281.
- He, P., Sahoo, S., Ng, K.S., Chen, K., Toh, S.L., and Goh, J.C. (2013). Enhanced osteoinductivity and osteoconductivity through hydroxyapatite coating of silk-based tissue-engineered ligament scaffold. *Journal of biomedical materials research Part A* 101, 555-566.
- Hench, L.L., and Polak, J.M. (2002). Third-generation biomedical materials. *Science* 295, 1014-1017.
- Holt, G., Arthur, A., Frame, D., and Muirhead, A. (2004). Human skeletal allograft collection--room for improvement? *Scott Med J* 49, 146-148.
- Huiskes, R., Van Driel, W.D., Prendergast, P.J., and Soballe, K. (1997). A biomechanical regulatory model for periprosthetic fibrous-tissue differentiation. *J Mater Sci Mater Med* 8, 785-788.
- Isa, Z.M., Schneider, G.B., Zaharias, R., Seabold, D., and Stanford, C.M. (2006). Effects of fluoride-modified titanium surfaces on osteoblast proliferation and gene expression. *Int J Oral Maxillofac Implants* 21, 203-211.

- J. Y. Cheng, C.A.R., E. L. Thomas, H I. Smith, , and Vancso, G.J. (2002). Fabrication of nanostructures with long-range order using block copolymer lithography. *APPLIED PHYSICS LETTERS* 81, 3657-3659.
- Jager, M., Zilkens, C., Zanger, K., and Krauspe, R. (2007). Significance of nano- and microtopography for cell-surface interactions in orthopaedic implants. *J Biomed Biotechnol* 2007, 69036.
- Johansen, A., Evans, R.J., Stone, M.D., Richmond, P.W., Lo, S.V., and Woodhouse, K.W. (1997). Fracture incidence in England and Wales: a study based on the population of Cardiff. *Injury* 28, 655-660.
- Johnson, L.L. (1986). Arthroscopic abrasion arthroplasty historical and pathologic perspective: present status. *Arthroscopy : the journal of arthroscopic & related surgery : official publication of the Arthroscopy Association of North America and the International Arthroscopy Association* 2, 54-69.
- Jorgensen, N.R., Henriksen, Z., Sorensen, O.H., and Civitelli, R. (2004). Dexamethasone, BMP-2, and 1,25-dihydroxyvitamin D enhance a more differentiated osteoblast phenotype: validation of an in vitro model for human bone marrow-derived primary osteoblasts. *Steroids* 69, 219-226.
- Kantawong, F., Burgess, K.E., Jayawardena, K., Hart, A., Riehle, M.O., Oreffo, R.O., Dalby, M.J., and Burchmore, R. (2010). Effects of a surface topography composite with puerariae radix on human STRO-1-positive stem cells. *Acta Biomater* 6, 3694-3703.
- Kasai, Y., Takegami, K., and Uchida, A. (2003). Mixture ratios of local bone to artificial bone in lumbar posterolateral fusion. *J Spinal Disord Tech* 16, 31-37.
- Kashiwagi, K., Tsuji, T., and Shiba, K. (2009). Directional BMP-2 for functionalization of titanium surfaces. *Biomaterials* 30, 1166-1175.
- Katagiri, T., Yamaguchi, A., Komaki, M., Abe, E., Takahashi, N., Ikeda, T., Rosen, V., Wozney, J.M., Fujisawa-Sehara, A., and Suda, T. (1994). Bone morphogenetic protein-2 converts the differentiation pathway of C2C12 myoblasts into the osteoblast lineage. *J Cell Biol* 127, 1755-1766.
- Key, J. (1931). Experimental Arthritis: The changes in joints produced by creating defects in the articular cartilage. *Journal of Bone and Joint Surgery Am* 13, 725-739.
- Khan, W.S., Rayan, F., Dhinsa, B.S., and Marsh, D. (2012). An osteoconductive, osteoinducti, and osteogenic tissue-engineered product for trauma and orthopaedic surgery: how far are we? *Stem Cells International* 2012.
- Khurana, J.S., ed. (2009). *Bone pathology*, 2nd edn (Humana press).
- Kilian, K.A., Bugarija, B., Lahn, B.T., and Mrksich, M. (2010). Geometric cues for directing the differentiation of mesenchymal stem cells. *Proc Natl Acad Sci U S A* 107, 4872-4877.
- Kobayashi, T., and Kronenberg, H. (2005). Minireview: transcriptional regulation in development of bone. *Endocrinology* 146, 1012-1017.
- Krishnamoorthy, S., Pugin, R., Brugger, J., Heinzelmann, H., Hoogerwerf, A.C., and Hinderling, C. (2006). Block copolymer micelles as switchable templates for nanofabrication. *Langmuir* 22, 3450-3452.
- Kwan, A.P., Cummings, C.E., Chapman, J.A., and Grant, M.E. (1991). Macromolecular organization of chicken type X collagen in vitro. *J Cell Biol* 114, 597-604.
- Langer, R., and Vacanti, J.P. (1993). Tissue engineering. *Science* 260, 920-926.
- Lee, C.H., Cook, J.L., Mendelson, A., Moiola, E.K., Yao, H., and Mao, J.J. (2010). Regeneration of the articular surface of the rabbit synovial joint by cell homing: a proof of concept study. *Lancet* 376, 440-448.
- Leinco (2013). Immunohistochemical protocol for frozen sections (Leinco technologies inc.).
- Lian, J.B., and Stein, G.S. (1995). Development of the osteoblast phenotype: molecular mechanisms mediating osteoblast growth and differentiation. *Iowa Orthop J* 15, 118-140.

- Lian, J.B., Stein, G.S., Javed, A., van Wijnen, A.J., Stein, J.L., Montecino, M., Hassan, M.Q., Gaur, T., Lengner, C.J., and Young, D.W. (2006). Networks and hubs for the transcriptional control of osteoblastogenesis. *Rev Endocr Metab Disord* 7, 1-16.
- Liu, H., Lin, J., and Roy, K. (2006). Effect of 3D scaffold and dynamic culture condition on the global gene expression profile of mouse embryonic stem cells. *Biomaterials* 27, 5978-5989.
- Lopez-Garcia, C., Klein, A.M., Simons, B.D., and Winton, D.J. (2010). Intestinal stem cell replacement follows a pattern of neutral drift. *Science* 330, 822-825.
- Macchiarini, P., Jungebluth, P., Go, T., Asnaghi, M.A., Rees, L.E., Cogan, T.A., Dodson, A., Martorell, J., Bellini, S., Parnigotto, P.P., *et al.* (2008). Clinical transplantation of a tissue-engineered airway. *Lancet* 372, 2023-2030.
- MacDermott, R.P., and Bragdon, M.J. (1983). Fetal calf serum augmentation during cell separation procedures accounts for the majority of human autologous mixed leukocyte reactivity. *Behring Inst Mitt*, 122-128.
- MacLaine, S.E., Gadhari, N., Pugin, R., Meek, R.M., Liley, M., and Dalby, M.J. (2012). Optimizing the osteogenicity of nanotopography using block co-polymer phase separation fabrication techniques. *Journal of orthopaedic research : official publication of the Orthopaedic Research Society* 30, 1190-1197.
- Mankin, H.J., Springfield, D.S., Gebhardt, M.C., and Tomford, W.W. (1992). Current status of allografting for bone tumors. *Orthopedics* 15, 1147-1154.
- Marom, R., Shur, I., Solomon, R., and Benayahu, D. (2005). Characterization of adhesion and differentiation markers of osteogenic marrow stromal cells. *J Cell Physiol* 202, 41-48.
- McBeath, R., Pirone, D.M., Nelson, C.M., Bhadriraju, K., and Chen, C.S. (2004). Cell shape, cytoskeletal tension, and RhoA regulate stem cell lineage commitment. *Dev Cell* 6, 483-495.
- McMurray, R.J., Gadegaard, N., Tsimbouri, P.M., Burgess, K.V., McNamara, L.E., Tare, R., Murawski, K., Kingham, E., Oreffo, R.O.C., and Dalby, M.J. (2011). Nanoscale surfaces for the long-term maintenance of mesenchymal stem cell phenotype and multipotency. *Nature Materials* 10, 637-644.
- McNamara, L.E., Sjostrom, T., Burgess, K.E., Kim, J.J., Liu, E., Gordonov, S., Moghe, P.V., Meek, R.M., Oreffo, R.O., Su, B., *et al.* (2011). Skeletal stem cell physiology on functionally distinct titania nanotopographies. *Biomaterials* 32, 7403-7410.
- McNamara LE, S.T., Burgess K, Lim J, Liu E, Gordonov S, Moghe PV, Meek RMD, Oreffo ROC, Su B, Dalby M (Manuscript in Preparation). Metabolomics provides a unique functional readout of skeletal stem cells on distinct nanotopographies evidenced by the alteration from a quiescent to an active phenotype on a 15 nm pillar.
- Miller, M.D. (2008). Review of Orthopaedics, 5th edn (Saunders).
- Moro-Barrero, L., Acebal-Cortina, G., Suarez-Suarez, M., Perez-Redondo, J., Murcia-Mazon, A., and Lopez-Muniz, A. (2007). Radiographic analysis of fusion mass using fresh autologous bone marrow with ceramic composites as an alternative to autologous bone graft. *J Spinal Disord Tech* 20, 409-415.
- Myers, G.J., Abudu, A.T., Carter, S.R., Tillman, R.M., and Grimer, R.J. (2007). The long-term results of endoprosthetic replacement of the proximal tibia for bone tumours. *J Bone Joint Surg Br* 89, 1632-1637.
- NCBI (2013). PCR (NCBI Probe Database).
- Nishida, J., and Shimamura, T. (2008). Methods of reconstruction for bone defect after tumor excision: a review of alternatives. *Med Sci Monit* 14, RA107-113.
- Nishimura, I., Huang, Y., Butz, F., Ogawa, T., Lin, A., and Wang, C.J. (2007). Discrete deposition of hydroxyapatite nanoparticles on a titanium implant with predisposing substrate microtopography accelerated osseointegration. *Nanotechnology* 18.
- Oh, S., Brammer, K.S., Li, Y.S., Teng, D., Engler, A.J., Chien, S., and Jin, S. (2009). Stem cell fate dictated solely by altered nanotube dimension. *Proc Natl Acad Sci U S A* 106, 2130-2135.

- Ong, J.L., Carnes, D.L., Cardenas, H.L., and Cavin, R. (1997). Surface roughness of titanium on bone morphogenetic protein-2 treated osteoblast cells in vitro. *Implant Dent* 6, 19-24.
- Oreffo, R.O., Cooper, C., Mason, C., and Clements, M. (2005). Mesenchymal stem cells: lineage, plasticity, and skeletal therapeutic potential. *Stem cell reviews* 1, 169-178.
- Park, J.M., Koak, J.Y., Jang, J.H., Han, C.H., Kim, S.K., and Heo, S.J. (2006). Osseointegration of anodized titanium implants coated with fibroblast growth factor-fibronectin (FGF-FN) fusion protein. *Int J Oral Maxillofac Implants* 21, 859-866.
- Petit, R. (1999). The use of hydroxyapatite in orthopaedic surgery: a ten year review. *European journal of orthopaedic surgery and traumatology* 0, 71-74.
- Petrie T, R.J., Reyes C, Burns K, Collard D, Garcia A (2008). The effect of integrin-specific bioactive coatings on tissue healing and implant osseointegration. *Biomaterials* 29, 2849-2857.
- Pittenger, M.F., Mackay, A.M., Beck, S.C., Jaiswal, R.K., Douglas, R., Mosca, J.D., Moorman, M.A., Simonetti, D.W., Craig, S., and Marshak, D.R. (1999). Multilineage potential of adult human mesenchymal stem cells. *Science* 284, 143-147.
- Pountos, I., Jones, E., Tzioupis, C., McGonagle, D., and Giannoudis, P.V. (2006). Growing bone and cartilage. The role of mesenchymal stem cells. *J Bone Joint Surg Br* 88, 421-426.
- Pridie, K. (1959). A Method of Resurfacing Osteoarthritic Knee Joints. . *Journal bone and joint surgery Br* 41-B, 618-619.
- Qiagen (2009). Quantitect reverse transcription handbook (Qiagen).
- Ramachandran, M., ed. (2007). Basic orthopaedic sciences, The Stanmore guide (Hodder Arnold).
- Rea, S.M., Brooks, R.A., Schneider, A., Best, S.M., and Bonfield, W. (2004). Osteoblast-like cell response to bioactive composites-surface-topography and composition effects. *J Biomed Mater Res B Appl Biomater* 70, 250-261.
- Reid, R.L. (1968). Hernia through an iliac bone-graft donor site. A case report. *J Bone Joint Surg Am* 50, 757-760.
- Robey, P.G., and Bianco, P. (2006). The use of adult stem cells in rebuilding the human face. *J Am Dent Assoc* 137, 961-972.
- Rokkum, M., Reigstad, A., and Johansson, C.B. (2002). HA particles can be released from well-fixed HA-coated stems: histopathology of biopsies from 20 hips 2-8 years after implantation. *Acta orthopaedica Scandinavica* 73, 298-306.
- Sacchetti, B., Funari, A., Michienzi, S., Di Cesare, S., Piersanti, S., Saggio, I., Tagliafico, E., Ferrari, S., Robey, P.G., Riminucci, M., *et al.* (2007). Self-renewing osteoprogenitors in bone marrow sinusoids can organize a hematopoietic microenvironment. *Cell* 131, 324-336.
- Scharstuhl, A., Schewe, B., Benz, K., Gaissmaier, C., Buhning, H.J., and Stoop, R. (2007). Chondrogenic potential of human adult mesenchymal stem cells is independent of age or osteoarthritis etiology. *Stem Cells* 25, 3244-3251.
- Shaw-Dunn J, M.S., Payne A.C. *et al.* Functional anatomy and biomechanics (Glasgow).
- Simmons, P.J., and Torok-Storb, B. (1991). Identification of stromal cell precursors in human bone marrow by a novel monoclonal antibody, STRO-1. *Blood* 78, 55-62.
- Sjostrom, T., Dalby, M.J., Hart, A., Tare, R., Oreffo, R.O., and Su, B. (2009a). Fabrication of pillar-like titania nanostructures on titanium and their interactions with human skeletal stem cells. *Acta Biomater* 5, 1433-1441.
- Sjostrom, T., Fox, N., and Su, B. (2009b). Through-mask anodization of titania dot- and pillar-like nanostructures on bulk Ti substrates using a nanoporous anodic alumina mask. *Nanotechnology* 20, 135305.
- Sodek, J., Ganss, B., and McKee, M.D. (2000). Osteopontin. Critical reviews in oral biology and medicine : an official publication of the American Association of Oral Biologists 11, 279-303.

- Sotiropoulou, P.A., Perez, S.A., Salagianni, M., Baxevanis, C.N., and Papamichail, M. (2006). Characterization of the optimal culture conditions for clinical scale production of human mesenchymal stem cells. *Stem Cells* 24, 462-471.
- Standal, T., Borset, M., and Sundan, A. (2004). Role of osteopontin in adhesion, migration, cell survival and bone remodeling. *Experimental oncology* 26, 179-184.
- Stein, G.S., and Lian, J.B. (1993). Molecular mechanisms mediating proliferation/differentiation interrelationships during progressive development of the osteoblast phenotype. *Endocr Rev* 14, 424-442.
- Stephens, M., Kwan, A.P., Bayliss, M.T., and Archer, C.W. (1992). Human articular surface chondrocytes initiate alkaline phosphatase and type X collagen synthesis in suspension culture. *J Cell Sci* 103 (Pt 4), 1111-1116.
- Stevens, M.M., and George, J.H. (2005). Exploring and engineering the cell surface interface. *Science* 310, 1135-1138.
- Tanner, K.E., Downes, R., Bonfield, W. (1994). Clinical applications of hydroxyapatite reinforced materials. *British Ceramic Transactions* 93, 104-107.
- Tare RS, K.J., Aavold A, Jones AH, Dunlop DG, Oreffo ROC (2009). Skeletal stem cells and bone regeneration: translational strategies from bench to clinic. *Engineering in Medicine* 224-H, 1-16.
- Termaat, M.F., Den Boer, F.C., Bakker, F.C., Patka, P., and Haarman, H.J. (2005). Bone morphogenetic proteins. Development and clinical efficacy in the treatment of fractures and bone defects. *J Bone Joint Surg Am* 87, 1367-1378.
- Thoms, S., Gadegaard, N., Macintyre, D.S., Mcghee, K., Gallagher, J., Casey, B., and Wilkinson, C.D.W. (2003). Arrays of nano-dots for cellular engineering. *Microelectron Eng* 67-8, 162-168.
- Till, J.E., and McCulloch, E.A. (1963). Early repair processes in marrow cells irradiated and proliferating in vivo. *Radiat Res* 18, 96-105.
- Tuli, R., Seghatoleslami, M.R., Tuli, S., Wang, M.L., Hozack, W.J., Manner, P.A., Danielson, K.G., and Tuan, R.S. (2003). A simple, high-yield method for obtaining multipotential mesenchymal progenitor cells from trabecular bone. *Mol Biotechnol* 23, 37-49.
- Urist, M.R. (1965). Bone: formation by autoinduction. *Science* 150, 893-899.
- Verhage, M., and Toonen, R.F. (2007). Regulated exocytosis: merging ideas on fusing membranes. *Current opinion in cell biology* 19, 402-408.
- Vieu C, C.F., Pépin A, Chen Y, Mejias M, Lebib A, Manin-Ferlazzo L, Couraud L, Launois H (2000). Electron beam lithography: resolution limits and applications. *Applied Surface Science* 164, 111-117.
- Wakitani, S., Nawata, M., Tensho, K., Okabe, T., Machida, H., and Ohgushi, H. (2007). Repair of articular cartilage defects in the patello-femoral joint with autologous bone marrow mesenchymal cell transplantation: three case reports involving nine defects in five knees. *J Tissue Eng Regen Med* 1, 74-79.
- Wang, L.S., Boulaire, J., Chan, P.P.Y., Chung, J.E., and Kurisawa, M. (2010). The role of stiffness of gelatin-hydroxyphenylpropionic acid hydrogels formed by enzyme-mediated crosslinking on the differentiation of human mesenchymal stem cell. *Biomaterials* 31, 8608-8616.
- Webster, T.J., Yang, L., and Sheldon, B.W. (2009). The impact of diamond nanocrystallinity on osteoblast functions. *Biomaterials* 30, 3458-3465.
- Wheless (2013). wheless' textbook of orthopaedics, C.R. Wheless, ed.
- Whiteside, L.A., White, S.E., Engh, C.A., and Head, W. (1993). Mechanical evaluation of cadaver retrieval specimens of cementless bone-ingrown total hip arthroplasty femoral components. *J Arthroplasty* 8, 147-155.
- Wilkinson, A., Hewitt, R.N., McNamara, L.E., McCloy, D., Dominic Meek, R.M., and Dalby, M.J. (2011). Biomimetic microtopography to enhance osteogenesis in vitro. *Acta Biomater* 7, 2919-2925.

- Woo, E.J. (2012a). Adverse Events After Recombinant Human BMP2 in Nonspinal Orthopaedic Procedures. *Clin Orthop Relat Res*.
- Woo, E.J. (2012b). Recombinant human bone morphogenetic protein-2: adverse events reported to the Manufacturer and User Facility Device Experience database. *The spine journal : official journal of the North American Spine Society* 12, 894-899.
- Yamashita, F., Sakakida, K., Suzu, F., and Takai, S. (1985). The transplantation of an autogeneic osteochondral fragment for osteochondritis dissecans of the knee. *Clin Orthop Relat Res*, 43-50.
- Yang, L., Tao, T., Wang, X., Du, N., Chen, W., Tao, S., Wang, Z., and Wu, L. (2003). Effects of dexamethasone on proliferation, differentiation and apoptosis of adult human osteoblasts in vitro. *Chinese medical journal* 116, 1357-1360.
- Zhao, G., Zinger, O., Schwartz, Z., Wieland, M., Landolt, D., and Boyan, B.D. (2006). Osteoblast-like cells are sensitive to submicron-scale surface structure. *Clin Oral Implants Res* 17, 258-264.
- Zhao, H., Ito, Y., Chappel, J., Andrews, N.W., Teitelbaum, S.L., and Ross, F.P. (2008). Synaptotagmin VII regulates bone remodeling by modulating osteoclast and osteoblast secretion. *Dev Cell* 14, 914-925.
- Zimmer (1999). Calcicoat ceramic coating (HA/TCP).
- Zimmer (2003a). Cancellous-Structured Titanium (CSTi).
- Zimmer (2003b). Porous surfaces for fixation of orthopaedic implants. 3146-3150.
- Zimmer (2006). Zimmer MAYO conservative hip prosthesis.
- Zimmer (2010). VerSys hip system fiber metal taper.

Appendix

The media, solutions and run protocols are detailed below. Unless otherwise stated the reagents were obtained from Sigma-Aldrich, UK.

9 Acellular substrate analysis

Simulated Body Fluid (SBF)¹

Reagents obtained from BDH lab supplies (UK) unless otherwise stated.

MilliQ water	50 ml
NaCl (VWR, Prolab, Belgium)	780 mg
NaHCO ₃ (Fisher Scientific, UK)	35 mg
KCL	22 mg
K ₂ HPO ₄ .3H ₂ O	23 mg
MgCl ₂ .6H ₂ O	31 mg
HCL (1M)	4 ml
CaCl ₂	28 mg
Na ₂ SO ₄	7 mg
(CH ₂ OH) ₃ CNH ₂ (Sigma Aldrich, St Louis)	606 mg

Reagents were added sequentially on a low temperature magnetic stirrer, pH adjusted to 7.40 with HCL / NaOH and the solution made up to 100ml with MilliQ water. The solution was filtered before use. The ion concentrations of human plasma and this form of simulated body fluid are equated with respect to sodium, potassium, magnesium, calcium, hydrogen phosphate, and sulphate ions. Chloride ion concentrations are 149 mM in SBF and 103 mM in human plasma, whereas hydrogen carbonate ions are 4.2 mM in SBF and 27 mM in human plasma.¹

2 Cell culture

Antimicrobial solution: 1% Antimicrobial/antifungal/ L-Glutamine

Penicillin	
Streptomycin	
Amphotericin B (Gibco, Invitrogen UK)	250 µg/ml
L Glutamine	200 mM

Modified DMEM

DMEM	500 ml
FBS	50 ml
Antimicrobial solution	10 ml
Nonessential amino acids 100X (Invitrogen, UK)	5 ml
Sodium Pyruvate (100mM)	5 ml

Modified αMEM

αMEM	500 ml
FBS	75 ml
Antimicrobial solution	13 ml

Osteogenic Media

Modified DMEM	250 ml
Ascorbic acid	4.4 mg
Dexamethasone (39.2 mg in 100ml HS)	2.5 µl

3 HBMC harvest and HOBs

Bone marrow transport medium

PBS	200 ml
EDTA	149 mg
Antimicrobial solution	4 ml

Ficoll Paque Premium

1.077 g/ml

GE healthcare biosciences AB, SE-751 84 Uppsala

Collagenase type XI

256U/ml

HOBs

Obtained from Promocell GmbH (Germany)

Bone Morphogenic Protein (BMP2)

BMP2	0.0012 mg
Modified DMEM	12ml

Trypsin-Versene Solution

Trypsin	10X
Versene	

4 Cell microscopy

Fixative

Formaldehyde 37-41% (Fisher Scientific, UK)	10ml
PBS	90ml
Then sucrose (Fisher Scientific, UK)	2000 mg

1% PBS/BSA

BSA (Sigma Aldrich, St Louis)	1000 mg
PBS	100 ml

PBS Tween 0.5%

PBS	200ml
Tween 20 (Promega Corporation, Madison)	1ml

Permeabilising buffer

PBS	100 ml
Sucrose	10300 mg
Sodium Chloride (VWR, Prolab, Belgium)	292 mg
Magnesium Chloride Hexa Hydrate (BDH lab supplies, UK)	60 mg
Hepes (Fisher Scientific, New Jersey)	476 mg

The reagents were dissolved sequentially and the pH adjusted to 7.2 using 1 M Sodium Hydroxide (Fisher Scientific, UK). Finally 0.5 ml Triton X 100 was added (Sigma-Aldrich, Saint Louis).

Antibodies

OCN (OC4-30 and sc-73464), OPN (Akm2A1 and sc-21742), COL2a (sc-59958), MYOD (sc-32758), TUBB₃ (sc-51670), PPARG (sc-51984) and PSELECTIN (sc-59935) obtained from Autogen Bioclear (UK) and Santa Cruz Biotechnology (USA) were used.

5 RNA Extraction

Stratagene RNA extraction

The elution buffer was warmed to 60°C. Mix 1 prepared: lysate buffer 6300 µl and 45 µl BME (for 16 samples). 350 µl added per well, cell scraper used and lysate passed through 18 gauge needle then vortexed. 'Absolutely mRNA protocol' followed using 30 µl elution buffer followed by incubation and centrifugation prior to a second elution stage of 20 µl elution buffer, re-incubation, and re-centrifugation.

6 RT

All of the reaction mixes were vortexed and microcentrifuged prior to thermocycling.

Omniscript RT (50) (Qiagen)

10ng RNA was used for ORT to yield 20 µl of ~1500 ng/µl cDNA for use in qPCR. 9 µl ORT mix* was added to each tube of RNA/ water control and centrifuged 8000 g for 1 min. RNA and water were incubated at 65°C for 5 min and then held at 4°C. Incubation at 37°C for 60 min, inactivation at 93°C for 5 min and holding at 4°C until use or subsequent freezing at -20°C was undertaken.

*ORT mix (for 4 test samples and a control water sample)

10X Buffer RT 12 µl, dNTP mix (5 mM of each dNTP) 12 µl, Random Primer 12 µl, RNasin (40 U/µl) 1.5 µl, Omniscript RT 12 µl, and water 10.5 µl.

Quantitect RT

Genomic DNA elimination was undertaken by incubation of the following suspension at 42°C for 2 min prior to placing on ice: gDNA wipeout (7x) 2 µl and RNA (up to 1 µg) and RNase free water 12 µl.

RT was undertaken using the following mix and incubation undertaken at 42°C for 15 min, inactivation of the qRTase at 95°C for 3 min and storage at -20°C for use in qPCR. RTase 1 µl, Quantiscript RT Buffer (x 5) 4 µl, RT primermix 1 µl, Template RNA from above reaction 14 µl.

7 QPCR

Sybr green and Taqman qPCR kits were used as described below.

The **SYBR Green PCR** method was used. The master mix consisted of:

Quantifast SYBR green PCR mix for 12 reactions was 160 µl; forward primer (10 µM) 12 µl; backward primer (10 µM) 12 µl; RNase free water 120 µl.

The run method was undertaken using the 7500 Fast Real-Time PCR system (Applied Biosystems) and was as follows:

Hold	95°C 5 min
Cycle x 40	(95°C 10 s, 60°C 30 s, 76°C 15 s)
Melt Curve	(95°C 15 s, 60°C 1 min, 95°C 15 s, 60°C 15 s)

The **Brilliant III Ultra-Fast Sybr Green qPCR** method was also used. The master mix for 1 reaction consisted of: Brilliant III Ultra-Fast Sybr Green QPCR master mix 10 µl; Forward primer (10 µM) 1 µl; Backward primer (10 µM) 1 µl; RNase free water 5.7 µl; and diluted reference dye (1:500) 0.3 µl. 2 µl cDNA was added per test well and 2 µl RNase free water to each control well. The run method was undertaken using the 7500 Fast Real-Time PCR system (Applied Biosystems) and was as follows:

Settings: Quantitation CT, SYBR green, Fast

Hold	95°C 3 min
Cycle x 40	(95°C 5 s, 60°C 20 s)
Melt Curve	(95°C 1 min, 55°C 30 s, 95°C 30 s)

The **Taqman qPCR** was used for the definitive results. The master mix was as follows (1 x mix): Taqman gene expression master mix 10 µl; Primerprobe 1 µl and water 7 µl. The reaction mixes were vortexed and microcentrifuged prior to thermocycling, and the plates centrifuged at 3600r.p.m. for 30 seconds (Eppendorf 5804R) prior to thermocycling.

Settings: Quantitation CT, Taqman, Standard

Hold	50°C 2 min, 95°C 10 min
Cycle x 40	95°C 15 s, 60°C 1 min

The Taqman primerprobe reference numbers were:

RUNX2	HS 00231692-m1
OPN (SPP1)	HS 00959010-M1
BGLAP (OCN)	HS 01587814-g1
SOX9	HS 01001343-g1
TUBB ₃	HS 00801390-s1
PPARG	HS 001115513-m1
MYOD	HS 00159528-M1
18S	HS 99999901-s1)

8 RNA yield and integrity

Table A-1 Relative gene expression at day 11 (chapter 3)

RNA sample	ng/ μ l	A260	A280	260/280
Planar 1	5.85	0.146	0.070	2.09
Planar 2	5.23	0.131	0.065	2.01
Planar 3	5.77	0.144	0.101	1.43
NSQ50 1	5.01	0.125	0.067	1.88
NSQ50 2	8.41	0.210	0.091	2.32
NSQ50 3	3.54	0.088	0.052	1.71
Osteogenic 1	5.38	0.135	0.076	1.77
Osteogenic 2	4.89	0.122	0.056	2.18
Osteogenic 3	4.81	0.120	0.055	2.17
NSQ50 HAPCL 1	13.01	0.325	0.165	1.97
NSQ50 HAPCL 2	4.67	0.117	0.056	2.08
NSQ50 HAPCL 3	5.18	0.129	0.070	1.84

Table A- 2 Relative gene expression at day 28 (chapter 3)

RNA sample	ng/ μ l	A260	A280	260/280
Planar 1	2.08	0.052	0.022	2.38
Planar 2	1.73	0.043	0.013	3.31
Planar 3	1.64	0.041	0.010	4.26
NSQ50 1	2.48	0.062	0.027	2.26
NSQ50 2	1.95	0.049	0.017	2.91
NSQ50 3	3.29	0.082	0.052	1.57
Osteogenic 1	2.28	0.057	0.036	1.59
Osteogenic 2	1.74	0.044	0.015	2.99
Osteogenic 3	2.36	0.059	0.023	2.53
NSQ50 HAPCL 1	2.54	0.063	0.039	1.64
NSQ50 HAPCL 2	1.61	0.040	0.035	1.14

NSQ50 HAPCL 3	5.42	0.014	0.075	1.81
---------------	------	-------	-------	------

Table A-3 RUNX2 expression at 25 days (chapter 4)

RNA sample	ng/ μ l	A260	A280	260/280
Planar 1	2.64	0.066	0.006	10.51
Planar 2	1.85	0.046	0.016	2.88
Planar 3	2.44	0.061	0.016	3.87
14 nm nanoisland 1	3.54	0.088	0.021	4.24
14 nm nanoisland 2	1.94	0.048	0.014	3.36
14 nm nanoisland 3	7.79	0.195	0.108	1.81
18 nm nanoisland 1	2.02	0.051	0.008	6.43
18 nm nanoisland 2	2.62	0.066	0.018	3.71
18 nm nanoisland 3	3.20	0.080	0.010	7.65

References

- 1.Kokubo T, Kushitani H, Sakka S, et al. 1990. Solutions able to reproduce in vivo surface-structure changes in bioactive glass-ceramic a-w. J Biomed Mater Res 24:721-734.

